University of Alberta

SPECIMEN THICKNESS EFFECTS ON MODE I & MODE II INTERLAMINAR TOUGHNESS OF COMPOSITES USING FINITE ELEMENT ANALYSIS

By

ARUN AGRAWAL

A thesis submitted to the Faculty of Graduate Studies and Research in partial fulfillment of the requirements for the degree of Master of Science

Department of Mechanical Engineering

Edmonton, Alberta

Spring 2002

National Library of Canada
Acquisitions and Bibliographic Services
395 Wellington Street
Ottawa ON K1A 0N4
Canada

Bibliothèque nationale du Canada
Acquisitions et services bibliographiques
395, rue Wellington
Ottawa ON K1A 0N4
Canada

Your file Votre référence

Our file Notre référence

The author has granted a non-exclusive licence allowing the National Library of Canada to reproduce, loan, distribute or sell copies of this thesis in microform, paper or electronic formats.

L'auteur a accordé une licence non exclusive permettant à la Bibliothèque nationale du Canada de reproduire, prêter, distribuer ou vendre des copies de cette thèse sous la forme de microfiche/film, de reproduction sur papier ou sur format électronique.

The author retains ownership of the copyright in this thesis. Neither the thesis nor substantial extracts from it may be printed or otherwise reproduced without the author's permission.

L'auteur conserve la propriété du droit d'auteur qui protège cette thèse. Ni la thèse ni des extraits substantiels de celle-ci ne doivent être imprimés ou autrement reproduits sans son autorisation.

0-612-69793-2

Canada

University of Alberta

Library Release Form

Name of Author: **Arun Agrawal**

Title of the Thesis: **Specimen Thickness Effects on Mode I & Mode II Interlaminar Toughness of Composites Using Finite Elements Analysis**

Degree : **Master of Science**

Year this Degree Granted: **2002**

Permission is hereby granted to the University of Alberta Library to reproduce single copies of this thesis and lend or sell such copies for private, scholarly, or scientific research purposes only.

The author reserves all other publication and other rights in association with the copyright in the thesis, and except as herein before provided, neither the thesis nor any substantial portion thereof may be printed or otherwise reproduced in any material from whatever without the author's prior written permission.

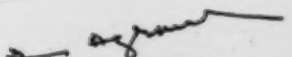

Arun Agrawal

9008, 112 Street, #3B
Edmonton T6G 2C5
Alberta, Canada

Dated:
Jan 30 2002

University of Alberta

Faculty of Graduate Studies and Research

The undersigned certify that they have read, and recommend to the faculty of Graduate Studies and Research for acceptance, a thesis entitled Specimen Thickness Effects on Mode I & Mode II Interlaminar Toughness of Composites Using Finite Element Analysis submitted by Arun Agrawal in partial fulfillment of the requirements for the degree of Master of Science.

Dr Pean-Yue Ben Jar

Dr Donald Raboud

Dr Gary Faulkner

Dr Jung-June (Roger) Cheng

Jan 24, 2002

Abstract

Laminated fibre-reinforced polymer composites are highly susceptible to delamination damage. Their delamination resistance, characterized by the interlaminar fracture toughness (IFT), is of major concern. Owing to orthotropy, it is believed that pure Mode I, as well as pure Mode II interlaminar failures are possible. Experimental measurement of Mode I IFT has been standardized through DCB specimen. For Mode II testing, ENF specimen is widely used. Nonetheless, controversies amongst various test configurations to obtain the representative values stall the standardization of Mode II IFT test.

The present focus is to investigate specimen thickness effects on IFT values through finite element analysis of 2-dimensional linear elastic models of composite DCB and ENF specimens. Our results conclude thickness independence for both the specimens. Such evidence is significant towards the development of an acceptable Mode II IFT test standard. However, various unaccounted corrections may mischievously manifest as distinguishable thickness / other geometry effects.

Acknowledgements

I would like to take this opportunity to express my sincere thanks and gratitude to Dr. Ben Jar, Department of Mechanical Engineering, University of Alberta, under whose supervision the present research work is carried out. I would like to acknowledge his constant guidance and encouragement during the course of this work.

My sincere thanks are due to the various faculty members, non-academic staff, and grad students of the Mechanical Engineering department, interactions with whom had been an invaluable support and inspiration for this work. I would also like to acknowledge the financial support available to me from the department and other research funds for this work.

CONTENTS

Chapter 1
Introduction 1

1.1 General Introduction 1

1.2 Classification of Composites 3

1.3 Role of Laminated Fibre-Reinforced Polymer (LFRP) Composites as Structural Components 5

1.4 Mechanical Behaviour of LFRP Composites: Macromechanics 10

1.5 Mechanical Behaviour of LFRP Composites: Micromechanics 15

1.6 Fracture strength of LFRP Composites 19
1.6.1 Fracture Toughness of Isotropic Materials 19
1.6.2 Failure and Fracture Toughness Issues for Composites 22
1.6.3 Micro-Damage Modes in Fracture Mechanics of Composites 24
1.6.3.1 Fibre Fracture 25
1.6.3.2 Fibre Matrix Deboning 25
1.6.3.3 Intralaminar Matrix Cracking 25
1.6.3.4 Delamination 27
1.6.4 Micro Fracture Analysis of FPRP Composites 28

1.7 Overview of the Present Study 29

Chapter 2
Delamination of Composite Materials 31

2.1 Introduction 31

2.2 Mechanics of Delamination: The Interlaminar Stresses 33
2.2.1 Free Edge Delamination 33
2.2.2 Delamination Caused by Impact 38
2.2.3 Delamination caused by Matrix Cracks 38
2.2.4 General 38

2.3 Delamination Prediction 40

2.4 Delamination Control. 41

Chapter 3
Characterization of Mode I and II Interlaminar Fracture Toughness 43

3.1 Introduction 43

3.2 Mode I Interlaminar Fracture Toughness Testing 45

3.3 Long Road to Mode II Interlaminar Fracture Toughness Testing 47

3.4 Other Interlaminar Fracture Tests 51

3.5 The DCB Specimen 52
3.5.1 Specimen Details 52
3.5.2 Data Analysis 55

3.6 The ENF Specimen 61
3.6.1 Specimen Details 63
3.6.2 Data Analysis 64

ANNEX 3.1 Large Displacement and End Block Corrections in Mode I DCB specimen. 72

ANNEX 3.2 Large Displacement Corrections in Mode II ENF specimen. 74

Chapter 4
Finite Element Model of the Test Specimens 75

4.1 Introduction 75

4.2 The DCB Specimen Model 80
4.2.1 Results and Discussion 84

4.3 The ENF Specimen Model 87
4.3.1 Results and Discussion 91

4.4 Discussion 99

Chapter 5
Conclusions 105

5.1 General 105

5.2 Composite Interlaminar G_{IIc}: Sheer Myth or True Shear Measurement? 106

5.3 Concluding Remarks 107

5.4 Future Work 108

References 109

Appendix I:
A Note on the Graphical Representation in ANSYS: 120

List of Tables

Table 1.1	Typical mechanical properties of common fibres	6
Table 1.2	Typical mechanical properties of common resins	6
Table 1.3	Mechanical properties of popular composites	8
Table 1.4	Typical mechanical properties of traditional materials	8
Table 4.1	Large deformation corrections	83
Table 4.2	Study on dependence of Mode I fracture toughness on specimen thickness	84
Table 4.3	Study on dependence of crack tip-corner stresses on ENF specimen thickness	91
Table 4.4	Study on dependence of interface stresses on ENF specimen thickness	96
Table A1.1	Actual deformed crack contour from numerical nodal deflection values	122

List of Figures

Fig 1.1 Popular commercial applications of composites 3

Fig 1.2 A typical multi-directional laminate with Reference coordinate axes 7

Fig 1.3 Lamina orientation in 2-D plane 12

Fig 1.4 Typical transverse section of a unidirectional composite 17

Fig 1.5 Basic delamination modes in composite materials 21

Fig 1.6 Intra-laminar matrix cracks 27

Fig 1.7 Delamination cracks in a cross ply laminate 27

Fig 2.1 Common delamination sites and interlaminar stresses 32

Fig 2.2 Mechanism of set-up of interlaminar shear stress τ_{xz} in $(\theta/-\theta)_n$ laminate 34

Fig 2.3 Mechanism of set-up of interlaminar shear stress τ_{yz} in $(0/90)_n$ laminate 36

Fig 2.4 Mechanism of set-up of interlaminar direct stress σ_{zz} in (0/90) laminate 37

Fig 2.5 Interlaminar stresses due to matrix crack in off-axis plies 39

Fig 3.1 The DCB specimen 46

Fig 3.2 Popular Mode II test specimens 49

Fig 3.3 DCB specimen under loading 55

Fig 3.4 Displacement fields showing Mode II crack-driving mechanisms 62

Fig 3.5 Free-body diagram of the ENF specimen 66

Fig 3.6 Definition of various displacement components for the ENF specimen 66

Fig 3.6 End block effects for the DCB specimen 73

Fig 4.1 Starter defect crack contour 77

Fig 4.2 Finite element discretization of DCB/ENF specimen model 77

Fig 4.3 Mesh details of crack tip elements and Ref axes 78

Fig 4.4 Model of the DCB specimen 81

Fig 4.5 Maximum principal stress near crack tip of the DCB specimens 85

Fig 4.6 Variation of the max principal stress (S1) for path along crack tip of 10mm DCB specimen 86

Fig 4.7 Model of the ENF specimen 88

Fig 4.8 Use of bar elements to constraint opposite crack faces 90

Fig 4.9 Stress contours near crack tip for 10mm thick ENF specimen 92

Fig 4.10 Variation of max principal stress (S1), shear stress τ_{xz}, and von Misses stress (Ψ) for path along crack tip of 10mm ENF specimen 94

Fig 4.11 Vector plot showing the orientation of max principal stress near the crack tip 95

Fig 4.12 Variation of max principal stress (S1), normal Stress σ_z and Von Misses stress (Ψ) for path along interface of 10mm ENF specimen 97

Fig A1.1 Original and deformed configurations showing that the top and bottom faces cross over each other 121

Fig A1.2 Actual deformed crack contour configuration 124

Chapter 1

INTRODUCTION

1.1 GENERAL INTRODUCTION

Composites have emerged as a valuable class of engineering materials because they offer attributes not attainable from other conventional materials. A composite material is one, which is made up of macroscopic combination of two or more materials of different mechanical, electrical, optical, chemical, thermal, or hygral properties. The composite material is designed from its constituents to achieve an advantageous functional property, for example, specific strength, which is superior to that of the individual constituents. It is common that a composite exhibits the best qualities of their constituents and offer some qualities that neither constituent possesses.

Composite materials can be broadly classified into natural composites like wood, bones, stone etc., and the man-made composites like straw-reinforced clay walls, concrete etc. Even the man-made composites have a long history of usage. For example, laminated wood and development of strengthened mud bricks and pottery by straw reinforcement dates back to many ancient civilizations and has been in use for more than 3000 years. Also, the use of plywood with superior strength, moisture resistance, and resistance to thermal expansion, dates back to the ancient Egypt [1]. These can be considered precursors to modern composite materials.

Modern structural composites, frequently called the advanced composites, are a recent arrival, compared to their long history. With invention of first polyester resin in 1847 by Swedish chemist Berzelius, and introduction of plastic technology to make cellulose nitrate plastic in 1862 by English technologist Parkes, polymers came up as relatively cheap structural materials comparable in importance to metals. During the Second World War thrust was to replace natural rubber by synthetic material emerged and soon, the idea of reinforced structural plastic composite was 'rediscovered'. Glass fibre reinforced plastic (GRP) was commercially exploited as early as 1931 and first fibre-glass boat was made in 1942 [5]. Carbon fibres were perhaps first used by Edison in electric light bulbs in industrial application, and attracted the structural use primarily in the aerospace industry on account of their high performance and high cost by 1968. The first reported

high strength structural use of fibre was of Boron fibre in 1959, which attracted introduction into aerospace applications in 1960s. Kevlar aramid-49 fibre composites came up in 1970s. Thus, composites provide an alternative class of materials with tailored properties and attract an amazingly rapid industrial application, mostly in aerospace industry.

The impact of composites on our civilization can be limited only by the imagination. The specific properties which can be improved to a desired practical use include strength, weight, stiffness, fatigue life, corrosion resistance, temperature dependent behaviour, thermal insulation, thermal conductivity, wear resistance, acoustical insulation, etc. Composites, thus, have tailor-made properties and have a wide range of applications. Some of the popular applications of composites in structural non-structural use are shown in Fig 1.1. The outer surface of the stealth bomber aircraft with tailored optical and electrical properties is the most conspicuous non-structural aerospace use. The most widespread use of structural composites is in aircraft components, where high strength-to-weight ratio materials capable of sustaining increasing loading conditions while maintaining structural integrity are always required. It is anticipated that up to 35% weight saving can be achieved with the use of structural composites [4]. Composites also have tremendous applications in space vehicles where structural weight optimization is the prime objective to have higher payload. In civil structures, composites are attracting wide use, for example, the roof structure of Dubai airport, and a swimming pool in Aberdeen are made of glass fibre reinforced plastics. They have made uses in other fields like racing cars, commercial boats, pedestrian bridges, telescopic antennas, orthopedic bio-materials, tennis and squash racquets, golf shafts and so on. A detailed description covering various aspects of composites is available [2,5,6].

1.2 CLASSIFICATION OF COMPOSITES

Based on the arrangement of the constituents, which make the composite, there are three commonly accepted types: *Fibrous Composites* - which consists of fibres in a matrix; *Laminated Composites* - which consists of layers of various materials; and *Particulate Composites* - which consists of particles in a matrix. In fibrous composites the fibres are characterized geometrically by very high length-to-diameter ratio and higher strength. A short form is called a whisker. The fibres or whiskers are bound together by binder material usually called matrix to from a structural element. Fibre (or whisker) are much stronger and stiffer than same material in bulk form. This is due to a more perfect micro structure of a fibre. There are fewer internal defects (or dislocations) in the fibre than in the bulk material. Fibre has near crystal-sized diameter, and crystals are aligned in the fibre along the fibre axis. Typically, the diameter can be about 7 microns for carbon fibre. Typically, the matrix is of considerably low density, stiffness, and strength than fibre, or whisker. The purpose of matrix is manifold : support, protection, stress transfer, etc.

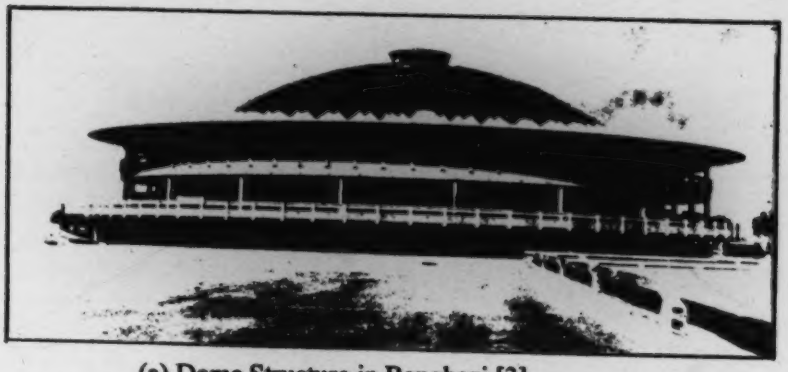

(a) Dome Structure in Benghazi [3]

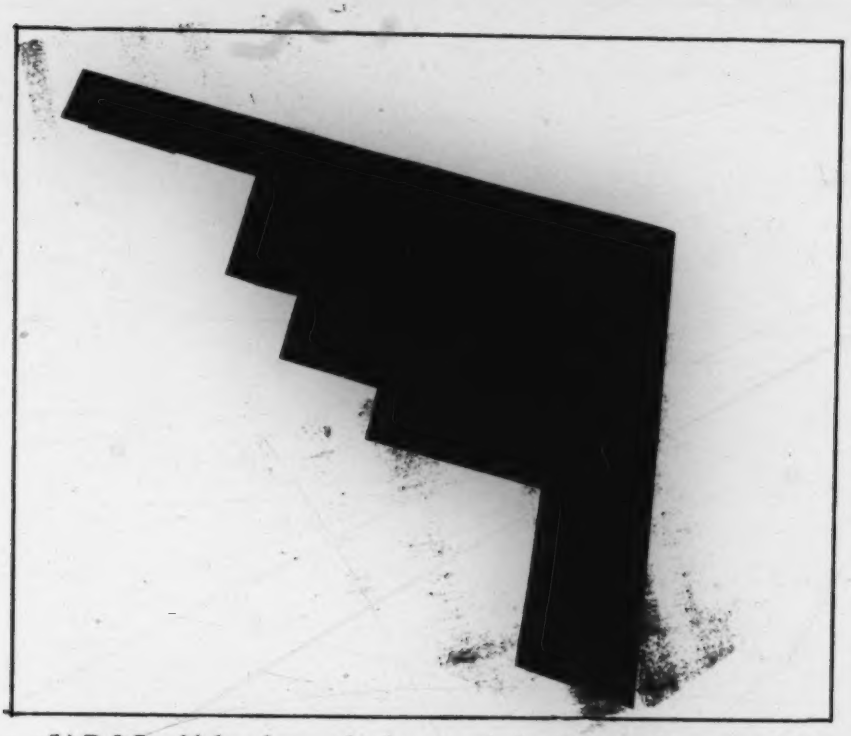

(b) B-2 Stealth bomber made almost entirely of composite materials [5].

Fig 1.1 Popular Commercial Applications of Composites

Laminated composites consist of at least two different materials that are bonded together. Lamination is used to combine the best aspects of the constituent layers in order to achieve a more useful material. For example, bimetals for temperature measuring devices, clad metals for corrosion protection or electro-thermal property, laminated glass for increased toughness applications, plastic-based laminates in forms like formica sheets, laminated fibrous composites, etc. Laminated fibrous composites are a hybrid class of composites involving both fibrous composites and lamination techniques. A more common name is *laminated fibre-reinforced composites*. Here the layer of fibre-reinforced material are built up with the fibre directions of each layer typically orientated in different directions to give different strengths and stiffness in various directions. Specific applications include missile cases, fibre-glass boat hulls, golf shafts, tennis rackets, etc.

Particulate composites have particles of one or more materials suspended in a matrix of another material. The particles can be either metallic or non-metallic, as can be the matrix. For example, lead particles in a steel or copper alloy to improve the machineability has metal particles in a metallic matrix composite. Concrete, having particles of sand and rock in cement paste is an example of nonmetallic matrix composite with nonmetallic particles. Example of nonmetallic composite with metallic particles is aluminum powder and perchlorate oxidizer in a flexible organic binder such as polysulphide rubber in rocket propellants to achieve steady burn reaction. Ceramics suspended in metal matrix, called cermet, is an example of nonmetallic particles in a metallic (matrix) composite.

It will be prudent to include one more category of classification of composites based on the chemical composition of the matrix from the point of view of the different typical uses in the industry. The matrix can be polymeric (e.g. polyester, epoxy), metallic, or ceramic. In the present context the structural composites especially, the structural fibre reinforced composites are most relevant. Based on the type of the matrix composites are classified as *Polymer composites, Metal composites, and Ceramic composites*. Common commercially available fibres are glass, graphite, aramid, polyethylene, boron, silicon carbide, silica, alumina, and aluminum silica. *Metal matrix composites* can be made up of Al alloys, Ni alloys, Ti alloys. The compatible fibres are Al_2O_3, Al_3N, B, SiO_2; Al_2O_3, B, Be, C, Mo, SiC; B, Be, Mo, SiC, respectively. *Polymer composites* can be thermosets (like epoxy, polysters, silicone, bismaleimid (BMI), polyimides etc.) which are amorphous and brittle, or the thermoplastics (which account for 75% tonnage of neat resin production and include polyether-ether-ketones (PEEK), nylon, polyether, polyimides(PI), polysulphones, etc.) and which have advantageous low density and low manufacturing cost. Fibre used in the polymer matrix composite can be carbon fibres (e.g. polyacrylonitrile based, graphite fibres), aramid fibre (e.g. kevlar), glass (e.g. E glass, S glass), ceramic fibres (e.g. oxide: silica; monoxide: SiC, silicon nitride, boron nitride), or any of the miscellaneous compatible fibres like boron and polyethylene. *Ceramic composites* have comparatively low tensile strength are not popular in structural applications.

1.3 ROLE OF LAMINATED FIBRE-REINFORCED POLYMER (*LFRP*) COMPOSITES AS STRUCTURAL COMPONENTS

Laminated fibre reinforced composites are by far the most important category of composite in terms of the structural use. Most commonly used matrices in the fibre-reinforced composites are polymeric. For the primary structural applications the laminated fibre-reinforced polymer-matrix composites have significant advantages over the conventional engineering materials. This is on account of their superior strength, strength-to-weight ratio, good fatigue and damping characteristics, corrosion resistance, ease of fabrication, and aesthetic qualities. Here in the present study, the term composites now onwards will, in general, refer to the LFRP composites.

The principal constituents of the composite, i.e. the reinforcing fibres, the matrix, and the interface, influence the strength and stiffness. The fibre reinforcement is the backbone that determines the stiffness and strength of composite in the direction of the fibres. The fibres are long and have high modulus of elasticity and high ultimate strength, and are generally orthotropic. Fibres generally exhibit a linear elastic behaviour. A comparison of their relevant mechanical properties is given in Table 1.1. They need to have uniform diameter and surface. They can be continuous or discontinuous (short fibre, i.e. those where length of the fibre affects the structural properties). Typically in LFRP composites fibres are continuous. The matrix, on the other hand, provides the support and protection to the sensitive fibres, and transfers local stress from one fibre to another. Resinous matrix materials are generally ductile (sometimes, brittle) and viscoelastic, and sometimes viscoplastic. Typical properties of the common matrix are given in Table 1.2.

As discussed earlier, laminated fibre-reinforced composites typically have layers of laminae or plies stacked over one-another. For instance, graphite-epoxy prepreg unidirectional ply is such basic system. Thickness of a lamina is very small, typically 0.1 mm, and therefore cannot be directly used. Each lamina may actually be made from several distinct layers with each layer having the same orientation and properties. The laminae can be of various thickness and can consist of different materials. Various laminae (or plies), however, generally have different orientation of the principal material direction in a laminate. A typical laminate is shown in Fig 1.2. A laminate may have as many as 100 layers. Sometimes, as in woven lamina, the reinforcement may be provided in a single lamina in two mutually perpendicular directions. In the present case only unidirectional laminae are considered with reinforcement only in one direction. The layers of a laminate are usually bound together by the same matrix material that is used in the laminae. The structural properties of the composite laminae depends upon the individual properties of the constituent materials, i.e. the fibre and the matrix, fibre volume fraction, fibre orientation, fibre thickness, degree of fibre-matrix adhesion at the interface, void ratio, etc. The mechanical properties of popular commercial composites are given in Table 1.3. The laminates considered are unidirectional and a strong directional character can be seen clearly from the values. The material constants referred

Table 1.1

Typical Mechanical Properties of Common Fibres
Reproduced from Refs [2,3,5,6,7]

Fibre	Density	Young's Modulus	Specific Modulus	Tensile Elongation	Tensile Strength	Specific Strength
	Kg/m3	GPa	MNm/kg	%	MPa	MNm/kg
E Glass	2600	72	27.7	2.4	1720	0.66
S Glass	2500	87	34.8	2.9	2530	1.01
High Strength Graphite	1800	230	128	1.1	2480	1.38
High Modulus Graphite	1900	370	195	0.5	1790	0.94
IM-7 Hercules	1800	290	161		5170	2.87
Graphite T-50 UC	1670	393	235		2070	1.24
Kevlar 29	1440	83	57.6	2.8	2270	1.58
Kevlar 49	1440	124	86.1	1.8	2270	1.58
Boron-AVCO	2100-3000	365-414			3280-3660	
Silicon Carbide(SCS-2)	3050	400	131		4140	1.36
Alumina FP-2 Du Point	3700	380	102		1725	0.47
Tungsten	19300	414	21		4140	0.214
Cotton	1500	0.05			500-880	
Jute	1500	NA			460	
Sisal	1450	NA			850	

Table 1.2

Typical Mechanical Properties of Common Resins (at room temp)
Reproduced from Ref [2,6]

Resin	Type	Density Kg/m3	Tensile Modulus GPa	Tensile Strength MPa
Epoxy	Thermoset	1100-1400	2.1- 5.5	40 - 85
Polyester	Thermoset	1100-1400	1.3 - 4.1	40 - 85
Nylon	Thermoplastic	1100-1100	1.3 - 3.5	55 - 90
Polyester	Thermoplastic	1300-1400	2.1 - 2.8	55 - 60
PEEK	Thermoplastic	1300-1400	3.5 - 4.4	100 -120

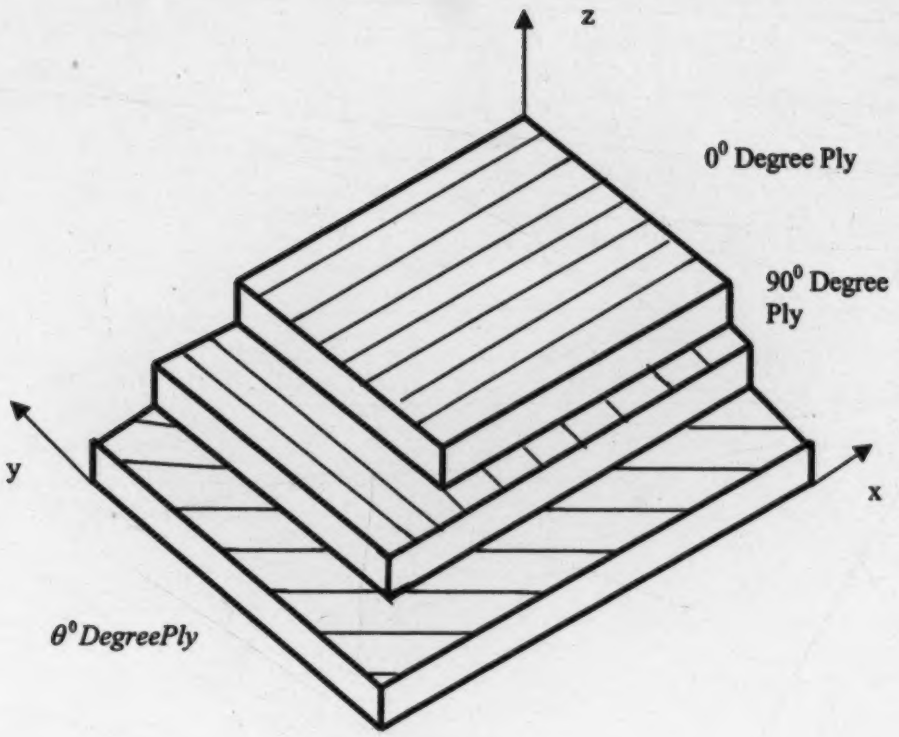

Fig 1.2 A typical multidirectional laminate with reference coordinate axes.

Table 1.3

Mechanical Properties of Popular Composites (fibre vol fraction= 0.6)
Reproduced from Refs [5,6,9]

Composite (unidirectional)	Longitudinal Modulus (E1) GPa	Transverse Modulus (E2) GPa	Shear Modulus (G12) GPa	Major Poisson's Ratio
E Galss/Epoxy	45	12	5.5	0.28
S Glass/Epoxy	55	16	7.6	0.28
Kevlar 49/ Epoxy	76	5.5	2.1	0.34
high str Graphite/ Epoxy	145	10	4.8	0.25
high Mod Graphite/Epoxy	220	6.9	4.8	0.25
Carbon /PEEK(vf=.58)	131	8.7	5	0.28
Boron /Aluminium(Vf=.5)	235	137	47	0.27
Boron /Epoxy (Vf=.5)	207	20	6.9	0.3

Table 1.4

Typical Mechanical Properties of Traditional Materials

Material	Density Kg/m3	Tensile Modulus GPa	Tensile Strength MPa
Mild Steel	7800	210	370-700
Aluminium	2800	70	450
Timber	500	1.0-10	74

in the table are the *engineering constants* and are explained in section 1.4, subsequently. For a comparison, the material properties of some conventional materials are given in Table 1.4.

The major purpose of lamination is to tailor the directional dependence of strength and stiffness of the laminae to match the loading environment of the structural component. The amount of fibre volume fraction alters the ratio of longitudinal to transverse strength in a lamina. Also, for most applications, the transverse properties of a unidirectional laminae would be unsatisfactory. But a multi-axial laminate may have an astonishing range of uses. In the laminate the fibre orientation drastically changes the directional mechanical properties of the composite. So the chosen fibre lay-up (stacking sequence) in a laminated structure can give a preferred 'controlled' anisotropy. The designer has a large flexibility, and the design can be suitably tailored and optimized [8]. Because of the directional laminae, the tensile, flexural, torsional, or shear properties of a composite structure can be dissociated from one another to some extent. A golf shaft for example, can be tailored in torsional stiffness without altering the flexural or tensile stiffness. However, these same lamination variables also influence the laminate failure modes in a way that differs fundamentally from the conventional materials.

For the composite materials (due to anisotropy, often orthotropy) there exists a coupling between normal and shear loading and deformation modes. For example, application of a normal stress leads not only to extension in the direction of the stress and contraction perpendicular to it, but also the shearing deformation. In addition, the behaviour of fibre-reinforced composite materials is complicated by the fact that they are, on a micro scale, inhomogeneous. So in addition to the strength and stiffness requirements, safeguard against local damage, to which composite materials are most susceptible, must be ensured in the design. In fact, laminate failure has been found to constitute a complex load-dependent processes, which can have a variety of geometry regulated material damage modes. Composites may have a variety of failure mechanisms: e.g. matrix cracking, fibre debonding (or pull-out), interlaminar cracking (delamination), or, microscopic defects. Any of these damage mechanisms may ultimately lead to the global structural failure.

To understand the physical behaviour of the composites many studies have been carried out in the past. To make the problem mathematically tractable some assumptions and idealizations are necessary. Basically two approaches are popular : firstly, the macro mechanics approach, where the material is presumed homogeneous and only average apparent properties of composite are considered; and secondly, the micro mechanics approach, where the interaction of the constituent materials of the composite is examined. Each of them has its distinct advantages and limitations.

1.4 MECHANICAL BEHAVIOUR OF LFRP COMPOSITES: MACROMECHANICS

The macro approach is concerned with the gross structural behaviour of the composite. The basic premise used is that the average material behaviour can be predicted from the properties of its constituents. This analysis considers the unidirectional lamina as quasi-homogeneous anisotropic material with its own average apparent stiffness and strength properties. It doesn't take into account the individual constituents i.e. the fibre, the matrix, and the interface in the analysis, and regards the lamina material as a whole. Though not very rigorous, this approach is quite elegant in its physical formulation of the composite laminate. The approach looks attractive, and also fruitful, as most applications of the composites are at macro scale size and the physical model can be easily visualized.

The macro analysis is based on classical continuum mechanics for elastic or elastic-plastic, orthotropic material. The macro analysis approach assumes material continuity at all phases in the laminate. The mechanical behaviour of the laminate can be analyzed from the *classical (thin) laminate theory*. Properties of the laminate are derived from the properties of the individual laminae i.e. the overall elastic or elastic-plastic response of the laminate is based on the interaction of the individual laminae in the laminate. The analysis assumes that the orthotropic mechanical properties of each individual lamina are already known, which are actually determined either from the experiments, or analytically by the micromechanics.

Individual laminae are the basic entities to arrive at the analysis of the laminated structure. Because of orthotropy the mechanical properties show a strong directional dependence. The stress-strain behaviour of a lamina is derived from the *generalized Hooke's Law* for the orthotropic materials. In the case of anisotropic materials, using the symmetry of the stiffness matrix, the stress-strain relations for a 3-dimensional analysis can be expressed from the general framework of linear elasticity:

$$\begin{Bmatrix} \sigma_{11} \\ \sigma_{22} \\ \sigma_{33} \\ \tau_{23} \\ \tau_{31} \\ \tau_{12} \end{Bmatrix} = \begin{bmatrix} c_{11} & c_{12} & c_{13} & c_{14} & c_{15} & c_{16} \\ c_{12} & c_{22} & c_{23} & c_{24} & c_{25} & c_{26} \\ c_{13} & c_{23} & c_{33} & c_{34} & c_{35} & c_{36} \\ c_{14} & c_{24} & c_{34} & c_{44} & c_{45} & c_{46} \\ c_{15} & c_{25} & c_{35} & c_{45} & c_{55} & c_{56} \\ c_{16} & c_{26} & c_{36} & c_{46} & c_{56} & c_{66} \end{bmatrix} \begin{Bmatrix} \varepsilon_{11} \\ \varepsilon_{22} \\ \varepsilon_{33} \\ \gamma_{23} \\ \gamma_{31} \\ \gamma_{12} \end{Bmatrix} \qquad 1.1$$

where σ_{11} , σ_{22} , σ_{33}; and $\varepsilon_{11}, \varepsilon_{22}, \varepsilon_{33}$; are the normal stresses and strains, respectively. Here, σ_{11}, σ_{22} , σ_{33}; and $\varepsilon_{11}, \varepsilon_{22}, \varepsilon_{33}$; are synonymous with $\sigma_{xx}, \sigma_{yy}, \sigma_{zz}$, and

$\varepsilon_{xx}, \varepsilon_{yy}, \varepsilon_{zz}$ respectively. And $\tau_{12}, \tau_{31}, \tau_{23}$; and $\gamma_{23}, \gamma_{31}, \gamma_{12}$, are shearing stresses and strains, respectively, synonymous with $\tau_{xy}, \tau_{zx}, \tau_{yz}$; and $\gamma_{yz}, \gamma_{zx}, \gamma_{xy}$ respectively.

The coefficients c_{ij} , i=1....6, j=1...6, are called the stiffness coefficients, or the elastic constants. For anisotropic materials there are no planes of symmetry for the material properties. If there are two planes of material property symmetry for a material, symmetry exists relative to the third mutually orthogonal plane also. These are termed the *orthotropic materials*. So the stress-strain relations for orthotropic materials in terms of coordinates aligned with the principal material directions can be expressed as:

$$\begin{Bmatrix} \sigma_{11} \\ \sigma_{22} \\ \sigma_{33} \\ \tau_{23} \\ \tau_{31} \\ \tau_{12} \end{Bmatrix} = \begin{bmatrix} c_{11} & c_{12} & c_{13} & 0 & 0 & 0 \\ c_{12} & c_{22} & c_{23} & 0 & 0 & 0 \\ c_{13} & c_{23} & c_{33} & 0 & 0 & 0 \\ 0 & 0 & 0 & c_{44} & 0 & 0 \\ 0 & 0 & 0 & 0 & c_{55} & 0 \\ 0 & 0 & 0 & 0 & 0 & c_{66} \end{bmatrix} \begin{Bmatrix} \varepsilon_{11} \\ \varepsilon_{22} \\ \varepsilon_{33} \\ \gamma_{23} \\ \gamma_{31} \\ \gamma_{12} \end{Bmatrix} \qquad 1.2$$

So we can see that for the orthotropic materials, there is no interaction between normal stresses σ_{11} , σ_{22} , σ_{33} and the shearing strains $\gamma_{23}, \gamma_{31}, \gamma_{12}$, as occurs in the anisotropic materials. Similarly there is no interaction between the shearing stress and the normal strains. In addition there is no interaction between shearing stresses and shearing strains in different planes. So there are only nine independent material constants.

In case of the isotropic materials there are infinite number of planes of material property symmetry, with only two material constants, namely, E and ν. For a unidirectional reinforced lamina, we have one plane (perpendicular to the fibre direction, say '1') in which the material properties are equal in all directions, and material is called the *transversely orthotropic*. It has five elastic constants, viz., c_{11}, c_{22}, c_{12} , c_{23}, c_{55}. For this case $c_{44} = (c_{22} - c_{23})/2$, and it is no longer an independent material constant. We refer '1' as the (major) principal material direction. The material properties are commonly referred in terms of the *engineering constants*: $E_{11}, E_{22}, G_{12}, \nu_{12}$, and ν_{23}. For a two-dimensional case only first four engineering constants are needed.

In most structural applications, composite materials are used in the form of thin laminates loaded in the plane of the laminate. Assuming all the stress components in the out-of-plane direction being zero, the stress-strain relations for a lamina are derived considering the plane stress condition for the composite lamina having orthotropic engineering constants. Let us consider a 2-dimensional problem with a lamina as shown in Fig 1. 3. The principal material axes of a lamina are, say, 1^{on} and 2^{on}, and the respective on-axis moduli of elasticity of the lamina are $E_{11}{}^{on}$, and $E_{22}{}^{on}$. Let the major and minor Poisson's ratios be $\nu_{12}{}^{on}$ and $\nu_{21}{}^{on}$. The *major Poisson's ratio* ν_{12} is defined as the ratio of strain in

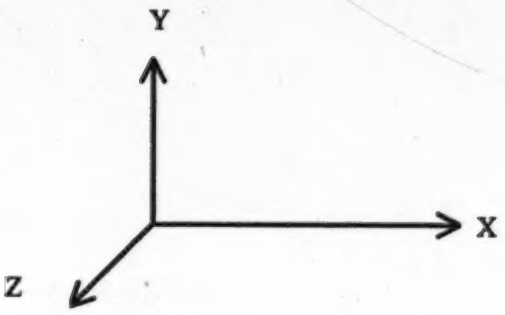

Global laminate axes.

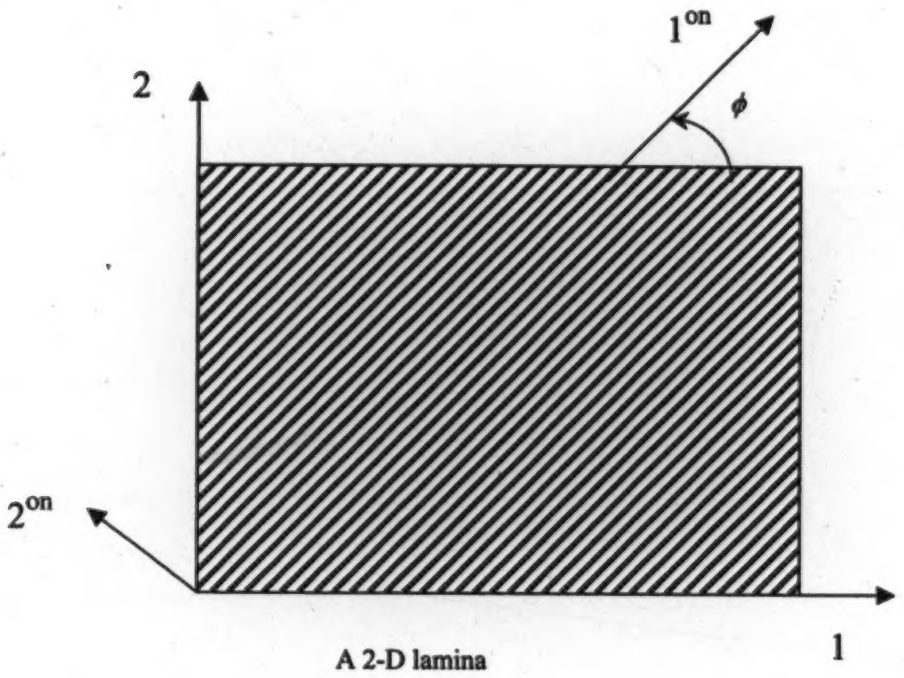

A 2-D lamina

Fig 1.3 Lamina Orientation in 2-D plane

direction '2' on account of stress being applied in the direction '1'. Similarly we can define the minor Poisson's ratio as the ratio of strain in direction '1' on account of stress being applied in the direction '2'. This is most common definition of the major and minor Poisson's ratio used by standard texts on composite materials [9]. The terminology used by ANSYS is, however, reverse of this. Here, we stick to standard terminology, and using the reciprocal relation:

$$\nu_{21}^{on} = (E_{22}^{on} / E_{11}^{on})\nu_{12}^{on} \qquad 1.3$$

If '3' is the direction normal to the plane of the laminate and if we denote $\sigma_1^{on} = \sigma_{11}^{on}$, $\sigma_2^{on} = \sigma_{22}^{on}$, $\sigma_3^{on} = \sigma_{33}^{on}$, $\sigma_4^{on} = \sigma_{23}^{on}$, $\sigma_5^{on} = \sigma_{13}^{on}$, $\sigma_6^{on} = \sigma_{12}^{on}$; and also $\varepsilon_1^{on} = \varepsilon_{11}^{on}$, $\varepsilon_2^{on} = \varepsilon_{22}^{on}$, $\varepsilon_3^{on} = \varepsilon_{33}^{on}$, $\varepsilon_4^{on} = \gamma_{23}^{on}$, $\varepsilon_5^{on} = \gamma_{13}^{on}$, $\varepsilon_6^{on} = \gamma_{12}^{on}$, corresponding to the lamina on-axis directions, the stress-strain relations for a 2D linear elastic case can be expressed as:

$$\begin{Bmatrix} \sigma_1^{on} \\ \sigma_2^{on} \\ \sigma_6^{on} \end{Bmatrix} = \begin{bmatrix} Q_{11}^{on} & Q_{12}^{on} & 0 \\ Q_{21}^{on} & Q_{22}^{on} & 0 \\ 0 & 0 & Q_{66}^{on} \end{bmatrix} \begin{Bmatrix} \varepsilon_1^{on} \\ \varepsilon_2^{on} \\ \varepsilon_6^{on} \end{Bmatrix} \qquad 1.4$$

where Q_{ij}^{on} denote the *on-axis elastic constants* for the single lamina computed as below:

$$Q_{11}^{on} = \varpi \, E_{11}{}^{on}$$
$$Q_{22}^{on} = \varpi \, E_{22}{}^{on}$$
$$Q_{12}^{on} = Q_{21}^{on} = \varpi \, E_{11}{}^{on} \nu_{21}^{on} = \varpi \, E_{22}{}^{on} \nu_{12}^{on}$$
$$Q_{66}^{on} = \frac{1}{G_{12}^{on}}$$

where $\varpi = (1 - \nu_{12}^{on}\nu_{21}^{on})^{-1}$

The off-axis elastic constants of a lamina can be obtained from the on-axis elastic constants and the fibre orientation angle (ϕ) i.e. the angle the major principal material axis makes with the global x-axis of the composite. This is shown in Fig 1.3.
Let $m = \cos(\phi)$, and $n = \sin(\phi)$ The off-axis elastic constants of a single lamina can be expressed as

$$\begin{Bmatrix} Q_{11} \\ Q_{22} \\ Q_{12} \\ Q_{66} \\ Q_{16} \\ Q_{26} \end{Bmatrix} = \begin{bmatrix} m^4 & n^4 & 2m^2n^2 & 4m^2n^2 \\ n^4 & m^4 & 2m^2n^2 & 4m^2n^2 \\ m^2n^2 & m^2n^2 & m^4+n^4 & -4m^2n^2 \\ m^2n^2 & m^2n^2 & -2m^2n^2 & (m^2-n^2)^2 \\ m^3n & -mn^3 & mn^3-m^3n & 2(mn^3-m^3n) \\ mn^3 & -m^3n & m^3n-mn^3 & 2(m^3n-mn^3) \end{bmatrix} \begin{Bmatrix} Q_{11}^{om} \\ Q_{22}^{om} \\ Q_{12}^{om} \\ Q_{66}^{om} \end{Bmatrix} \qquad 1.5 \quad \ldots$$

where, Q_{ij} are the off-axis elastic constants of the single laminate. It should be noted that it still has four material constants (five material constants in 3D), and shows (transversely) orthotropic character in principal material directions.

In a laminated plate to take care of the transverse shear deformations γ_{xz} and γ_{yz} the corresponding off-axis stress-strain relationships for transverse shear stresses τ_{xz} and τ_{yz} are given in terms of transverse shear elastic constants:

$$\begin{bmatrix} \tau_{xz} \\ \tau_{yz} \end{bmatrix} = \begin{bmatrix} Q_{44} & Q_{45} \\ Q_{45} & Q_{55} \end{bmatrix} \begin{Bmatrix} \gamma_{xz} \\ \gamma_{yz} \end{Bmatrix}$$

where,
$Q_{44} = G_{13}\ m^2 + G_{23}\ n^2$
$Q_{45} = (G_{13} - G_{23})\ m\ n$
$Q_{55} = G_{23}\ m^2 + G_{13}\ n^2$

The complete stress-strain relation for a general transversely orthrotopic plate of a lamina with arbitrary fibre orientation with respect to global axis is expressed as:

$$\begin{Bmatrix} \sigma_1 \\ \sigma_2 \\ \\ \sigma_4 \\ \sigma_5 \\ \sigma_6 \end{Bmatrix} = \begin{bmatrix} Q_{11} & Q_{12} & 0 & 0 & Q_{16} \\ Q_{12} & Q_{22} & 0 & 0 & Q_{26} \\ & & & & \\ 0 & 0 & Q_{44} & Q_{45} & 0 \\ 0 & 0 & Q_{45} & Q_{55} & 0 \\ Q_{16} & Q_{26} & 0 & 0 & Q_{66} \end{bmatrix} \begin{Bmatrix} \varepsilon_1 \\ \varepsilon_2 \\ \\ \varepsilon_4 \\ \varepsilon_5 \\ \varepsilon_6 \end{Bmatrix} \qquad 1.6$$

From the above, we see that in body coordinates, even an orthotropic material appears to be anisotropic. Such lamina is called *generally orthotropic*. A generally orthotropic lamina needs to be oriented at specific angle to have various stiffness in required directions to be zero.

For a given stacking sequence of the laminae in a laminate, finally, the compliances and stiffnesses can be derived as coefficients of the stress-strain relation for the laminate. Alternatively, the elastic constants for the laminate relating the force and moment resultant versus the strain field vector can be derived in form of *composite laminated shell(or plate) stiffness matrix*, which will have contribution from each lamina. The overall elastic constants of laminate are commonly expressed as summation over n-ply laminate [8]:

$$A_{ij} = \sum_{k=1}^{n} (Q_{ij})_k (z_k^{\,1} - z_{k-1}^{\,1}) \qquad i = 1, 2, 6 \qquad 1.7(a)$$

$$B_{ij} = \frac{1}{2} \sum_{k=1}^{n} (Q_{ij})_k (z_k^{\,2} - z_{k-1}^{\,2}) \qquad i = 1, 2, 6 \qquad 1.7(b)$$

$$D_{ij} = \frac{1}{3} \sum_{k=1}^{n} (Q_{ij})_k (z_k^{\,3} - z_{k-1}^{\,3}) \qquad i = 1, 2, 6 \qquad 1.7(c)$$

and $$S_{ij} = f \sum_{k=1}^{n} (Q_{ij})_k (z_k^{\,1} - z_{k-1}^{\,1}) \qquad i = 4, 5 \qquad 1.7(d)$$

where, z_k and z_{k-1} are the distances measured from the mid-surface of laminate to the bottom of the k^{th} and $(k-1)^{th}$ lamina, respectively. The parameter f denotes the shear correction factor [93]. Additional terms are required if the laminae have inelastic response.

1.5 MECHANICAL BEHAVIOUR OF LFRP COMPOSITES: MICROMECHANICS

The macro mechanical analysis of composite laminate describes the gross in-plane elastic behaviour in terms of four lamina properties $E_{11}, E_{22}, G_{12}, \nu_{12}$, but gives no information about stress/strain states in fibre, matrix or at the interface, which are the individual physical constituents of the lamina. And since most damage mechanisms initiate at fibre-matrix level, it is necessary to investigate stresses and deformations at micro scale. Micro scale analysis is immensely more challenging and, essentially, considers the lamina to be heterogeneous material, with distinct phases, viz. the matrix, the fibre, and the interface. Local failures in composites can be *matrix failure* (tensile, compressive, shear), *fibre failure* (tensile, buckling, splitting) and *fibre-matrix interface failure* (debonding), and *delamination*. These are described in section 1.6.3. Such analysis is particularly important in the study of fracture toughness, fatigue life, etc., which are strongly influenced by local characteristics and cannot be averaged.

The continuum mechanics analysis assumes that the matrix and the fibre are perfectly bonded together all the time, which is not true. In high performance structural composites, when one fibre breaks, there is no continuous loading path, and the load from one side of broken fibre is transferred to the matrix and subsequently to the other side of the broken fibre as well as to the adjacent fibres. The load transfer arises as result of the different physical properties of the fibre and the matrix e.g. different elasticity. *Micromechanics* investigation involves study of the matrix and the fibre-matrix interface in transmitting the loads to fibre in such heterogeneous medium. The load is transferred from the matrix by shear stresses along the edges of the fibre and by direct stress at the fibre ends. Matrix materials generally have higher ultimate fracture strain compared to the ultimate failure strain of the fibre. At the ultimate strength, as it carries only small proportion of load, and by the virtue of its lower elastic modulus, the matrix stays normally uncracked.

Fibre-matrix interface is a significant micro parameter and its role on the macro performance of composite is being increasing realized by the scientific community [10]. *Interface* relates to the bonding between the matrix and the fibre, and shows a coupling character i.e. mutual interaction between the individual constituents. The interface is an anisotropic transition region exhibiting a gradation of properties. Although small in size, it can play an important role in controlling the failure mechanisms, fracture toughness, and overall stress-strain behaviour of the composite. The interactions at the interface are rheological. At the atomic scale level, the surfaces are quite rough and give rise to irregularities in the geometry of the interface and this in turn can give rise to the stress concentrations along the fibre-matrix interfaces. Expression for the variation of shear stress, and the tensile stress along the fibre-matrix interface, and tensile stress in the fibre can be obtained by considering the equilibrium of the forces acting on the element of the fibre. Usually, the interface is the weakest link in the structural performance of the composite. It is interesting to note that, in case of chopped fibre end, or a matrix crack front reaching the fibre, a modified interface (treated with coupling and coating agents) will reduce the stress concentration in the region by spreading the high stress zone to a larger volume. The performance of the interface actually enhances, or limits the use of composites.

It was presumed that the four engineering constants $E_{11}, E_{22}, G_{12}, \nu_{12}$, required in macro mechanical analysis are already known, supposedly from the experimental characterization. In practice these properties vary a great deal for the same composition of the material, as constituent properties and geometric characteristics vary from batch to batch. Typical transverse cross-sections of unidirectional lamina are shown in Fig 1.4 [5]. It is clear that composites with low fibre volume ratio tend to have a random fibre distribution, whereas fibres in composites with high fibre volume ratio tend to nest in near hexagonal packing. Understandably, when the fibre volume fraction is high, orthotropic model is in close agreement with the experimental finding. There are various models available that allow a reliable prediction of average behaviour (primarily elastic modulii (or stiffness) and complementary, the strength) of the lamina as a function of the

constituent properties and local conditions. The constituent material properties have the following broad effect on the properties of the composite. Elastic modulus of fibre makes significant contribution to E_{11}. The Poisson's ratios of the fibre and matrix have no effect on E_{11}, and little effect on E_{22} and G_{12}. Elastic modulus of matrix makes significant contribution to E_{22} and G_{12}.

Various analysis approaches available, primarily rely on the definition of the *representative volume element*, or unit cell, which is supposed to replace the complex microstructure of the composite. It is the smallest region or piece of material over which

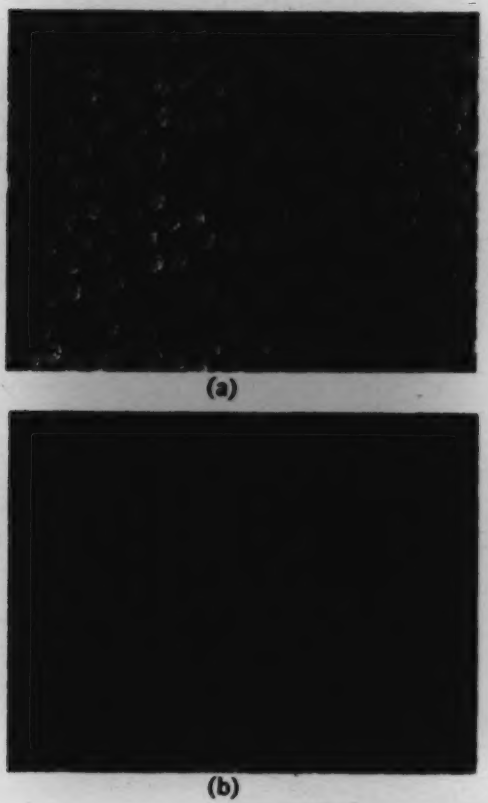

Fig 1.4 Typical transverse section of a unidirectional composite [5]: (a) Silicon Carbide / glass ceramic - ave. fibre dia. 15 μ, fibre volume ratio = 0.40, (b) Carbon / Epoxy – fibre dia. 8 μ, fibre volume ratio = 0.70.

the stresses and strains are macroscopically uniform. Microscopically, however, the stresses and strains are nonuniform owing to the heterogeneity of the material. Generally, only a single fibre appears in a representative volume element. In unidirectional lamina fibre spacing constitutes one dimension of the *representative volume element.* The other dimension is lamina thickness or fibre spacing in thickness direction. The mechanical properties of the composite depend upon the volume fraction of the fibres. All the approaches assume perfect bonding between the fibre and the matrix at the interface with no voids, and overestimate material properties for a degraded composite with imperfect bond. In addition, all micromechanical stiffness approaches make following assumptions: lamina is macroscopically homogeneous, and orthotropic, initially stress free (no residual stresses) and linearly elastic; matrix is homogeneous, isotropic, and linearly elastic; fibre is homogeneous, isotropic, linearly elastic, perfectly aligned, and regularly spaced.

The simplest micro approach is the mechanics of materials approach that assumes the continuity of the strains in the fibre direction at the interface. This implies equal strain for the matrix and the fibre, or *iso-strain* at the interface. Further, it implies that sections normal to the '1-direction' that were plane before stressing remain plane after stressing. This statement is employed in developing the theory for a beam, plate, or shell. The mechanics of materials approach does not consider the effect of fibre shape and its distribution, and generally, adequately predicts the longitudinal properties such as E_{11} and ν_{12}, but underestimates the transverse and shear properties, namely, E_{22} and G_{12}, respectively.

There is much controversy associated with micromechanical analyses [11]. In literature, there have been other popular approaches like self-contained field approach (a typical fibre embedded in a cylindrical matrix phase, which in turn is surrounded by infinite homogeneous medium with average orthotropic composite properties), variational methods based on energy principal (predicting upper and lower bounds of effective properties of composite), numerical methods (finite difference, finite element etc.), exact elastic solutions (Muskhelishvili's complex variable mapping for elastic inclusion in elastic matrix), and others. The predicted properties from micromechanical analysis need to match with the experimental findings. To account for realistic behaviour other variable such as fibre misalignment factor, and *contiguity factor* (no *contiguity* means isolated fibres) have been explored in the theoretical model, especially if the ratio of elastic moduli of fibre to matrix is high.

Semi-empirical relationships were employed by Halpin-Tsai to give an approximate representation of a more complicated micromechanics model [12]. A factor ξ was introduced as a measure of reinforcing efficiency (or load transfer), that basically relates to fibre geometry, packing geometry, and loading conditions. They gave the expression for $E_{11}, E_{22}, G_{12}, \nu_{12}$, that are in good agreement with experimental data.

1.6 FRACTURE STRENGTH OF LFRP COMPOSITES

It is known that the occurrence of crack-like flaws or imperfections in structures, though undesirable, cannot be eliminated completely. Cracks can be very costly. A US national committee had estimated that the costs on account of the fracture amounted to almost 4% of the Gross National Product [13]. The term 'failure' or 'strength' is basically used to specify the condition where the structure is unable to adequately perform its primary intended use. The global effect can range from simple loss of structural stiffness due to gross inelastic deformation (e.g. yielding), to a reduction in load carrying capacity due to localized deformation and damage growth, to complete loss of load-carrying capacity by gross macroscopic deformation and separation (fracture). So a fracture failure occurs when the material loses stiffness or strength. Clearly the strength will depend on the failure mode under consideration.

1.6.1 FRACTURE TOUGHNESS OF ISOTROPIC MATERIALS

For the fullest extent safe use of a material, fracture mechanics is being widely accepted as a mandatory requirement in the design of structures. For a homogeneous, isotopic material, like most metals, whose global behaviour is linearly elastic (or, conforms to small scale yielding, i.e. small plastic zone limiting to vicinity of crack tip), and provided that the cracks are detected, the safety of the structure can be assessed by the criterion of *linear elastic fracture mechanics*, using single parameter strength characterization.

Energy based approach is many times preferred over a stress based analysis. Griffith analyzed the crack stability in a body on the basis of global energy equilibrium. He proposed that on account of flaws, larger bodies generally exhibit smaller strengths, due to greater likelihood of bigger flaws. When flaws grow in a stressed body there is a decrease in the potential energy of the body, so energy released is available to form new surfaces of growing flaw. Griffith stated that for propagation to occur the energy released upon the crack growth should be sufficient to overcome all the surface energy of the material [14,15,16,17].

Under the equilibrium conditions,

$$\frac{dE}{dA} = \frac{d\pi}{dA} + \frac{dW_s}{dA} = 0 \qquad 1.8$$

where, dA is the incremental increase in crack surface area, E is the total energy, π is the potential energy supplied by internal strain energy and applied external forces, and W_s is the (dissipative) work required to create a new surface.

Irwin defined a term, called *energy release rate* by symbol G, to represent the energy available (loss of strain energy) for incremental crack extension. The crack may grow under a constant displacement or a constant loading configuration, however, the displacement control is more stable. It is the crack extension or crack-driving force and is given by:

$$G = -\frac{d\pi}{dA} = \frac{dW_s}{dA} \qquad 1.9$$

For example, for a crack in an infinite plate having Young's modulus E, with a flaw size 'a' subjected to a remote tensile stress σ , the energy release rate, for Mode I fracture is given by:

$$G = \frac{\pi.\sigma^2 a}{E} \qquad 1.10(a)$$

At fracture G = G_c, *the critical energy release rate* represents critical combinations of the failure stress σ_f and crack size a_c:

$$G_c = \frac{\pi.\sigma_f^{\ 2} a_c}{E} \qquad 1.10(b)$$

The *critical energy release rate,* G_c is a measure of *fracture toughness* of the material. As one of the fundamental assumptions of fracture mechanics, fracture toughness G_c is a material property, independent of the geometry of the cracked body. It is recognized as a relevant strength parameter for characterization of materials that are homogeneous and isotropic at macroscopic scale. Nonetheless, of all material properties, toughness is perhaps the least readily defined and yet the most critical in terms of confidence in a structural component. Fracture Toughness is referred to as the energy per unit area necessary to give a new crack surface. Sometimes, alternatively (fracture) surface energy per unit area is used a material property.

There are three kinematically admissible crack extension modes, namely Mode I or opening mode, where crack surfaces directly move apart; Mode II or in-plane (or forward) shear, or sliding mode, where crack surfaces slide over each other in crack plane perpendicular to the leading edge of the crack; and Mode III or the out-of-plane (or parallel) shear mode, or tearing mode, where crack surfaces move relative to one another in crack plane parallel to the leading edge of the crack. These are shown in Fig 1.5. Technically, Mode I is the most important. Generally, fracture toughness values for Mode I, Mode II, and Mode III loading are independent of each other. The superposition of these three modes is sufficient to describe the most general case of crack surface displacement.

The prediction of strength implies that processes have caused significant microscopic changes in the material behaviour and geometry, e.g. yielding, damage formation, and crack growth. The fracture process generally has three stages in homogeneous materials;

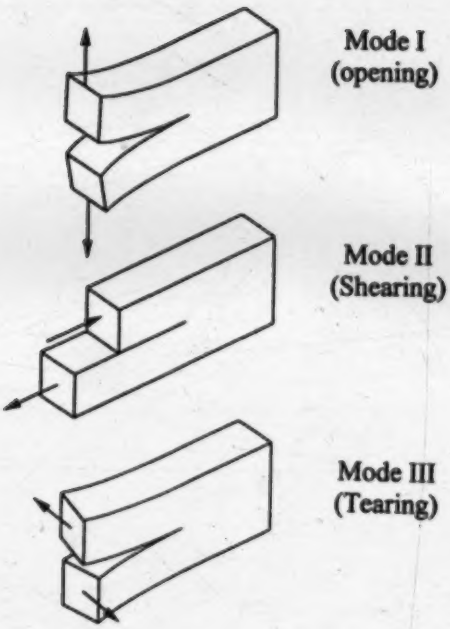

Fig 1.5 Basic Delamination Modes in composite materials

first, initiation of a microcrack (or initial crack-like flaw), second, microcrack grows in stable fashion and coalescence with other microcracks to form a macrocrack, and thirdly, propagation of the macrocrack in unstable fashion at critical stress level. Stage two is not found in brittle materials that have abrupt failure with unstable crack propagation generally below their yield strength. They have small crack-tip deformation and lower fracture toughness. Ductile materials have large crack-tip (plastic) deformation, higher fracture toughness and may have significantly different fracture initiation and fracture failure energies. Linear elastic fracture mechanics is applicable strictly to the materials undergoing a brittle fracture.

1.6.2 FAILURE AND FRACTURE TOUGHNESS ISSUES FOR COMPOSITES

In a laminate consisting of a number of plies of various orientations, the plies provide mutual restraint against Poisson's deformations and provide interlaminar shearing stresses as well as normal stresses in the thickness direction. The crack initiation may take place early in the loading period, and the layer that fails first initiates the so-called *first ply failure*. Under static tensile loading above 0.4% strain the first-ply-failure (mostly transverse cracks in laminate plies perpendicular to the loading direction) can occur. This is despite the fact that the matrix system has failure strain of about 2%. Incidentally, 0.4% is also the max allowable strain in most aircraft components. In most designs, due to overriding safety considerations only a small part of strength potential of laminate is used.

Composite materials on account of their high matrix ductility and fibre-structure have astonishingly high resistance to crack propagation. Generally the fibres have many times higher strength but are brittle, and the matrix is viscoleastic and ductile. Typically, the toughness of the composite is more than both the matrix and the fibre. It is attributed to the extra energy needed for fibre-matrix debonding and the pullout involving the redistribution of the stress and also the creation of a new surface. The properties of matrix supply only a certain portion of the fracture energy of the composite. Normally in a composite having brittle fibre in a brittle resin, the toughness will increase as the volume fraction of the fibre is increased, where as if the matrix is ductile, the toughness will decrease as the volume fraction of the fibre is increased. However, for a more ductile matrix, by increasing the plastic zone size (or, nonlinear viscoelastic zone) ahead of the crack tip, giving greater load redistribution away from the crack tip and more crack-tip blunting, the delamination fracture toughness can be increased [18].

To analyze the failure of composites associated with a certain range of stress, material properties, etc., some '*lamina based*' (macro) approaches are sometimes applied. Primarily, there are two lamina-based approaches. Namely, the non-interactive failure criteria- where *maximum stress criterion and maximum strain criterion* hold; and the stress interactive criteria- which has the *Tsai-Hill and Tsai-Wu tensor criteria* [5,9] giving the most general failure envelope for each ply. The failure envelope can be

generalized to arbitrary cross-plied laminate. Within the framework of such single failure formulae, various orthotropic strength constants are involved, that ultimately depend upon the constituents of the composite i.e. the fibre and the matrix.

However, the notion to attempt failure by a lamina based approach as if it were a homogeneous material, discarding micro damage modes, is a physically unrealistic oversimplification. A global failure criteria based solely on the assumption of uniform stresses in entire homogenized lamina, may give conservative prediction of matrix crcaking. In order to allow greater permissible strains in a structure and have greater weight savings, micro mechanisms need to be considered in the failure analysis of the composite. In addition, the use of a homogenized lamina automatically excludes the possibility of any thermal stress accounting within a lamina. This is because the resin matrix typically has relatively high coefficient of thermal expansion than the fibre, and in reality is prevented to shrink by the fibres during cool-down. As another limitation, the analysis based on assumption of homogeneity has large discrepancies with experimental results when there is significant separation of material phases in the composite because it cannot account for the extra energy necessary to create the free surfaces resulting from the fibre-matrix debonding in the composite. Significantly, the edge effects always call attention to micro-damage modes. While continuum laws may provide the answer to specific problems, they cannot be used in predicting the materials failure response which involves various damage modes [19].

The fracture mechanics of laminated structures has received unprecedented attention in the past two decades. The approaches that mimic the applications of linear elastic fracture mechanics are not adequate to study the composites. Metal failure at micro scale involves only one mode, initiation and propagation of a single crack. In contrast, toughness characterization in composites involves various modes. This is because unlike conventional isotropic materials, where the largest single crack with propagation in *self-similar* fashion controls the strength in terms of plain strain fracture toughness, crack growth in composites is not in a self-similar fashion in general. Self-similarity is observed when relative geometry of the loading and the notched composite stays the same with the crack growth. The composites due to their complex microstructure exhibit orthotrophy and non-homogeneity. Their toughness depends upon the crack propagation path, in addition to the fracture properties (strength and ductility) of the constituents and the geometrical arrangement of fibres. In characterizing the fracture strength of composites, there need be a separate failure criteria for the fibre, the matrix, and possibly the interface. Further, all the modes of failure need be considered if any ingredient can fail in more than one mode. All the micro-damage mechanisms that exist in a composite consume fracture energy and contribute to the fracture toughness. Hence no single material property can be identified to quantify the fracture resistance of cracked laminated fibre reinforced composites. The term toughness is used only for specific damage mode, such as delamination, and does not relate to the overall load carrying capacity of the composites.

1.6.3 MICRO-DAMAGE MODES IN FRACTURE MECHANICS OF COMPOSITES

Basically fracture mechanics is a macro theory. Initially, the application of fracture mechanics to composite materials was limited due to the suspicion on account of their distinctive characteristics such as anisotropy and non-homogeneity. Starting from a linear elastic behaviour, fracture mechanics has progressively included ductile materials, nonlinear behaviour, viscoelasticity, orthotropic materials, heterogeneous materials, and more recently damage mechanisms. Currently, there are two broad approaches out of the general framework of conventional linear elastic fracture mechanics for applicability to composite materials; macromechanical, and micromechanical. The essential difference between the two is the homogeneity/ non-homogeneity of the lamina.

Composite failure results from accumulation of complex fracture processes. It is widely accepted that local physical micro level damage events (which depend upon local physical micro level parameters like fibre diameter, fibre spacing, fibre ductility, strength, interface bonding etc.) significantly influence macro performance of composites. Depending upon the material properties, laminate stacking sequence, environment, the failure can be preceded by a global ensemble of discrete interacting damage modes. It is interesting to see how the fracture toughness and fracture energy of fibre composites can be examined on the basis of micro-damage mechanisms. The micro level damage modes include:

1. *Fibre fracture.*
2. *Fibre-matrix debonding* (and pull-out, if the matrix is brittle)
3. *Intralaminar matrix cracking*- Initiation, multiplication (not propagation) of transverse, longitudinal cracks.
4. *Delamination* (inter-ply separation), unique to laminated composites and initiated preferentially at specimen edge.

As observed earlier, a macro analysis assumes a uniform stress over entire homogeneous lamina, and is utterly unrealistic, for a generally orthotropic composite with arbitrarily positioned crack. In an orthotropic material, the direction of crack propagation may not be known even though applied load is normal to the crack and linear elastic fracture mechanics is hardly applicable in such case. However, if self similarity is observed, an appropriate (macro) fracture mechanics criterion can be applied for some composite damage cases containing a flaw of known length, by idealizing the composite as a homogeneous material with averaged linear elastic orthotropic properties. Self-similarity can be invoked if applied loads and material properties are aligned symmetrically with reference to a crack such that it runs straight [20,21,22].

Qualitatively similar failure mechanisms are always applicable. Composite materials can suffer any of the modes of above failure modes of its constituents, together with a few arising from their combination. The relative amount of each of these failure modes can vary from ply to ply as a result of different fibre orientations and loading conditions.

Essentially many damage modes interact making them coupled. The various damage modes are examined as below in sections 1.6.3.1 to 1.6.3.4

1.6.3.1 Fibre Fracture

It can be said that a longer fibre has a higher probability of individual fibre breakage below average fibre strength on account of defects given by the Weibull distribution. After a single fibre break, more fibre breakage plus debonding and separation of the fibre and matrix will result.

In advanced composites such as carbon-epoxy, the longitudinal stresses in the fibres are almost directly proportional to the corresponding stress in the lamina. Such condition is valid if the laminate is well-designed where only the fibre-dominated fracture is meaningful; and matrix dominated failure is considered premature and an inferior design, as the maximum strength potential of the expensive fibres is not utilized. Omitting considerations for matrix failures, this permits reliable use of failure theory much simpler than conventional micromechanics with no loss of accuracy [23]. Such theory is basically an orthotropic adaptation of classical maximum-shear-stress (Tresca) yield criteria for ductile isotropic materials. It must be emphasized that although such analysis may seem to be a macro analysis, it is actually not. So the final failure of a composite is by nature associated with fibre fracture.

1.6.3.2 Fibre-Matrix Debonding

The fibre-matrix interface bond is a very important factor controlling the resistance to the crack propagation. With good interface bond, the material requires higher plastic deformation and higher fracture energy absorption. Debonding needs to be considered if failure is initiated from the matrix. This will however require a micro analysis approach [24,25]. For example, value of G_c can be deduced for debonding and pullout of fibre from the matrix. Normally, smaller the diameter of the fibre, better is the resistance to fibre-pullout.

1.6.3.3 Intralaminar Matrix Cracking

The awareness of matrix cracking in composite laminates was originally raised by O'Brien [26]. Matrix stresses, are very definitely not proportional to applied mechanical loads, and need to be analyzed at discrete constituent level. Matrix-dominated failure, when encountered, requires comprehensive micromechanics analysis, in general. Matrix fracture can be shear or tensile. A matrix crack is a crack that either propagates in the matrix phase of the material or is wandering through fibre-matrix interfaces. Its physical size is large enough to be identifiable on a

macroscale, although it is usually prevented from reaching a catastrophic dimension. G_c can be found for inelastic deformation and fracture of matrix material. Due to the laminate internal fibre and layer structure crack gets arrested before it can grow. Hence, during a given loading, matrix cracks can be developed in the laminate, whose distribution pattern is almost always regulated by the reinforcement structure. With the increased loading, however, either an unstable coalescence of matrix cracks occurs, or a fibre- breakage in the major load-carrying plies is precipitated. Matrix cracks can be classified as intralaminar and translaminar.

Under monotonic tensile or transverse impact loading, in the continuous fibre-reinforced laminates containing 90° degree plies, the general sequence of damage accumulation begins with *transverse cracks* in 90° degree plies near the *free edge* [27]. They grow in the thickness direction. However, intralaminar matrix cracks are caused, normally, by the in-plane stresses in a lamina. Formation of longitudinal cracks in cross-ply laminates occurs when the transverse tensile strain in 0° degree plies exceeds transverse fracture strain of a unidirectional laminate. Their size in the thickness direction is limited to the thickness of such ply. These longitudinal cracks are said to be in the so-called *L-orientation* configuration as shown in Fig 1.6(a), and their resistance to crack propagation is minimal. Fracture mechanics approach seems to be applicable by assuming a cracked isotropic layer sandwiched between two anisotropic solids.

Alternatively, a crack can run transverse to the fibre orientation as shown in Fig 1.6(b). This is called T-orientation. At some distance ahead of the crack, fibres are intact. In high stress region near the crack-tip, the fibres are broken. Immediately behind the crack-tip the fibres undergo *pull-out* and absorb energy if the shear stresses at interface are maintained (i.e. in the absence of debonding). In a ductile matrix, the fibres are generally bonded to the matrix. Alternatively, it is possible for a fibre to be left intact as the crack propagates by *fibre-bridging*. Such micro cracks occur at multiple matrix sites. These cracks can grow easily as translaminar into adjacent 0° degree plies. High crack resistance is obtained in T-orientation. However, the application of fracture mechanics concepts is not very effective, unless fibre and matrix fail simultaneously along smooth plane normal to the applied load.

1.6.3.4 Delamination

Delamination cracking is mainly due to the interlaminar stresses associated with the interactions of the various laminating plies. These stresses tend to intensify near localities where there is a abrupt change in material or geometry. Unlike the bulk behaviour of laminate where reinforcement takes most of the load, free boundaries are susceptible to initiation of various types of damage [27]. Near the free edge of a specimen, the loads are transmitted from ply to ply by matrix shear, or normal stress in the thickness direction. There are, therefore, high interlaminar shear stresses and peel stresses at the edge, which can cause delamination. A typical delamination crack

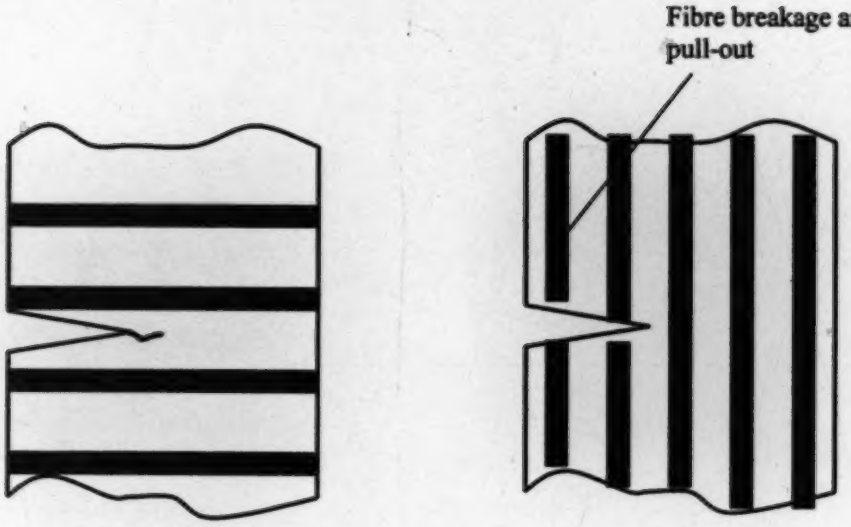

(a) L-orientation cracks

(b) T-orientation cracks

Fig 1.6 Intralaminar Matrix Cracks

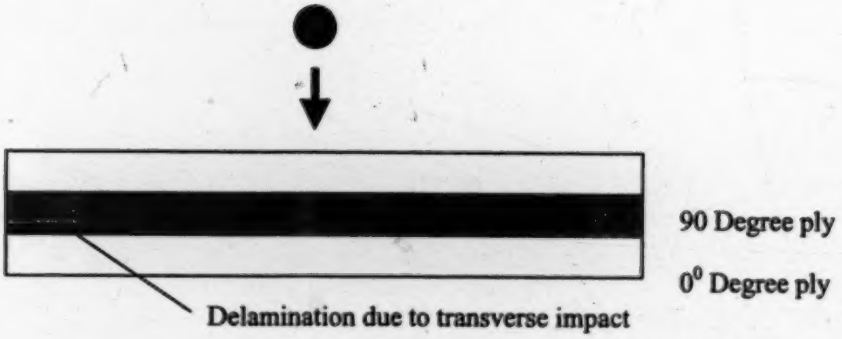

Fig. 1.7 Delamination crack in a cross ply laminate

is shown in Fig 1.7 The circumstances under which delamination precedes the failure of fibres can arise from local manufacturing defects, free edge effects, surface impacts, and compressive loads parallel to the laminate axis. This is discussed in detail in sections 2.1 to 2.5.

Principal mechanisms during interlaminar fracture are: fibre breakage, crack bridging by fibre, formation of side cracks, plastic deformation and microcrcaking of the matrix. The resistance to interlaminar crack growth can be expressed as the Mode I delamination fracture toughness, G_{Ic} or the Mode II delamination fracture toughness, G_{IIc}. The major contribution to energy absorption comes from the deformation and fracture of the polymer matrix between the fibres, and the minor but an important effect can be attributed to the fibre fracture. Bond quality also plays a significant role. The transition condition from an assumed flaw to a delamination is provided by a criterion from the theory of brittle fracture. Since the size and location of the flaw are known, crack-tip strain energy release rate, or crack driving force, can be calculated based on ply elasticity and method of fracture mechanics as crack propagation is self-similar.

1.6.4 MICRO FRACTURE ANALYSIS OF LFRP COMPOSITES

In micro approach, the material is essentially heterogeneous and failure analysis is based on behaviour of individual lamina layers and interface between them. Although the observations can be made on (micro) failure mechanisms, constructing a quantitative theory accounting various damage modes in fracture process relating to the useful macroscopic variables will be extremely cumbersome [28]. In addition the usefulness of such micromechanical theory is questionable in light of the numerous material input parameters it is supposed to account for [23].

Consequently, micromechanics should never be the preferred method to calculate the strength of fibre-dominated laminates, unless absolutely necessary. In most cases a relatively simple failure theory gives better results, as in fibre-dominated composites. Many authors have tried to bridge the gap between micromechanics and desired laminate level strength prediction. [29]. Such trade-off between micromechanical failure analysis and macromechanical failure analysis can yield interesting practical predictions. This can be achieved by merging a micro failure analysis with macro analysis [30]. The approach treats the material as heterogeneous at and near the crack site where required; and homogeneous when it is practically away from the damage zone. The growth of the flaw in a stable manner under increasing load up to a catastrophic failure can thus be determined from structural configuration and the applied loads.

1.7 OVERVIEW OF THE PRESENT STUDY

The present work deals with the study of mechanical behaviour of fibre-reinforced polymeric composite materials. On account of micro-defects, and other causes the polymer composites are susceptible to delamination failure. Delamination is considered as the most important damage mode in LFRP composites. Hence, the main issue to be addressed in evaluating the mechanical properties of composites is the delamination resistance, characterized by the interlaminar fracture toughness. The focus of the study is on the characterization and standardization of delamination fracture toughness of LFRP composites as a material property.

In the present chapter, we have dealt with various aspects pertaining to the analysis of the mechanical behaviour (stiffness and strength) of the LFRP composites. Chapter 2 aims to explain the causes and mechanics of delamination onset under various situations in terms of the interlaminar stresses in a laminate. Finally, effort is made to explain various aspects regarding characterization of delamination resistance and the current hurdles which prevent the characterization of Mode II toughness in chapter 3. Various test methods used to measure the interlaminmar fracture toughness are based on the assumptions of linear elastic fracture mechanics and small deformations. For the Mode I test, the Double Cantilever Beam (DCB) specimen is widely used and the ASTM test standards for the DCB specimen are already available. For mode II the End-Notched Flexure (ENF) specimen is widely popular, but ASTM standard is yet to evolve. The test configurations of the DCB and the ENF specimens and methods of data analysis are examined in detail. Beam theory analysis with and without the effect of shear deformation for the DCB and ENF specimens is also attempted in this chapter. Other necessary correction parameters to be included in the beam theory solutions are also examined. Suitable expressions for the delamination fracture toughness in Mode I and Mode II are derived from theories prevalent in the literature.

In the chapter 4, a finite element analysis is conducted on the two–dimensional linear elastic models of the DCB and ENF specimens. The focus of the finite element study is to investigate the specimen thickness effects on the Mode I and Mode II interlaminar fracture toughness. For this purpose the stress fields at the corner of the crack tip and at the interface are analyzed for specimens of various thicknesses under appropriate loading conditions. For the DCB specimen model the max principal stress field is considered. However, for ENF model the max principal stress, shear stress τ_{xz}, normal stress σ_x, normal stress σ_z, and the von Misses stress are considered as discussed subsequently.

The conclusions are laid in chapter 5. The interlaminar fracture toughness for the Mode I and the Mode II fracture is believed to be an important property for design with composites. It should be determined precisely to expand the confident use of polymer composites for primary load bearing applications. To correctly measure the interlaminar fracture toughness the test methods need to be standardized. Geometry independence of

the test results is the first step leading the standardization of a method. Particularly, for ENF specimen, there has been considerable controversy on the reliability and reproducibility of the test results, and a consensus on the test method is yet to emerge.

Such standardization may lead to a more fundamental understanding of the mechanical behaviour of the composites. And only in this way can reliable estimates of the failure loads expected in service be made using strengths determined in small-scale laboratory tests.

Chapter 2

DELAMINATION OF COMPOSITE MATERIALS

2.1 INTRODUCTION

Superior specific strength and stiffness coupled with a designer's ability to selectively reinforce critical load paths have made composite materials ideal for weight saving structures. In a wide range of high performance primary load bearing civil, marine, automotive, and aerospace applications, laminated composites are increasingly being used. However their mechanical behaviour is not fully understood, and they are susceptible to various failure modes. For the last 20 years, the unprecedented attention to the failure analysis of laminated composite materials has singled-out delamination as the weakest failure mode for the composites. Delamination is considered as the most prevalent life-limiting growth mode in composite structures with regards to their durability and damage tolerance. Resistance to delamination has thus become synonymous with "toughness"[31]. This, however, doesn't undermine the fact that interlaminar fracture toughness of composites does not have the same significance to design as fracture toughness does for metals.

Laminated composites have excellent in-plane properties, but are weak when subjected to out-of-plane stresses (τ_{xz}, τ_{yz}, and σ_{z}). They are susceptible to delamination damage during manufacturing or service on account of two-dimensional fibre structure of the material with lack of reinforcement in the thickness direction. The occurrence of delamination can be attributed to the low tensile strength of the matrix in the resin rich interlaminar region. A crack can form and propagate in the interface of the laminating plies and such plane crack is commonly called a delamination crack. A delamination crack may grow leading to redistribution of the stresses in the plies of the laminate.

Delaminations are of special interest because they take place underneath the surface of a laminated structure. Although delaminations may not be easily detected, they can lead to enormous reduction in strength and stiffness of the structural component. It is observed that tensile behaviour of the laminate may not be significantly affected, but the compressive behaviour may be critical [32]. It may cause localized buckling and high

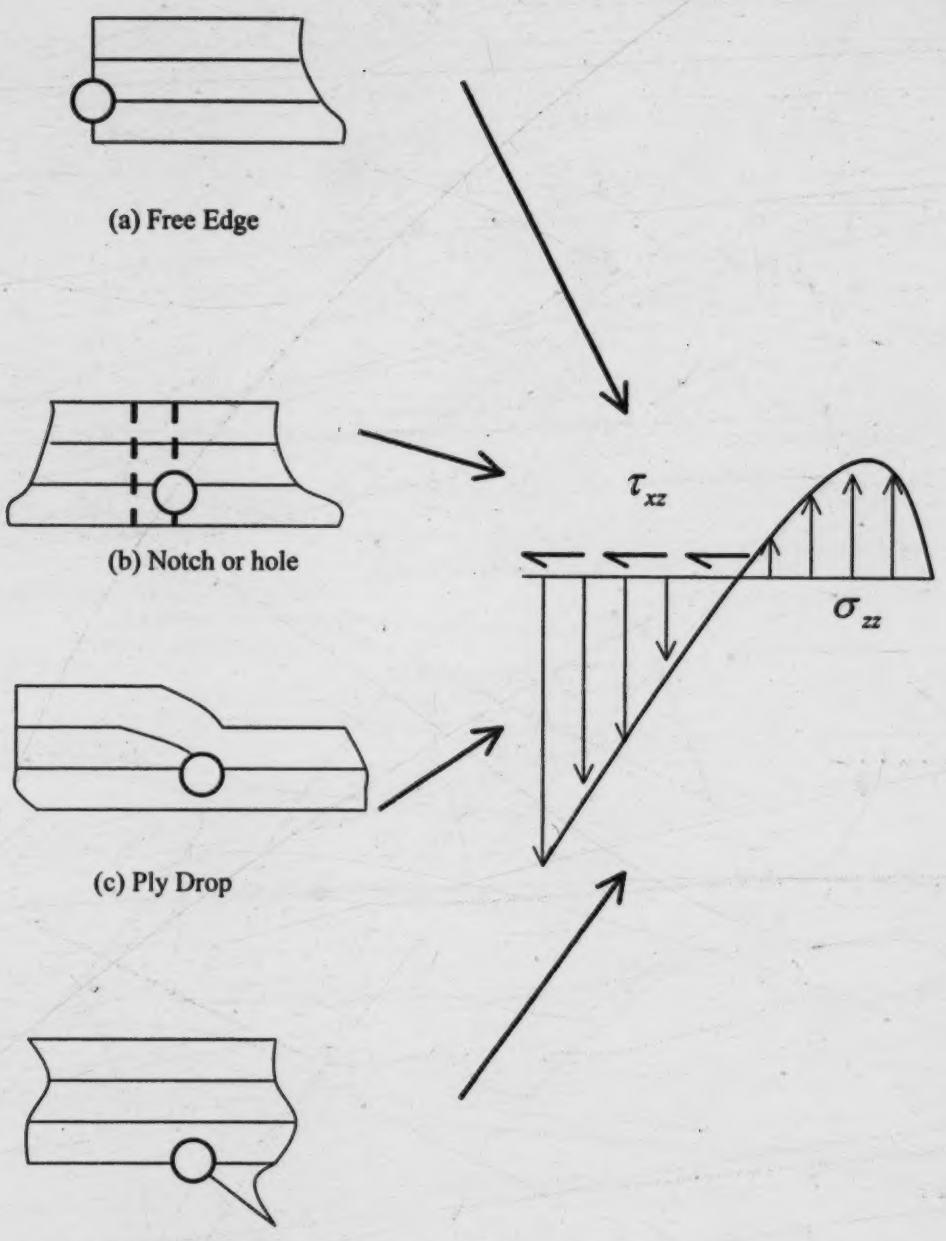

Fig 2.1 Common Delamination Sites and Interlaminar Stresses.

interlaminar shear and normal stresses at the edges of the buckled regions, and, hence delamination may be considered as a subcritical failure mode. So delamination may be indirectly responsible for the failure of composite.

2.2 MECHANICS OF DELAMINATION: THE INTERLAMINAR STRESSES

Delamination, or interlaminar cracking is mainly due to the interlaminar stresses associated with the interactions of the various laminating plies. It may be noted that the classical laminate theory assumes a plane stress state involving σ_{xx}, σ_{yy}, and τ_{xy} which is valid for thin elements. But due to the different orthotropy of each ply, the interlaminar stresses (τ_{xz}, τ_{yz}, and σ_{zz}) exist [33,34,38]. The fundamental reason for the presence of interlaminar stresses is the existence of a mismatch in engineering properties between the layers. Hence, the interlaminar stress analysis is a 3-dimensional problem. With reference to width effects, a two-dimensional plane strain analysis gives a conservative value and is normally employed. The mechanisms of delamination initiation are regulated by the lamination variables (ply stacking sequence, ply fibre orientation, etc.) as well as the geometrical discontinuities i.e. the flaws, free edge. In this sense multiple delaminations can occur throughout the laminate, forming a pattern of localized damages.

Delamination may occur at a variety of sites that result in eccentricities/discontinuities in loading path [35]. The favoured delamination sites include stress concentrations at holes, free edges or discontinuities, ply termination or ply drop sites for thickness tapering, or manufacturing flaws. It may also be caused by transverse concentrated loading such as low velocity impact or even static tensile loading for some lay-ups. These effects are shown in Fig 2.1. In all these cases the remote loading may be out-of plane or in-plane, but significantly the local effect is an out-of-plane load, causing interlaminar shear and normal stresses. Important cases for the analysis of interlaminar stresses are discussed below.

2.2.1 FREE EDGE DELAMINATION

Free edge delamination has been the most widely studied damage mode by far [35,36]. The interlaminar stresses tend to intensify near the localities where there is abrupt change in geometry or in material. In the neighbourhood of free edge under in-plane loading, the interlaminar stresses are highly localized, and free edge delamination may occur. It is fruitful to understand the analysis of interlaminar stresses at the free edge.

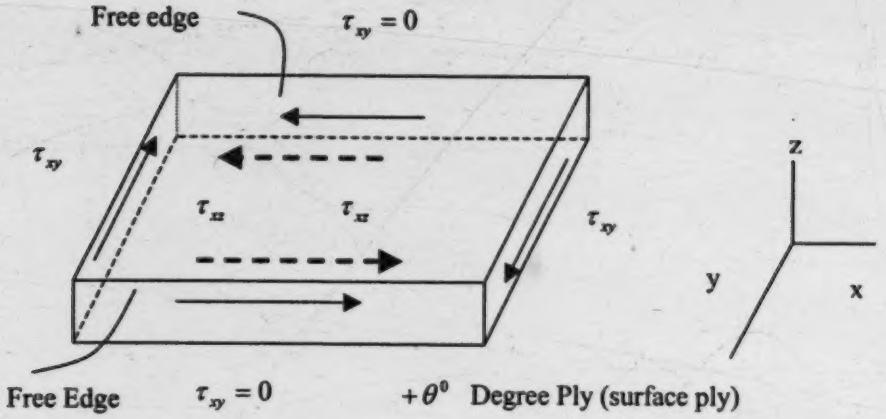

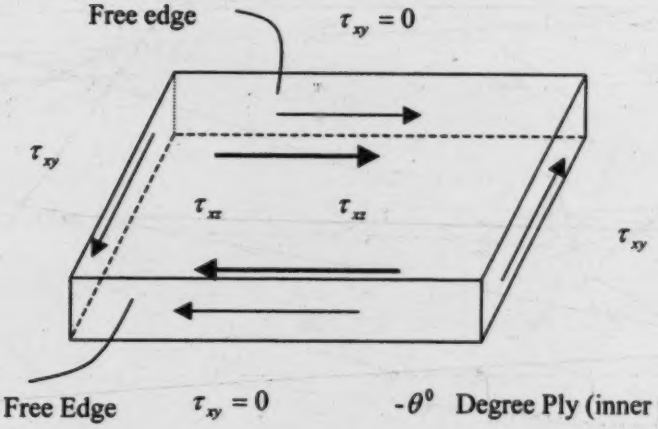

Mid –Plane of Laminate

Fig 2.2 Mechanism of set up of interlaminar shear stress τ_{xz} – $in(\theta/-\theta)_n$ laminate loaded in x-direction

Consider an angle ply laminate. Two top half plies of the four ply-laminate are considered as in the Fig 2.2. A slice of the laminate cut in the x-direction is shown. The laminate is loaded in x-direction. So we have,

$$\sigma_{xx}(+\theta^\circ) = \sigma_{xx}(-\theta^\circ) = nonzero$$
$$\sigma_{yy}(+\theta^\circ) = \sigma_{yy}(-\theta^\circ) = 0$$
$$\tau_{xy}(+\theta^0) = +ve, \quad \tau_{xy}(-\theta^0) = -ve,$$

Hence, the shear stresses τ_{xy} on the faces of the y-z plane are non-zero. The direction of these stresses in $+\theta^\circ$, and the $-\theta^\circ$ plies are opposite. However, the complementary shear stresses on the faces of x-z plane are zero as it is the free edge. This is in contradiction to the laminate analysis. So additional stress system must be introduced to counterbalance the moment due to shear stresses τ_{xy}. This can be achieved by the interlaminar shear stress τ_{xz}. Again as τ_{xz} cannot act on top surface being free surface, it acts only on the bottom surface of the $+\theta^\circ$ ply. Interlaminar shear stress τ_{xz} will be non-zero in a small region from both the free edges to some interior distance of the laminate in the y-direction. This interlaminar stress τ_{xz} is effective within a distance of approximately one laminate thickness away from the free edge. This region is called a *boundary layer*. The laminate analysis is valid in the inner region outside the boundary layer. So near the free edges, 3-dimensional analysis is necessary and confirms the presence of the interlaminar shear stress τ_{xz}.

Next consider a cross-ply laminate consisting of four plies. The laminated is again loaded in x-direction. Again we consider only two top half plies, as shown in Fig 2.3. We have,

$$\sigma_{xx}(0^\circ) = \sigma_{xx}(90^\circ) = nonzero$$
$$\tau_{xy}(0^\circ) = \tau_{xy}(90^\circ) = 0$$
$$\sigma_{yy}(0^\circ) = +ve, \sigma_{yy}(90^\circ) = -ve,$$

The shear stress τ_{xy} is zero as there is no external shear load in the x-y plane. At the free edges the normal stress σ_{yy} has to be zero in contradiction with the prediction of laminate theory. Hence, again, additional stress system should be introduced which can balance the forces, and, this is the interlaminar shear stress τ_{yz}. This will act on the bottom face of the 0° degree ply, as top surface is load free. This nonzero stress will be effective in the boundary layer region again. Similarly we have τ_{yz} in the top face of the 90° degree ply. Focusing the attention back to the top ply, we see that in the boundary layer region the τ_{yz} stress on the bottom face, replaces the direct stresses σ_{yy}. But these two stress systems are not collinear, as shown in fig 2.4. The unbalanced moment at the

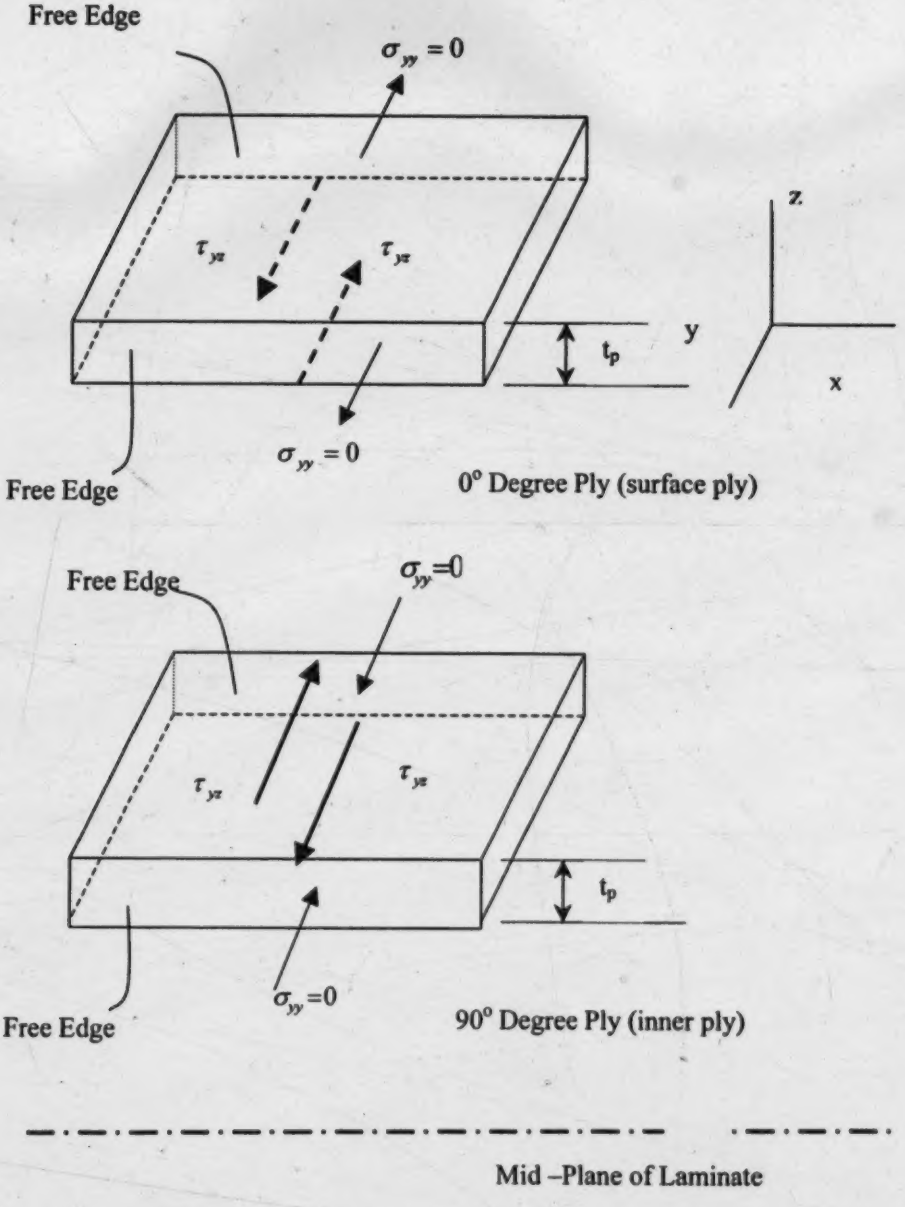

Fig. 2.3 Mechanism for set up of interlaminar shear stress τ_{yz} in $(0/90)_n$ laminate loaded in the x-direction

interface can be put in equilibrium by another stress system with introduction of direct stresses σ_{zz}. Their distribution gives net zero resultant force but a nonzero couple. These again act in the vicinity of the free edge in the boundary layer region. In the inner region where laminate analysis is valid both these interlaminar stresses vanish. The normal interlaminar stress σ_{zz} is maximum at the free edge itself. In fact the free edge is a singularity point for σ_{zz} [42]. The presence of σ_{zz} has important consequences for the laminate design, as tensile stress may cause adjacent plies at the interface to peel off. It has been shown that the presence of interlaminar stresses τ_{yz} and σ_{zz} is due to the mismatch of the Poisson's ratio values between adjacent plies [37].

The lay-up sequence has a considerable influence on the magnitude and direction of the interlaminar stresses. For angle ply laminates, there is shear coupling, and τ_{xz} will occur even in the absence of the Poisson's ratio mismatch. In cross-ply laminate, there is no shear coupling, and the Poisson's ratio mismatch will result in interlaminar stresses τ_{yz} and σ_{zz}. For laminate configurations, other than angle-ply and cross-ply, a combination of interlaminar stresses will result. Delamination often occurs between plies of different orientation due to stress concentration associated with material discontinuity there. But can also occur between layers of same orientation if there is an interface moment caused by neighbouring plies of different orientation or elastic properties. For an arbitrary ply stacking configuration all the three interlaminar stress τ_{xz}, τ_{yz}, and σ_{zz} will be present. The magnitude of the interlaminar stresses is related to the magnitude of the mismatch between the adjacent plies.

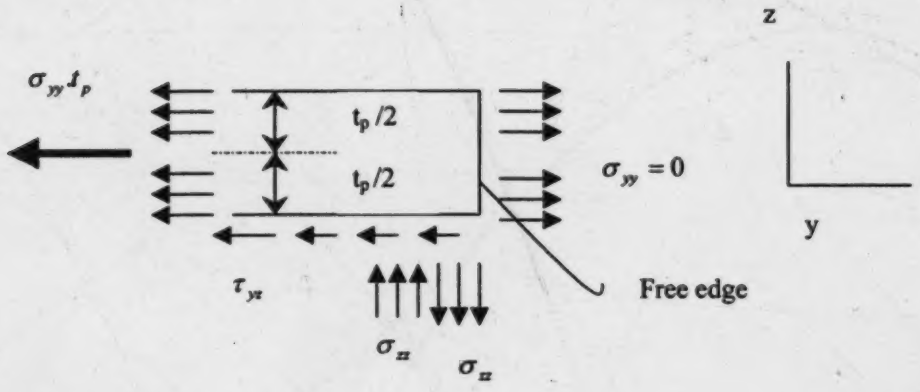

Fig 2.4 Mechanism of set up of interlaminar direct stress σ_{zz} in (0/ 90).

The magnitude of interlaminar normal stresses through the thickness at free edge varies widely and symmetry indicates that maximum occurs in most cases (depending upon the stacking sequence), at the mid-plane of the laminate, where shear stresses vanish. Thus, provided the maximum stress criterion is applicable, delamination would be expected at the mid-plane if normal interlaminar stresses exceed the interlaminar strength that can be assumed equal to the transverse strength of the ply. Such crack propagation along laminate mid-plane is driven by only normal stress, and hence can lead to pure Mode I fracture.

2.2.2 DELAMINATION CAUSED BY IMPACT

Transverse concentrated loading, such as low velocity impact by a projectile or even static tensile load for some lay-ups, results in highly localized deformation gradient. This causes large transverse shear and normal interlaminar stresses [49]. This may lead to the failure of the laminate.

A high velocity impact may also create a compression stress wave, which travels from the impact surface through the thickness of the laminate. This wave is reflected from the back surface as a tension wave, which can cause failure at the first weak interface.

Both internal stress waves and local out-of-plane deformations may initiate delamination at interfaces where there is major change in the angle between the plies. At higher velocity impact, additional damage may occur, such as fibre failure, matrix cracking etc.

2.2.3 DELAMINATION CAUSED BY MATRIX CRACKS

Another cause of the delamination development in a laminate is the matrix cracking in off-axis plies.[35] These off-axis cracks create interlaminar stresses as shown in fig 2.5. The interlaminar stresses have local maximum near the crack tip, and go to zero on the end faces of the laminate ($z = \pm 1$). These interlaminar stresses frequently cause local delamination, which grows along ply interfaces near the matrix cracks. In general, greater the crack length, the less is the stress required for the onset of delamination.

2.2.4 GENERAL

Besides mechanical loads, moisture and temperature effects cause residual stresses that may also lead to delamination damage. Also thicker plies tend to encourage higher interlaminar stresses thus causing early delamination.

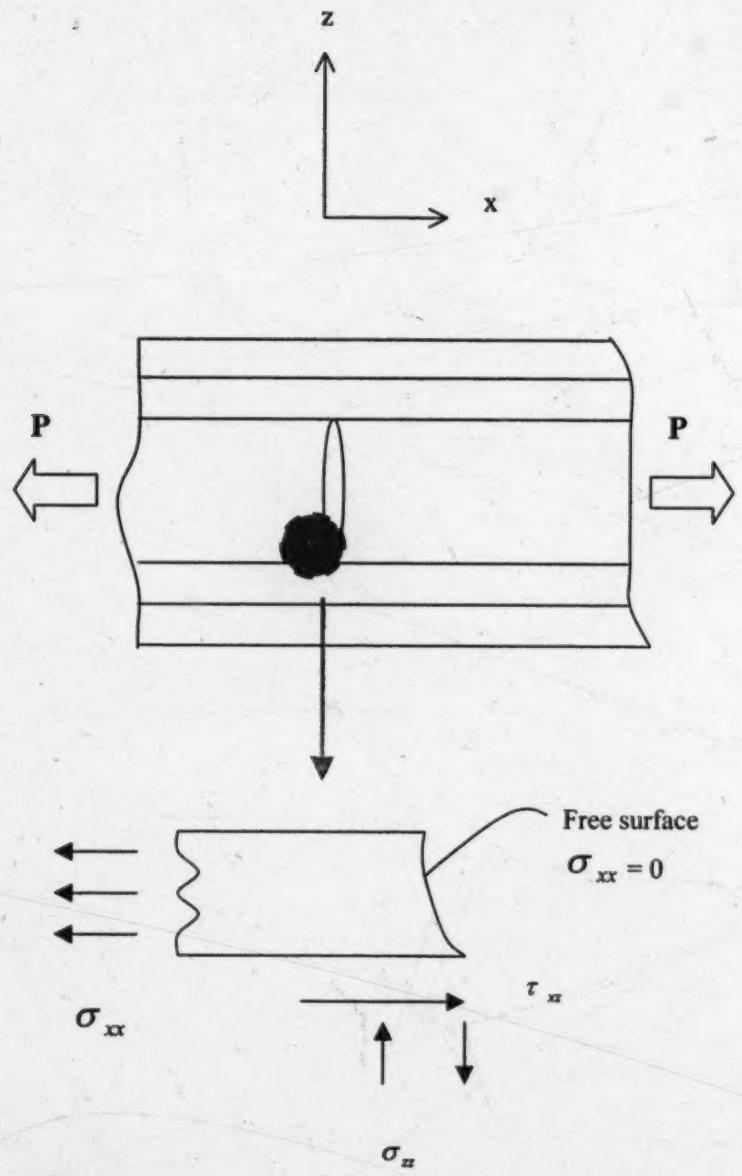

Fig. 2.5 Interlaminar stresses due to matrix crack in off-axis plies.

Delamination in composite laminates may interact with other damage mechanisms and result in growth behaviour different than that is anticipated from an elastic analysis [32]. For example, edge delamination is followed by matrix cracking in 90° degree plies, which can extend throughout the laminate width causing perturbation in the stress-field at the delamination front. Such interaction results in stable delamination growth. If the composite has tougher matrix, matrix cracking may be suppressed. Also for a delamination between plies of similar orientation, fibre-bridging may occur, causing nonlinear response. This again results in stable delamination growth and increase in G_c from the initiation value.

2.3 DELAMINATION PREDICTION

Prediction of delamination behaviour in composites has been a subject studied for many years. There are two approaches to account for delamination in design. The first is the classical laminate strength analysis approach, to calculate the *interlaminar stress components* [38,39,40]. This stress state is then compared with a failure criterion, which may be simply the transverse shear strength, or, a more involved three-dimensional criteria. Sometimes, higher order shear deformation theory is also used. However, because of complexities the analytical solutions to edge delamination are limited and more emphasis is placed on the numerical techniques like the finite difference, or the finite element. Again, most procedures for thick realistic laminates are computationally expensive. An elegant approximate solution to determine the normal component of interlaminar stress σ_z is available [41].

The second approach is the *fracture mechanics approach* based on strain energy release rate. Here, the requirement of self-similar crack growth and that of damage zone being small relative to the specimen size (thickness of specimen is sufficient), allowing damage zone to be considered confined, are fulfilled. Among the fracture mechanics criterion, more popular among the investigators is the energy approach, rather than the stress intensity factor approach. For the material showing limited ductility the crack propagation will occur when crack driving energy release rate exceeds a critical G_C. Equation 1.9 is useful for mathematical representation. If nonlinear inelastic behaviour is significant, J-integral based parameter may be used. A measure of the resistance of the material to delamination crack propagation is the interlaminar fracture energy of the material and can be characterized with critical energy release rate or fracture toughness criteria. The stress level at the onset of delamination can be determined from the response of a stress-strain plot. A sharp increase in both axial and transverse strain from the linear elastic response is an indication of onset of delamination.

Sometimes fracture mechanics approach based on the strain energy release rates is more promising compared to the stress criterion to describe the onset of delamination. At the edge, the linear elastic analysis suggests the interlaminar stresses at ply interface can become singular [42]. There is no rigorous explanation for the inability of the stress approach to tackle such case. However, the most logical explanation is that, the interlaminar micro cracks created by the singular stresses at the edges, or those initially present as inherent flaws, do not form delamination of a finite size until a critical G value is reached for the delamination extension [26] The ability of strain energy release rate to correlate delamination behaviour from various sources and to account for volumetric effects in the form of thickness dependence is the compelling reason for adopting fracture mechanics criterion to delamination problems.

Because the delamination is constrained to grow between individual plies, both interlaminar shear and tension are commonly present at the front. There, delamination is a mixed-mode fracture process. The resistance of the material can be characterized by a combination of Mode I, Mode II, and Mode III fracture toughness values. In order for the composite fracture resistance to be properly assessed, the fracture toughness parameters for each mode and mixed modes must be determined. Because of a complex mixed-mode nature, no closed form solutions have been developed to lay a strong theoretical foundation for understanding the parameters that control the delamination, except for a general analysis based on anisotropic composite laminate elasticity. Alternatively, however, the fracture toughness parameters can be determined, either experimentally, or computationally. A virtual crack closure method (and virtual crack extension techniques) has been combined with displacement based finite element analysis to calculate various G components [43,44,45] as a very popular technique. Some investigators have developed a modified finite element technique using methods such as the interlayer shear slip theory to study delamination simulation [46]. Another computational procedure currently gaining popularity is the essential fracture work method [47].

2.4 DELAMINATION CONTROL

The root cause of delamination is the poor interlaminar toughness. It causes deterioration in the structural performance of the composite. Since delamination forms an important factor in the structural performance of a laminate, it is important to understand this mode thoroughly and also design techniques to prevent it. It can be improved by the following methods:

1. designing a proper stacking sequence for the laminate
2. using a tougher resin
3. interleafing
4. providing a through thickness reinforcement

The design considerations are most effective, as the interlaminar stresses basically depend upon the lay-up sequence. One should avoid using angle plies together. A free-edge stress analysis based on ply elasticity [48] revealed that tensile interlaminar stresses act along the free edges of [± 45/ 0/ 90] coupon, while compressive interlaminar stresses are induced for the [0/ 90/ ± 45] coupon. Hence, the former developed the free-edge delamination, while later did not. Proper stacking sequence can provide considerable reduction in interlaminar stress components, and alleviation of free-edge delamination. This, used in conjunction with suitable manipulation of free edge regions and reinforcement of free edges, can significantly delay onset of delamination initiation.

Secondly, tougher matrices are also often employed in practice. This can significantly reduce damage following impact [49]. Alternatively, interleafing of the laminate, i.e. sandwiching thin adhesive films etc. of high toughness is found to be an effective way to improve the damage tolerance of composites against delamination. Altering the mechanical properties of the potential delamination layers selectively in this manner, however, doesn't improve any safeguard against other failure modes. Lastly, as another viable method, various studies have shown that structures formed by 3-D braiding, or through-thickness stitching often improves the fracture toughness. However, stitching reduces the compressive and tensile strength of laminate compared to unstitched laminates.

Chapter 3

CHARACTERIZATION OF MODE I AND MODE II INTERLAMINAR FRACTURE TOUGHNESS

3.1 INTRODUCTION

The most common damage mode in composites limiting their use in primary structural application is delamination. The presence and growth of delamination in a composite structure may result in strength and stiffness degradation, and may also initiate a catastrophic failure. In some cases delamination alone is a strength limiting factor. Therefore, delamination toughness for Mode I and Mode II fractures must be characterized to help combat such fracture and expand more confident use of composites. Delamination fracture toughness is considered as one of the most important mechanical properties in the characterization of a composite material and its correct assessment by standard test methods is paramount to the safe structural use of composites.

By far the greatest amount of theoretical and experimental work on the fracture of composite materials has been reported in the opening mode i.e. the Mode I. For the isotropic materials, Mode I is lowest fracture energy mode, and a crack always propagates along a path normal to the direction of maximum local principal stress. Mode I is the dominant mode of fracture observed in unidirectional fibre reinforced epoxy composites. The first generation of composites exhibited low Mode I fracture toughness and were particularly susceptible to delamination when subjected to interlaminar normal stresses. It can be said that the initiation and growth of delamination in composites is in many cases caused by interlaminar normal stress, but may also be caused by interlaminar shear stresses. In composites, which are highly orthotropic materials, the initial interlaminar defect is constrained and usually continues to propagate in the same plane between the laminate, regardless of the orientation of the applied load. Thus, a genuine Mode II failure is possible. Also with emergence of new material systems exhibiting superior Mode I toughness, emphasis has now shifted more to Mode II and Mode III delamination fracture toughness.

In general, interlaminar fracture in angle-ply laminates is induced by individual or mixed-mode type (Mode I opening, Mode II forward shear, Mode III tearing) fracture or both.

In order for the composite fracture resistance to be properly assessed, the fracture toughness parameters for each mode and mixed modes must be determined. It has been found that for composite materials Mode II G_c is many times more than that for Mode I. There is a general trend that the more brittle materials (lower G_{Ic}) have G_{IIc} values much greater than the corresponding G_{Ic}, whereas the tougher matrix materials (higher G_{Ic}) have G_{IIc} values that are close (but still higher) than the corresponding G_{Ic}. However, for toughened matrix composites, G_{Ic} is approximately equal to G_{IIc}. Interestingly, through-thickness reinforcement in stitched composite laminates can increase Mode I toughness 10-fold, but increase in mode II toughness is only of the order of 25 percent. Furthermore, the toughness increment supplied by the through thickness reinforcement depends upon crack length, geometrical ratios, and loading conditions and is not a material constant. Hence it is critical to examine the characterization and testing of Mode II delamination fracture toughness, in addition to the Mode I delamination fracture toughness for toughened composites.

In the recent years considerable efforts have been made to produce standard test methods to measure the delamination resistance. For isotropic materials, the resistance to fracture could be expressed in the terms of plain strain Mode I fracture toughness. The testing of composites is complicated by the directional strength and stiffness brought about by orientation of the reinforcement, and their non-homogeneity and aniosotropy. However, the fracture mechanics approach is effective and widely accepted for characterization of delamination onset and growth in composites. The application of linear elastic fracture mechanics enables critical strain energy release rate, or fracture toughness G_c to be deduced using compliance measurement. However, experimental measurement of Interlaminar Fracture Toughness (IFT) involves complex data reduction because G_c is an energy-based parameter that is influenced not only by the accuracy of the measured load and displacement, but also by the accuracy of the measured crack length, and the change in compliance with the crack length. Furthermore, a complete description of IFT requires characterization of three unique fracture modes; Mode I, Mode II, and Mode III. As these properties are often used by manufacturers to qualify new composite materials efforts to standardize the tests have been increasing. In particular, standards sanctioned by the International Standards Organization (ISO) are desired due to the global nature of trade in composite materials [50].

ISO develops international standards through a 'one nation- one vote' balloting process involving officially designated national representatives. Within ISO, Interlaminar Fracture Toughness (IFT) test methods are considered within Committee TC61, Subcommittee SC13, Working Group WG16 on Composites. Research efforts to standardize IFT tests have been lead by three organizations; the American Society for Testing and Materials (ASTM) Committee D30 on Composites, the European Structural Integrity Society (ESIS) formerly known as the European Group on Fracture (EGF), and the Japanese Industrial Standards Organization (JIS).

The Double Cantilever Beam (DCB) and the End-Notch Flexure (ENF) provide the most viable method for delmaination tests for Mode I and Mode II fracture respectively, as

discussed subsequently. The focus in the current study is concentrated on the DCB and ENF specimens. The verification of specimen-geometry independence is clearly a critical step in the development of an acceptable test standard. To investigate the specimen geometry effects in the present study, fracture behaviour using DCB and ENF specimens is analyzed by computational finite element simulation of the tests.

3.2 MODE I INTERLAMINAR FRACTURE TOUGHNESS TESTING

Over the years, the double cantilever beam (DCB) specimen has emerged as the preferred configuration for measuring the opening-Mode I interlaminar fracture toughness of composites. Earlier the DCB specimen has been in use for the plane strain fracture toughness of isotropic materials. For composites the DCB specimen [51] is being used since more than 25 years and the origin can be found in the earlier similar works on the DCB specimen used for adhesive bond tests [52]. The DCB specimen is shown in Fig. 3.1. Since 1981 the ASTM task group (D30.02.02) is studying the DCB specimen through a series of round-robin tests in collaboration with the ESIS and the JIS. Consequently, a considerable guidance has been available for Mode I testing in the form of experimental test procedure. The specimen is believed to produce a truest Mode I fracture.

After a long history of testing, the Mode I interlaminar fracture toughness has been standardized by ASTM in 1994 [53]. During the same period the JIS and ESIS have also published a DCB test standard [54,55]. These methods are very similar. However, there are some differences. Both the ASTM and the ESIS do not recommend precracking, and use an insert film (alone, with no precrack) during the moulding of the specimen. The JIS suggests a wedge precrack of 2-5 mm growth from the insert film introduced by static Mode I fracture. Secondly, the thin insert film used to introduce the starting defect is recommended to be less than 13 μ m by the ASTM, 15 μ m by the ESIS, and 30 μ m by the JIS. The key requirement is availability of stable crack growth without aid or obstacle effect from the initial defect. A sharp starting defect will maximize the stress concentration and give a conservative toughness value. On the other hand, it is known that precracking may produce fibre-bridging and multiple cracking which may increase the toughness values. These effects become significant in composites with tough matrices like carbon-fibre / PEEK composites [56].

A single toughness value may be obtained if the insert thickness is small without having to resort to precracking. Incidentally, one of the main reasons for the delay in reaching a consensus test method is the dramatic increase in Mode I interlaminar toughness of composites over the years [61]. The fracture mechanics approach, which is well-suited to characterizing the linear elastic behaviour of first generation carbon epoxy composites

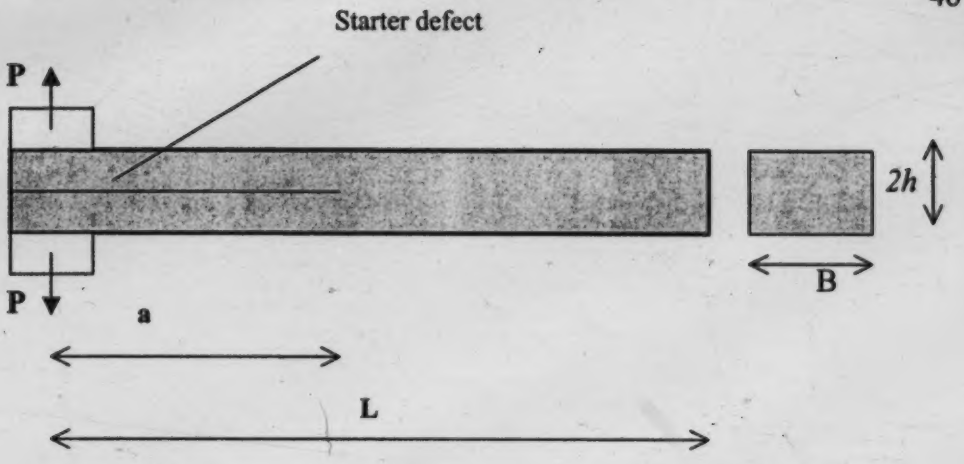

Fig. 3.1 The DCB Specimen

(G_{Ic} of 100-200 J / m^2), has proved less amenable when applied to tough composites (G_{Ic} of 1000-2000 J / m^2).

For isotropic materials and matrices, other test specimens like SENB- Single Edge Notch Bend specimen, CT – Compact Tension specimen are available to measure the plane strain fracture toughness [57]. The ASTM standards are available [58,59]. For fracture toughness testing of cylinders and thick bars the C- Shaped specimen is used with notch on the inner side of the 'C'.

3.3 LONG ROAD TO MODE II INTERLAMINAR FRACTURE TOUGHNESS TESTING

The majority of methods available to characterize the resistance of composites to delamination under shear are based on bending tests, using specimens with a starter delamination to promote a shear failure at the crack tip. During 1980s several tests methods were proposed by various groups to measure G_{IIc} of laminated fibre composites. However, these efforts have been less successful in reaching a consensus leading to a standard Mode II test method. It has been a difficult task, both in terms of achieving an adequate configuration to yield a pure shear loading at the crack tip, and in the interpretation of the results [60]. Consequently, again the ASTM undertook several interlaboratory round robin test programs to evaluate various test methods for determining interlaminar shear fracture toughness of laminated composite materials. The specific aim of these exercises has been to examine the effects of starter films, the effect of precracking, data reduction and calculation methods, choice of the critical load-deflection points, and benefits of stabilization and control methods in the test, benefits of crack shear displacement measurement etc. [64]. To date, as a result there is no widely accepted Mode II standard test method. Also, there is much controversy among the various test groups using different test configurations to get consistent and reproducible G_{IIc} values [61,62,63,64]. The common popular tests are:

(1) ENF-End Notch Flexure:
the most popular, three point bending test, the procedure for which was proposed by ASTM;

(2) ELS-End Loaded Split:
used extensively by the ESIS;

(3) SENF -Stabilized ENF:
proposed by the JIS in early 1990s to stabilize the test by feedback control of the test machine;

(4) 4ENF- 4 point ENF:
the latest and proposed by Martin and Davidson [65] and used for study program by the Materials Engineering Research Laboratory MERL, France.

The above specimens are shown in Fig 3.2.(a) to (d). Some other specimens used for the Mode II interlaminar fracture tests are; the Cantilever Beam Enclosed Notch (CBEN), and the Centre Notch Flexure (CNF), etc. [5,33]. Mode II fracture testing has not been limited to flexural specimen geometries. The other class of specimens is the compact specimens, which generally require a more complicated fixture. These are mentioned as follows. First, a proposition found long ago to use a modification of the Iosipescu shear test to produce a Mode II fracture. Another specimen used is, using a thin tubular section subjected to shear, and has been investigated for mode II fracture of unidirectional graphite/epoxy composites [66]. Some other beam and compact specimens, which are also used for mixed Mode I / II tests, are discussed in Sec 3.4. It may be mentioned that the suitability of a specimen depends upon its simple geometry, ease of manufacturing, simple loading system, and generation of a pure shear stress at the crack tip. Hence it is natural that not all the specimens are popular.

The ENF and the ELS tests are the two most popular Mode II test methods in the community. Both these tests have been analyzed to yield a pure sliding shear fracture Mode II at the delamination front. The ENF test was developed long time ago for testing wood [67], while the ELS test was developed at Texas A & M University in 1986 [68] and is used extensively by the ESIS. The ENF test is a simple three-point bend loading, but it results in an unstable delamination growth unless the initial crack is very long, or the test is controlled with special shear displacement gauge. ELS test has the advantage of stable crack propagation and allowing generation of an R curve (increase of fracture resistance with the crack length), but requires a more complicated test fixture.

Of the ENF and the ELS, the ENF is the most widely used test on account of its simple fixture. And the focus of the present study is subsequently concentrated on the ENF test in accordance with the imminent ASTM standards. The ENF specimen is a true Mode II test within the constraints of small deflection theory. The standard test method for the ENF test already exists, as adopted by JIS and European Association of Aerospace Industries (AECMA) [69]. It should be noted that one of the two methods in JIS standards requires a device to measure the end displacement between the top and the bottom halves of the specimen (termed shear displacement) during the deformation. This allows generation of the R curve, but involves an elaborate apparatus and tedious measurement of shear displacement. The ENF specimen is attractive as the test may be performed on slender specimens. Generally thickness greater than 3 mm is adequate to avoid flexural failure and to ensure the applicability of small displacement theory. Although the ENF test has been carried out at many institutions for many years there is still a need for some caution.

It is agreed that ENF specimen requires careful preparation and experience in order to obtain consistent results. There exists some disagreement regarding the best method to

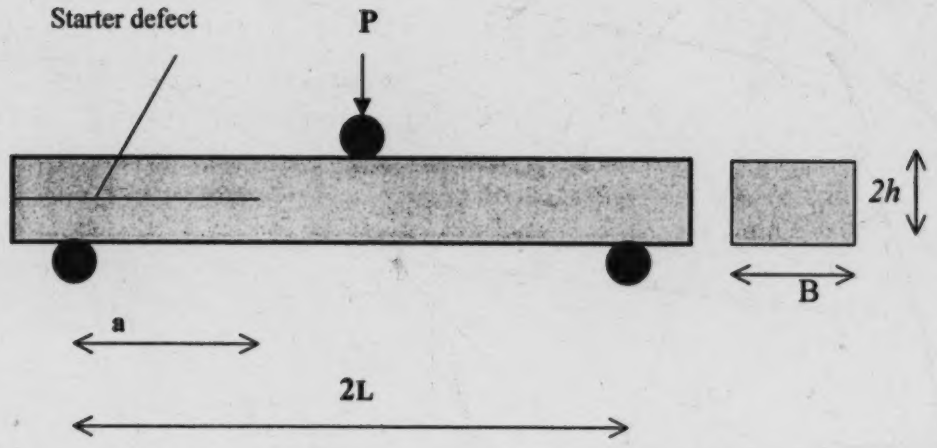

(a) The ENF Specimen

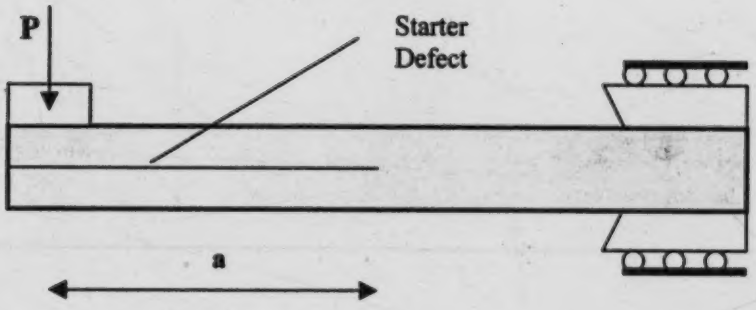

(b) The ELS Specimen

Fig 3.2 Popular Mode II test specimens

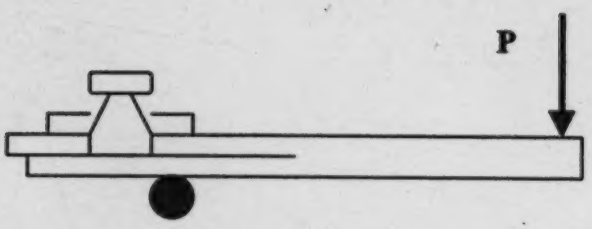

(c) Stabilized End Notched Flexure Specimen

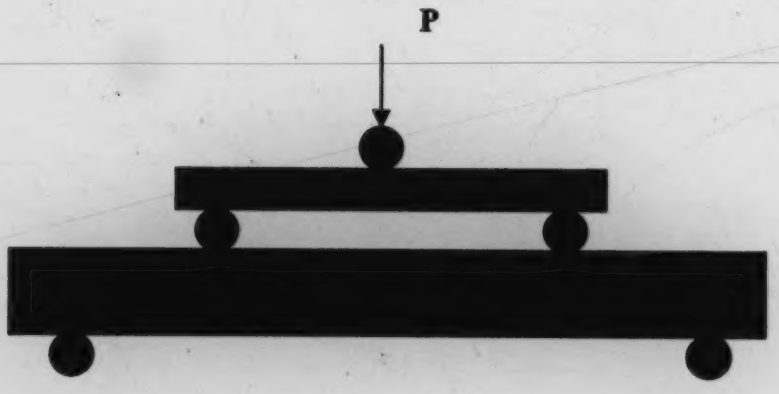

(d) Four Point ENF Specimen

Fig 3.2 (cont.) Popular Mode II test specimens

obtain critical point in load-deflection curve [64,107]. Also, for tougher composites a significant period of non-linearity is observed on the load-deflection curve. Furthermore, the problem of precrcaking is more complicated in Mode II, as even thin starter films tend to produce a higher G_{IIc} as discussed in section 4.4.

In the light of above, it is necessary to look into the analytical solutions of the ENF specimen from the beam theory to investigate the analysis of the specimen [71]. These expressions from a simple beam theory have been later suitably corrected to include the transverse shear deformation effects [72] and other crack tip effects. In addition much work has been performed using finite element analysis to check the validity of these expressions. Hopefully these studies will facilitate the standardization of the ENF specimen for the measurement of Mode II interlaminar fracture toughness in the near future.

3.4 OTHER INTERLAMINAR FRACTURE TESTS

For quite some time, the most widespread method in material characterization to measure the interlaminar shear strength was the Short Beam Shear (SBS) test [5,33]. The SBS test, while not a fracture mechanics test, was introduced in 1960s. It dominated in terms of its use and stood as the only standardized interlaminar test [73]. It is a three-point bending test with span-to-depth chosen such that an interlaminar shear failure is induced along the centerline rather than the tensile failure due to bending stresses, and measures the 'apparent' interlaminar strength. Evidently, better results are obtained for thicker laminates (>50 plies). Especially for the tough composites with improved interlaminar shear strength, the interlaminar fracture may not be reached and its use may be limited. Other serious limitations with the test are that the distribution of shear stresses is actually non-uniform over the width of the specimen, and that shear failure is a rare occurrence in thin composite laminates used commonly. Also the interlaminar shear stresses are not exactly parabolic as predicted by the beam theory, and in fact depend upon the stacking sequence with discontinuities at the ply interfaces. The test is basically used as a quality control tool in the lamination process, and screening new matrix materials.

In order to generate a delamination criterion in addition to the pure Mode I and the pure Mode II tests, the mixed mode tests are also needed. Various mixed mode test configurations are available [5,33,35,88]. The Mixed mode Bending (MMB) is the most popular configuration as it allows large range of mode ratios. There are other mixed mode specimens like; the Edge Delamination Tension (EDT) test to determine initiation value with G_I and G_{II} components at an interface, which is known priori to be delamination prone, in a general lay-up; the Cracked Lap Shear (CLS) specimen used for studying mixed mode fatigue crack propagation from total G_C obtained; the Symmetric Single Leg Bending (SSLB) test for mode mix of approximately 0.4; the Unsymmetric

Single Leg Bending (USLB) test for laminates with delamination not at the mid-palne ; a modification of the Arcan Test (used for biaxial stress studies) to investigate pure Mode I, pure Mode II, and mixed mode interlaminar fracture; the unsymmetrical DCB specimen [74] , the Compact Shear (CS) specimen, etc.

The development of a standard test method for mode III has lagged behind due to difficulty in identifying a configuration exhibiting pure mode III stress at the delamination front. Variations of the Split Cantilever Beam (SCB) have been examined to be less successful [5,50]. However recently developed Edge Crack Torsion (ECT) specimen appears promising [75].

3.5 THE DCB SPECIMEN

The DCB test aims to give the Mode I interlaminar fracture toughness using a modified beam theory or compliance calibration method. The test specimen consists of a unidirectional rectangular laminate beam of uniform thickness. The test involves peeling apart the upper and lower halves of the beam specimen due to tensile normal interlaminar stresses. The test is used to obtain the resistance to delamination initiation from an insert and its subsequent propagation in the form of an R curve. Linear elastic behaviour is assumed in the calculation, which is valid when the zone of damage or the nonlinear deformation at the delamination front, or both, is small relative to the smallest specimen dimension (typically, the thickness). The test standards as per the ASTM designation D5528 –94a [53] are followed in the description. The test is meant only for the unidirectional layups of fibre reinforced polymer matrix composites.

3.5.1 SPECIMEN DETAILS

(1) Specimen Dimensions:

The specimen must contain an even number of plies and shall be unidirectional with delamination growth occurring in the zero degree direction. The specimen has 20-25 mm nominal width, to minimize edge effects. The specimen length is nominally 125 mm (at least). The thickness of the specimen '2h' (thickness of each arm is 'h') can be chosen nominally be between 3 mm and 5 mm. The specimen is shown in Fig 3.1. Thinner specimens show geometrical non-linearity due to large displacements, and make the interpretation of the results more complicated. A ratio of opening displacement divided by crack length (δ / a) of less than 0.4, is necessary to keep the overestimation of G_{Ic} to less than 5%. For larger values, the corrections in Annex 3.1 need be applied.

(2) Starter Defect:

The starter defect is introduced at the laminate mid-thickness during moulding to ensure a controlled delamination. The insert is required to be properly implanted and inspected. The film is supposed to be as thin as possible to minimize the disturbance of the composite, recommended to be less than 13 μm. The specimen is not precracked. The initial delamination length 'a_0' (between the loading line and the crack tip), should be at least 50 mm from the loading line so that the influence of the hinges can be neglected (approx. 63mm film is required to account for the loading hinge arrangement). The polymer film made of Teflon, or Vak-Pak, or PTFE, is recommended normally; Polyimide film is recommended (instead of aluminum) for high melting point matrices such as PEEK [53]. The film is to be coated with a release agent, however, agents containing silicone may contaminate the laminate, so baking the film before placing is desired.

Different values of 'a_0' and '2h' may be required for materials with high interlaminar fracture toughness. The specimen thickness and initial delamination length shall be designed to satisfy [53]:

$$a_0 \leq 0.042\sqrt{\frac{(2h)^3 E_1}{G_{Ic}}} \qquad 3.1\ (a)$$

$$2h \geq 8.28\left(\frac{G_{IC} a_0^2}{E_1}\right)^{1/3} \qquad 3.1\ (b)$$

(3) Loading Configuration:

Typically, the test is displacement controlled. The specimen is tested at a low cross-head rate of 0.5 mm/ min to produce a stable crack growth. The loading rate may be increased after first 5mm delamination growth. The loading is introduced via either piano hinges or machined loading blocks. These must allow free rotation and a minimal stiffening effect at the load points in the specimen arms. The tabs should have adjustable slots in the hinges (that attach the specimen to the loading fixture), so that the load always remains vertical. The distance from the hinge pin to the center-line of the specimen should not exceed 10 mm, or a suitable criteria to minimize errors in the applied moment arm [53].

(4) Procedure & Interpretation of the Results:

The load, beam deflection δ, and the delamination length are recorded at each interval selected priori. Delamintion length is sum of distance from the loading line to the end of the insert plus the increment of delamination growth. The specimen edges

ahead of the insert may be coated with typewriter correction fluid to aid visual detection of delamination onset. The crack length can be tracked by marking the specimen edges at desired increments with a coloured pencil. An optical microscope or a precision dial caliper can also be employed for measuring the crack length. The graduation marks may be at an interval of 1mm for the first 5mm propagation, and at the interval of 5mm subsequently. When the delamination has extended for 25mm or more beyond the insert, the specimen may be unloaded. Unloading may be at quicker rate and the load-displacement plot need be recorded. If the load does not return to zero, damage may have been induced in the beam arms.

During the load and displacement measurement three definitions for an initiation value of G_{Ic} are available: (1) the point of deviation from linearity in the load-displacement curve (NL), (2) the point where delamination is visually observed on the edge, (VIS) measured with a microscope, and (3) at the point where compliance has an increase by 5% or where load has reached a maximum value (5% max). The NL G_{Ic} value, which is typically the lowest of the three initiation values, is recommended for generating delamination failure criteria. Physical evidence indicates that the NL value corresponds to physical onset of delamination from the insert in the interior of the specimen.

The resistance curve (R-curve) depicts G_{Ic} as a function of delamination length to characterize the initiation and propagation of delamination in the specimen. Increase occurs due to fibre bridging, which actually does not occur in multi-ply laminates. Hence, fibre bridging is considered to be artifact of the unidirectional specimen used; and generic significance of the G_{Ic} propagation values beyond implanted insert is questionable, and the initiation value is preferred.

(5) Conditioning, Precautions, & Application to Other Materials:

Five specimens are to be used for each test. In order to obtain baseline data specimens should be conditioned to contain a uniform moisture content throughout the specimen thickness. Test specimens be stored and tested in standard laboratory atmosphere having the temperature $23^0 \pm 3^0$ C and 50 ± 10 % relative humidity.

Delamination growth may proceed in two ways; (1) slow stable extension, or, (2) run-arrest extension. In the second case the unstable delamination front jump indicates problem with the insert, and the sample has to be discarded. Secondly, if the delamination growth is not uniform across the width, the delamination length need be measured on both the edges and the average be recorded. The difference between delamination lengths of two edges should not exceed 2 mm.

Non-unidirectional DCB configurations may experience branching of the delmination away from the mid-plane through matrix cracks in off-axis plies. Due to coupling between extension and shear, the fracture cannot be termed as pure Mode I. In

addition, significant anti-clastic bending effects may result in non-uniform delamination growth along the specimen width. Secondly, for tougher matrices, or metal matrix composites, or laminates with through-thickness reinforcement, failure of beam arm rather than the intended interlaminar failure may be experienced.

3.5.2 DATA ANALYSIS

For calculating G_{Ic} values, three data reduction methods are available; the modified beam theory, compliance calibration method, and, modified compliance calibration method. The values by these methods differ by only 3.1 %, and no method can be selected as superior to the others. There is another popular method known as the area method. The modified beam theory yields the most conservative values of G_{Ic} and is recommended by the ASTM [53].

(a) The Beam Theory

The specimen is assumed to consist of two identical cantilever beams with built-in ends at the crack tip, and length equal to the crack length. The specimen under load is shown in Fig. 3.3.

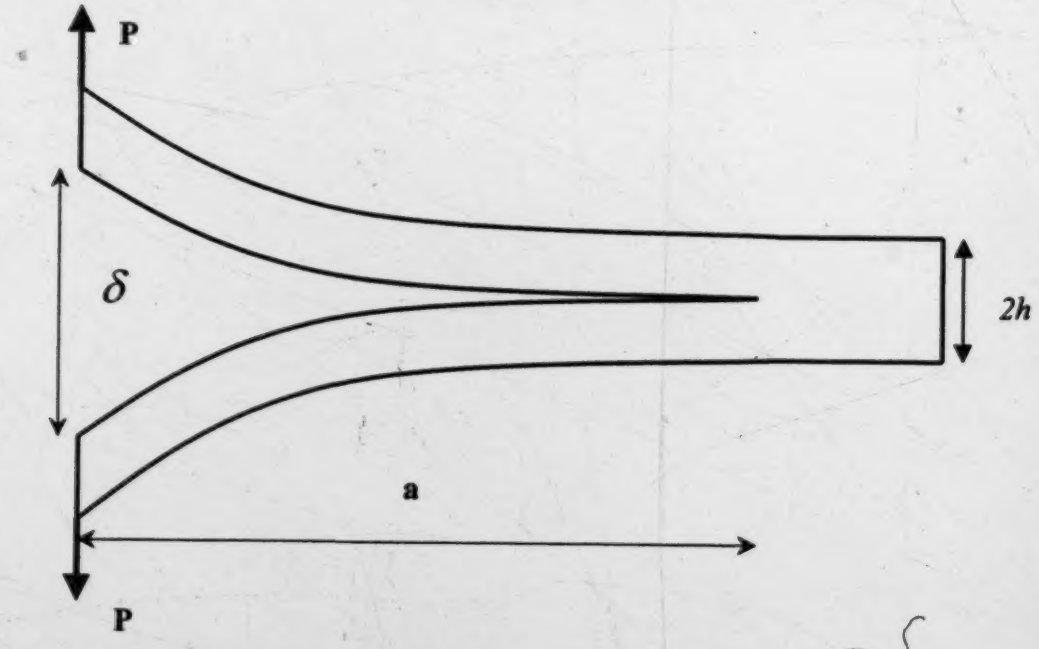

Fig 3.3 DCB Specimen under Loading.

Compliance is defined as $C = \frac{\delta}{P}$, where δ is the vertical load point displacement between two free ends and P is vertical load applied at each end. Under such assumption, and ignoring shear deformation and considering crack length to be sufficiently long to promote pure bending, the compliance C can be expressed as $C = \frac{2a^3}{3E_1 I}$, where $I = \frac{B(h)^3}{12}$, and B is the width of the specimen, and E_1 is the axial modulus of the laminate. Or compliance is given by:

$$C = \frac{8(a)^3}{Bh^3 E_1} \qquad 3.2$$

It should be noted that, in the equation 3.2, flexural modulus should be used instead of the in-plane axial modulus E_1. Such distinction has been made in the earlier works on delamination analysis [31,79]. The distinction between the flexural and tensile modulus is also detailed elsewhere [76]. And this has been retained in the Mode I interlaminar fracture toughness standards [53,54], which have used the notation E_{1f}, to denote modulus of elasticity in the fibre direction measured in flexure. However, for the unidirectional composite laminate specimen used in DCB test, the distinction is unwarranted. Subsequent works [81-84] have adopted only E_1, representing the axial modulus of the laminate. Hence in the present analysis only in-plane modulus E_1 is used.

From the equation 1.9, the strain energy release rate by definition is expressed as:

$$G = -\frac{d\pi}{dA}$$

where, A is the crack surface area, π is the potential energy, which is supplied by internal strain energy U stored in the body, and (applied) work done by external forces F_{ext}. Mathematically, potential energy can be put as:

$$\pi = U - F_{ext} \qquad 3.3$$

Now, the internal strain energy U can be expressed as

$$U = \int_0^{\delta} P.d\delta = \frac{P\delta}{2} \qquad 3.4$$

The DCB test is performed in a displacement controlled condition. So work done by external force F_{ext} is equal zero ($d F_{ext} = P^* d\delta = 0$, for change of P with crack length 'a' in a displacement controlled setup). Hence the potential energy is given by

$$\pi = U = \frac{P\delta}{2}$$

Therefore, using the relation δ = P.C, we get

$$G = -\frac{d\pi}{dA} = P^2 \frac{1}{2B}\frac{dC}{da} \qquad 3.5$$

The same expression has been derived by Irwin and Kies for calculation of Mode I critical energy release rate.

The compliance-crack length relation as in equation 3.2 can be employed in the above equation. Hence, if 'P' now represents the load corresponding to the fracture, by using *'uncorrected' beam theory*, by the *so-called load method*, we have the Mode I fracture toughness as:

$$G_I = 12\frac{P^2a^2}{B^2E_1h^3} \qquad 3.6$$

Now, we have the beam deflection given by the expression $\delta = \frac{8Pa^3}{E_1Bh^3}$

From the above, we can write G_I, by the *so-called displacement method*; where in the equation obtained in such manner is more convenient as it is expressed in terms of physical experimentally measured parameters alone.
The expression for G_I arrived at is:

$$G_I = \frac{3}{2}\frac{P.\delta}{B.a} \qquad 3.7$$

In practice equation 3.7 (or 3.6) will underestimate the compliance as beam is not perfectly built-in, i.e. rotation and small extension may occur at the delamination front and the slope and deflection at the root of the cantilever are not zero as assumed in the simple beam theory.

Correction for Beam Root Effects and Shear Deformations

The equation 3.7 assumes that compliance at the crack root is zero, but in reality there is some deflection and rotation at the root. Secondly, the shear deformations are not included in the beam theory. So a correction parameter needs to be applied for the *beam root extension, rotation and shear deformation effects*. This can be realized by treating the beam as of length $a+|\Delta|$ instead of 'a', where $|\Delta|$ is the correction factor. The increment $|\Delta|$ can be found experimentally by plotting cube root of compliance $C^{1/3}$ as a

function of crack length 'a'. The line doesn't pass through the origin, and the intercept on the x-axis determines the parameter $|\Delta|$. So the modified expression becomes,

$$G_I = \frac{3}{2}\frac{P\delta}{B(a+|\Delta|)} \qquad 3.8$$

This approach also allows the modulus to be determined as below [53,54,81].

$$E_1 = \frac{8(a+|\Delta|)^3 P}{\delta . B h^3} \qquad 3.9$$

Alternatively, we can examine the effect of shear deformations (alone) using the Timoshenko Beam theory [78,93] incorporating the shear modulus G_{13} , to the compliance and fracture toughness relations and arrive at expressions as below [5]

$$C = \frac{24}{E_1 B}[\frac{1}{3}(\frac{a}{h})^3 + \frac{1}{10}(\frac{E_1}{G_{13}})(\frac{a}{h})] \qquad 3.10(a)$$

$$G_I = \frac{12P^2}{E_1 B^2 h}[(\frac{a}{h})^2 + \frac{1}{10}(\frac{E_1}{G_{13}})] \qquad 3.10(b)$$

As a comparison between fracture toughness given by expressions 3.10(b) and 3.8, we take the isotropic case, with 2h=5mm and a=50mm. We can observe that for any typical case the expression 3.8 gives an increment, which is much larger as compared to increment in fracture toughness given by expression 3.10(b). Expression 3.8 is a better estimate. (This can be further confirmed by using a theoretical relation for the correction factor as given subsequently in equation 3.15.) So it is clear that equation 3.10(b) will grossly underestimate the fracture toughness due to neglection of the elastic supports at the beam roots, even though it accounts for shear deformations.

The most elegant analytical solution for the DCB specimen to account for $|\Delta|$ has been the one modeled on the basis of the beam on elastic foundations [77]. Even though the beam is slender, the local effects require a short beam analysis of the beam supported on elastic foundation with extension and rotational stiffnesses at the crack tip. The solution analyzes both the root rotation, and root extension displacement taking into account the necessary shear deformations. The shear deformations can be analyzed on the basis of Timoshenko Beam Theory. The root rotation effect is dominated by the shear effect since the deformations occur over a rather short distance. The result for the isotropic material gives the parameter $|\Delta|$ equal to '0.67 h', to be added as a correction to the crack length 'a'. It may be noted that for highly orthotropic materials shear deformations may have considerable effect (as shear modulus is lower in relation to the axial modulus).

It has been shown that the solution for the isotropic materials can be extended to the orthotropic materials by making a correction of '$\chi_1.h$' to the crack length 'a', where χ_1 is material parameter [79,80,81,82]. The values of χ_1 are typically near 2.5 for composite laminates. In reality, χ_1 depends upon the elastic properties of the material and is strongly dependent on the shear modulus. The above analytical model forms the basis for the experimentally derived correction factor $|\Delta|$ adopted in the ASTM Standard. Since C is proportional to a^3, a plot of $C^{1/3}$ against $(a+\chi_1.h)$ gives this necessary correction factor '$\chi_1.h$'. The actual theoretical expression for χ_1 can be found from the beam on elastic foundation model [80]

$$\chi_1 = \sqrt{\frac{1.(a_{66})}{18K.(a_{11})}}\sqrt{3-2(\frac{\Gamma}{(\Gamma+1)})^2} \qquad 3.11$$

where, $\Gamma = 1.18\frac{a_{66}}{\sqrt{a_{11}a_{22}}}$ 3.12

The coefficients a_{11}, a_{22}, a_{66} are the elastic compliances of the composite specimen.
And K is function of Poisson's ratio and is approximately 0.85. From empirical observation parameter '18K' can be replaced by '11' in the equation 3.11 for the DCB specimen [80,82,95].

Correction for Large Displacements

Secondly, to account for the non-linearity effect on account of *large displacement effects* as mentioned in section 3.5.1, a correction factor F is to be employed. This factor accounts for two effects, the shortening of the moment arm and tilting of the end blocks [81,82]. The tilting of the blocks, as the beam is distorted gives rise to further curvature to the beam, and further shortening. Both effects are included in F correction. Values for F correction are given in ANNEX 3.1

Correction for End Block Effects

Thirdly, for specimens using loading blocks with distance between the end of the insert to the load line less than 50mm, the influence of the end block effects is significant. Another correction factor, N, is a displacement correction required to correct the beam deflection δ. This is used in determination of compliance, delamination fracture energy, and Modulus E_1 to account for the stiffening of the specimen [81,82]. It should be noted that the value of N given in the equation also includes (in the last two terms) the corrections needed for the large displacement and the end block tilting. The values are given in the ANNEX 3.1.

The correction factors F and N have been adopted in the DCB standards. They are used as multiplying factors, and are less than 1.0.

(a-1) The Modified Beam Theory

Hence, in summary, using the *Modified Beam Theory*, we account for the following corrections to the expression 3.8

(1) χ - end rotation and deflection of the crack tip

(2) F – for large displacement geometrical non-linearity effects, (not required if ratio of opening displacement and crack length is less than 0.4.)

(3) N – stiffening effect due to end block.

To apply these corrections to either the modified beam theory or experimental compliance data analysis methods, first, the corrected compliance calibration is determined by plotting $(C / N)^{1/3}$ against the crack length 'a'. Subsequently the expression for the compliance and the Mode I fracture toughness becomes [81-85]:

$$C = \frac{8N(a+\chi h)^3}{Bh^3 E_1} \qquad 3.13$$

$$G_I = (\frac{F}{N}).\frac{3}{2}\frac{P\delta}{B(a+\chi h)} \qquad 3.14$$

The above equation 3.14 is very useful in the experimental analysis. It also has the advantage of not using the modulus E_1. However for the purpose of analytical or computational modeling, the deflection may be eliminated from the above equation. The expression for corrected Mode I interlaminar fracture toughness is then given by:

$$G_I = \frac{F}{1}12\frac{P^2(a+\chi h)^2}{B^2 E_1 h^3} \qquad 3.15$$

(b) Compliance Calibration Method

This is an experimental compliance calibration method, sometimes called Berry's Method [86,53,54]. Compliance vs the crack length is plotted on a log-log plot, from the visually observed delamination onset values and all propagation values. Using empirical relation:

$$C = \frac{a^n}{K}, \qquad 3.16$$

where n and K are to be determined from the plot. The values of n may be considerably lower than the ideal bending value of 3. Mode I interlaminar fracture toughness is calculated as:

$$G_I = \frac{nP\delta}{2Ba} \qquad 3.17$$

(c) Modified Compliance Calibration Method

It is again an empirical method. Delamination length normalized by specimen thickness, a / 2h is plotted as a function of cube root of compliance, $C^{1/3}$, using visually observed delamination onset and propagation values [53]. The slope of this line be A_1. Mode I interlaminar fracture toughness is calculated as:

$$G_I = \frac{3P^2C^{2/3}}{2A_1B(2h)} \qquad 3.18$$

(d) Area Method

This method is most popular on account of its simplicity. In this approach the specimen is not modeled as beam. It is based on direct energy. The energy released per unit area of crack extension is simply calculated as [31,33,79]:

$$G_{IC} = \frac{1}{2B[\Delta(a)]}(P_1\delta_2 - P_2\delta_1), \qquad 3.19$$

where, load P_1 corresponding to opening deflection δ_1 drops to load P_2 corresponding to deflection δ_2 after a finite increment $[\Delta(a)]$ in the crack length. The loss of strain energy is increment in the area under P-δ curve, which becomes $(P_1\delta_2 - P_2\delta_1)$. The relation is valid only for linear load-deformation response. However, the area method is not recommended by ASTM designation; as it will not yield an initiation value or delamination resistance curve.

3.6 THE ENF SPECIMEN

The ENF test is a three-point bend test of a unidirectional laminate, and is used to obtain the compliance and the Mode II, the in-plane shear mode, interlaminar fracture toughness G_{IIc} of the test specimen. The specimen is shown in fig 3.2(a). The specimen contains a starter delamination located at the neutral plane at one end of the beam and is subjected to transverse shear and flexural loadings on account of lateral load applied at the mid span. The presence of transverse shear stresses generates interlaminar shear stresses. The

mechanisms corresponding to bending and shear actions are shown in Fig 3.4. The dominant mechanism (which actually depends upon the specimen geometry i.e. crack length and the thickness dimension; and material properties i.e. flexural modulus and interlaminar shear modulus), however, corresponds to relative sliding or in-plane shear affected crack driving force at the crack tip. The test involves measurement of the load-deflection data of the cracked specimen and calculation of the shear mode strain energy release under Mode II affected fracture and crack growth from the starter delamination. The widely popular approach to the Mode II delamination characterization, is again, through the application of linear elastic fracture mechanics. A test coupon can produce two types of G_{IIc}, one from the onset of non-linearity in the force-displacement curve $G_{IIc,i}$, and other from the maximum load point $G_{IIc,max}$.

As noted earlier, the ENF standard test method already exists, as adopted by JIS and AECMA and the ESIS protocol [68,69,54]. The ESIS protocol covers the determintion of critical strain energy release rate for initiation of delamination, and describes methods from both starter films and shear pre-cracks. With regards to the ASTM adoption, there have been many ASTM task groups conducting round-robin test programs examining the ENF specimen with specific aims as discussed in section 3.3. These efforts are a prelude to developing an ASTM standard for the measurement of Mode II interlaminar fracture toughness of composites. For the present discussion, since ASTM standardization for this test is still in process, guidance in relation to specimen preparation, procedure and data analysis is borrowed from the similar three-point flexure test as covered by ASTM Standard D-790, the DCB standards, and standards adopted by the JIS and ESIS and other published works for the ENF specimen.

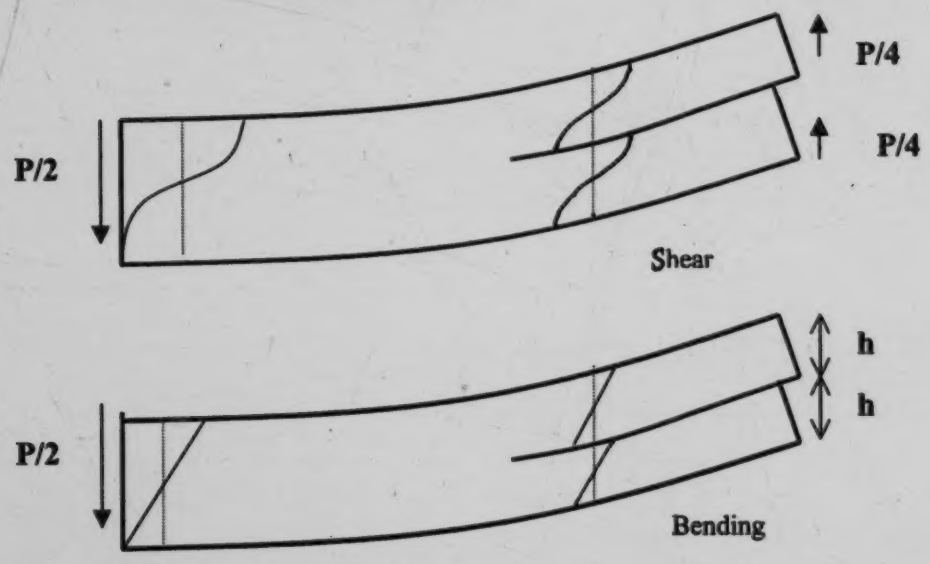

Fig. 3.4. Displacement fields of Mode II crack-driving mechanisms

3.6.1 SPECIMEN DETAILS

(1) Specimen Dimensions:

The specimen should be of unidirectional laminate. The specimen is nominally 20 mm wide. In general the specimen configuration, i.e. the thickness and distance between supports, is chosen to avoid large displacements and minimize transverse shear effects. The total specimen length is typically 120mm with distance between supports equal to 2L=100 mm [54]. Typical specimen thickness is 2h = 3-5 mm. Correction for variations resulting in large displacements are available in the ANNEX 3.2.

(2) Starter defects:

Consistent with the Mode I specimen, the ASTM prefers starter film at the laminate mid-thickness to be less than 13 μ m, (where as less than 15 μ m is recommended by the ESIS). Various polymer films like polyimide (PI), Teflon, or PTFE can be used. The film is to be sprayed with a release agent. The ratio of initial delamination length to half span **a / L** should be 0.5. ESIS recommends that ideally coupons with precrack and without precrcak, both, must be used in the test for new materials [54].

(3) Loading:

Typically, the ENF testing is performed under displacement control of 1mm/min with loading at the specimen mid-span. ESIS recommends loading rate of 1.0-0.5 mm/min. Unloading may be performed at higher rate of 5mm/min.

(4) Conditioning & Procedure:

Specimens should be conditioned to ensure consistent moisture content. For aerospace epoxies a temperature of 77^0 C for 10 days is suitable. Following the drying cycle, specimens should be stored in a dessicator for up to one day and removed before testing [54].

Crack-growth monitoring scheme consistent with Mode I may be used. Continuous plots of load versus loading point displacement should be recorded for both loading and unloading cycles. The crack shear displacement (CSD) measurement should also be made if possible.

Separate procedure and data analysis is applied for shear pre-cracked and Mode I pre-cracked specimens. Experimental compliance calibration is recommended for the

specimens precracked in Mode II, but it is not essential for specimens without precrack or specimens which are Mode I precracked. However, experimental compliance calibration is recommended for all specimens if experimental data analysis is preferred to the beam theory solutions. In all cases, if a corrected beam theory is used, at least one measurement is required for delamination length a='0' (insert outside the outer load point) in order to obtain a value of flexural modulus. Load and displacement valued may be tabulated for the crack length a= 0, 15, 20, 15, 30, 35, 40 mm.

(5) Interpretation of Results:

During the load and displacement measurement (at the load point) several values for an initiation value of G_{IIc} are available. (1) the point of deviation from linearity in the load-displacement curve (NL), (2) the point where delamination is visually observed on the edge (VIS), measured with a microscope, and (3) at the point where initial compliance C_0 (δ / P) has an increase of 5%; the offset line should be drawn from the original linear portion starting from the origin; the point of intersection of this line with the load-displacement curve defines the value of P and δ to be used. (4) if the 5% offset line is further along the curve than the maximum load point, the maximum load point is used to calculate G_{IIc}. The NL G_{IIc} value, is typically the lowest of the initiation values, but can show a significant scatter.

3.6.2 DATA ANALYSIS

In order to determine the values of G_{IIc}, two approaches are available;(a) experimental, and, (b) the beam theory methods. The data required are the P, δ, and the crack length 'a', and specimen dimensions.

(a) Experimental method

The procedure can be used to get G_{IIc} for the Mode I precracked specimens, shear precracked specimens, and specimens which are not precracked. Experimentally G_{IIc} has been obtained for machined cracked ENF specimens without insert [87]. Crack length is measured during the calibration load cycle. It should be noted that for the shear-precracked specimens G_{IIc} should be essentially determined from the experimental compliance calibration performed on the same specimen. Starter crack preparation (film thickness and pre-cracking) has very significant effect and CSD measurement gives the precise information on the crack initiation [64]. A least square regression analysis can then be carried out of the form:

$$C = C_0 + ma^3, \qquad 3.20(a)$$

where C_0 is the initial compliance and 'm' is a parameter.

and G_{IIc} is calculated as

$$G_{IIc} = \frac{3ma^2 P^2}{2B} \qquad 3.20(b)$$

The unstable nature of growth of crack in ENF specimen renders the data-reduction method much less useful. And the measurement of the fracture toughness relies heavily on the method of interpretation of the data. An analytical method described below is immensely useful in understanding the behaviour of the ENF specimen.

(2) The Beam Theory Method

The mechanics of ENF geometry is complex because of the presence of a crack in a finite domain, and an elasticity solution incorporating crack-tip singularity is not available. However, the crack-tip singularity is a local phenomenon that should not significantly influence the global deformation of the ENF specimen in the delaminated and undelaminated regions. Neglecting the effect of singularity and using linear elastic small-deflection approach, a theoretical estimation of the specimen compliance using a beam theory is often suitable to analyze the ENF specimen. It can also be used in correlating and predicting the results of experiments involving different material properties and specimen configurations. For this reason beam theory equations with and without shear deformations have been proposed in the literature [71,72].

An analysis, as used by Russell and Street [71] from simple beam theory is detailed below. A unidirectional composite beam with in-plane elastic modulus in fibre direction E_1, width B, and half span length L is considered with mid-plane delamination 'a'. A load P is applied at the mid-plane producing corresponding displacement δ at the mid-plane load point. A free body diagram is shown in Fig 3.5 [31].

Referring back, the compliance of the specimen is defined as the displacement δ at the central loading point divided by the applied load. Based on the notations defined in Fig 3.6, the deflection δ can be expressed [88]:

$$\delta = \frac{1}{2}(\Delta_{AB} + \Delta_{BC} + \Delta_{CD}) \qquad 3.21$$

Beams BC and CD are modeled as cantilever beams. The analysis is based on considering only the bending deformation, neglecting shear deformation. In addition, it is assumed that the cross-section at C does not warp because it is an approximate line of symmetry for the beam.

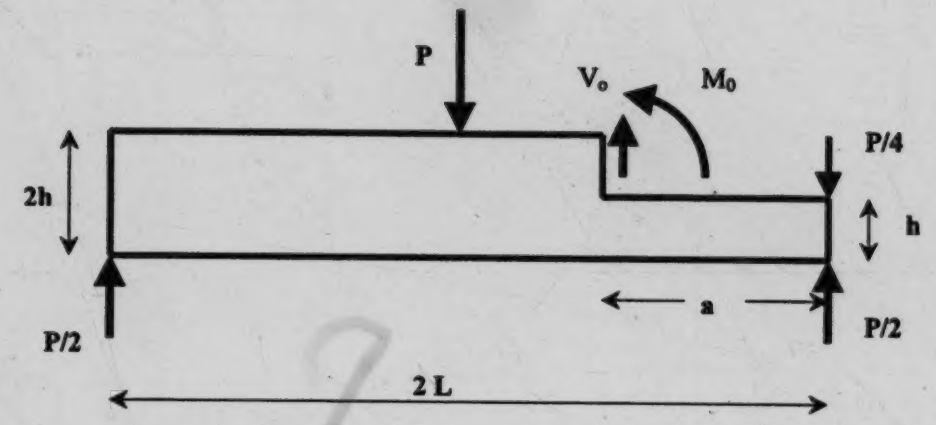

$V_0 = P/4$; $M_0 = Pa/4$

Fig 3.5 Free-Body Diagram for the ENF specimen

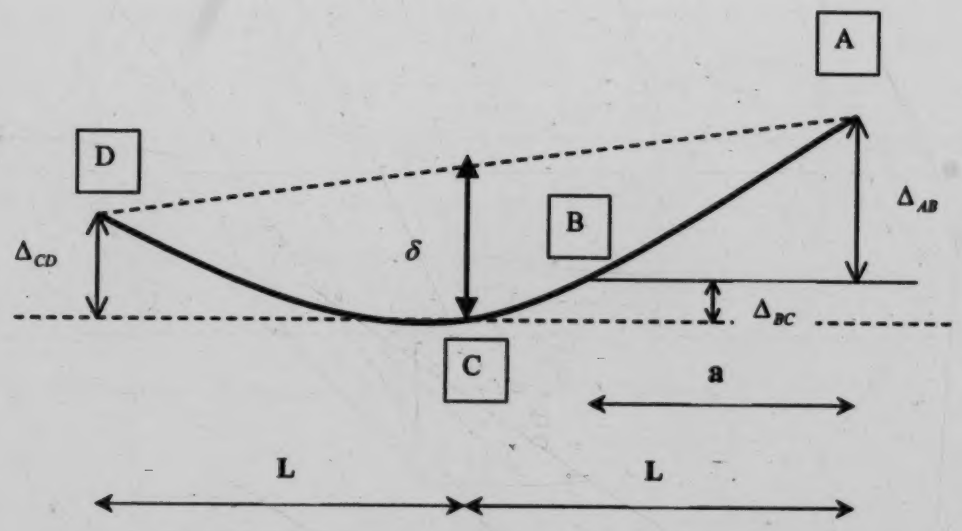

Fig 3.6 Definition of various displacements components for the ENF specimen

Under such assumptions, each of the above deflections may be determined from the classical beam theory approach [89,90,91,92].

Cantilever beam CD is fixed at C (x=0) and loaded with a load of P/ 2 at D (x=L). Hence

$$\Delta_{CD} = \frac{P/2.L^3}{3E_1 I}, \text{ with I= B(2h)}^3/12$$

Or,

$$\Delta_{CD} = \frac{P.L^3}{4E_1 Bh^3} \qquad 3.22$$

For the deflection Δ_{BC}, cantilever beam of length (L-a) and fixed at point C (x=0) with load P /2 and moment Pa /2 at the free end B (x=(L-a)) is considered. Moment at location 'x' is equal to $\frac{Pa}{2} + \frac{P}{2}\{(L-a)-x)\} = \frac{P}{2}(L-x)$. Integrating this expression twice between x = 0 and x = (L-a) gives:

$$\Delta_{BC} = \frac{P(2L^3 - 3aL^2 + a^3)}{8E_1 Bh^3} \qquad 3.23$$

For the deflection AB there are two components, one $\Delta_{AB,1}$, due to the rigid body rotation at B; and another $\Delta_{AB,2}$, due to the bending deformation of the beam. The two parallel cantilever beams of the delamination region AB carry a load of P/ 4 each at their ends. The parallel beams are assumed to deform freely under action of shearing stresses.

$$\text{Now } \Delta_{AB,1} = \{P\frac{(L^2 - a^2)}{4}.\frac{12}{E_1 B(2h)^3}\}.a = \frac{3P(aL^2 - a^3)}{8E_1 Bh^3} \qquad 3.24(a)$$

And component due to bending deformation is

$$\Delta_{AB,2} = \frac{P/4.a^3}{3E_1 I}, \text{ where I = B(h)}^3/12$$

Or,

$$\Delta_{AB,2} = \frac{Pa^3}{E_1 Bh^3} \qquad 3.24(b)$$

So Δ_{AB} can be obtained using 3.24(a) and 3.24(b) as below

$$\Delta_{AB} = \Delta_{AB,1} + \Delta_{AB,2} \qquad 3.25$$

Now, using equations 3.22 to 3.25, in equation 3.21 we get

$$\delta = \frac{1}{2} P \frac{(4L^3 + 6a^3)}{8E_1 Bh^3} \qquad 3.26$$

Finally, compliance can be found by using C= δ / P and is given by the expression

$$C_{II} = \frac{(2L^3 + 3a^3)}{8E_1 Bh^3} \qquad 3.27$$

The above expression can be used in the Irwin and Kies relation, similar to Mode I calculation, for the calculation of critical energy release rate as below:

$$G_{II} = -\frac{d\pi}{dA} = P^2 \frac{1}{2B} \frac{dC_{II}}{da} \qquad 3.28$$

Or,

$$G^{BT}{}_{II} = \frac{9P^2 a^2}{16E_1 B^2 h^3} \qquad 3.29$$

Alternative G_{II} may be expressed by the so-called displacement method as

$$G^{BT}{}_{II} = \frac{9Pa^2\delta}{2B(2L^3 + 3a^3)} \qquad 3.30$$

Correction for Transverse Shear Deformations

Equation 3.27 for compliance, and equations 3.29 and 3.30 for the fracture toughness need to be corrected for *transverse shear deformation effects* for materials that do not have large shear rigidity, and have large thickness-crack length ratio. The corrected value of G_{II} including the shear deformation effects can be derived by the exact same procedure as above incorporating shear modulus G_{13} [72,93]. Corrected fracture toughness is given by [5,54,72,88,94]

$$G^{SH}{}_{II} = G^{BT}{}_{II}\left(1 + 0.2\frac{E_1 h^2}{G_{13} a^2}\right)$$

Sometimes the above equation is expressed as $G^{SH}{}_{II} = G_{II}(1+S)$, *where* S represents the shear correction. Hence, the complete expression for the fracture toughness is given by

$$G^{SH}{}_{II} = \frac{9Pa^2\delta}{2B(2L^3 + 3a^3)}\left(1 + 0.2\frac{E_1 h^2}{G_{13} a^2}\right) \qquad 3.31$$

Alternatively in terms of load only expression, we have,

$$G^{SH}{}_{II} = \frac{9}{16}\frac{P^2a^2}{B^2E_1h^3}(1+0.2\frac{E_1h^2}{G_{13}a^2}) \qquad 3.32$$

The corrected compliance due to shear deformation effects is given by [94]:

$$C^{SH}{}_{II} = C_{II}\{1+(\frac{h}{L})^2(\frac{E_1}{G_{13}})(\frac{[1.2+0.9(\frac{a}{L})]}{[1+1.5(\frac{a}{L})^3]})\} \qquad 3.33$$

It may be noted that for polymer laminates the ratio E_1 / G_{13} can be large, up-to 20-50. So shear deformation effects can be very significant. For new materials E_1 and G_{13} may be measured using appropriate test methods such as ASTM D3039 and D4255 [54]. G_{13} is frequently assumed equal to G_{12}.

Focusing the attention on equation 3.32, similar to the behaviour of DCB specimen, it can be said that the beam theory result including the shear deformation effects may underestimate the strain energy release rate due to the neglection of the elastic supports at the beam roots. However, as opposed to the DCB specimen the beams (two cantilever beams at location AB) are bent in the same sense, and the correction factor does not involve root rotation. The correction parameter accounts only for the shear deformation effects (and shear at the root due to elastic support). Hence the correction χ_{II} is much less than the correction χ_I for the DCB specimen. Empirically it has been suggested that the parameter χ_{II} for the ENF test should be about half of that of the DCB specimen [95].

The span length 'L' needs to be modified by an addition of χ_0 and, the correction needed to the crack length 'a' is χ_{II}. The value of parameter χ_0 is close to that for mode I.
So the modified compliance and G_{II} becomes [82,95]:

$$C^{cor}_{II} = \frac{(2[L+\chi_0.h]^3+3[a+\chi_{II}.h]^3)}{8E_1Bh^3} \qquad 3.34$$

$$G^{cor}{}_{II} = \frac{9P[a+\chi_{II}.h]^2\delta}{2B(2[L+\chi_0.h]^3+3[a+\chi_{II}.h]^3)} \qquad 3.35$$

Interestingly, the expression using Timoshenko beam theory accounting for shear deformation as in 3.32 and the expression using the correction parameter χ_{II} as in equation 3.35 give very similar results. This is because both the expressions account for shear deformation effects alone. However, the procedure of using (compliance)$^{1/3}$ versus the crack length plot to get the correction factor as in DCB specimen is not readily

available for the ENF specimen. Hence the approach of using the parameter χ for the ENF specimen is not as popular as for the DCB specimen.

The actual theoretical expression for χ_{II} can be found from the beam on elastic foundation model as given by the equation below, similar to that for the Mode I; where in replacing '18K' by '63' [95].

$$\chi_{II} = \sqrt{\frac{1.(a_{66})}{63^{*}.(a_{11})}}\sqrt{3-2(\frac{\Gamma}{(\Gamma+1)})^{2}} \qquad 3.36$$

where, $\Gamma = 1.18\frac{a_{66}}{\sqrt{a_{11}a_{22}}}$

The coefficients a_{11}, a_{22}, a_{66} are, again, the elastic compliances of the composite specimen. The above equation gives χ_{II} about 0.42 times as that for the Mode I [85,95,96]. Such simple approximation for the correction χ_{II} to the ENF specimen from the DCB specimen correction χ_{I} is based on the realization that cantilever portion AB in the ENF specimen behaves the same as the ELS specimen and hence the correction factor for the ELS can be applied to the ENF specimen [85,95,96]. This could be advantageous, as χ_{I} from the DCB specimen is readily available.

Alternatively, the fracture toughness can be expressed via load method as below, where the correction parameter χ_{II} alone is satisfactory

$$G_{II} = \frac{9P^{2}(a+\chi_{II}.h)^{2}}{16B^{2}h^{3}E_{1}} \qquad 3.37$$

Corrections for Large Displacement Effects

Similar to the DCB specimen, correction factors due to *large displacements* and end block effects need to be taken into account [54,82]. The combination of high modulus ratios and slender thickness of the beams leads to large displacements in the specimens. However, very large effects are uncommon, and as a good approximation only the first term of the series expression is sufficient. Normally for $\delta / L < 0.2$, the correction can be neglected [54].

For the effective shortening of the beam arm, the correction factor F can be used. A correction factor also needs to be applied for the compliance values. Such a factor is represented as N. Hence, we have the modified expression for the so called displacement method as:

$$G_{II}^{Id} = G^{SH}{}_{II}[\frac{F}{N}] \qquad 3.38$$

The values of F and N depend upon the ratio **a / L** and also on the ratio δ / L. The values of the corrections are generally more than those for the DCB specimen. For a /L =0.5 , we get the corrections:

$$F = 1-(0.6099)\{\frac{\delta}{L}\}^2 \qquad 3.39$$

$$N = 1+(0.3766)\{\frac{\delta}{L}\}^2 \qquad 3.40$$

For other values of **a/L** , the correction factors F and N are given in ANNEX 3.2 .

ANNEX 3.1
Large Displacement and End Block Corrections in Mode I DCB Specimen [53,54,81-84].

Large displacements effects may be corrected for by inclusion of parameter F. If the end block effects are important a second parameter, N, a displacement correction should be included.

$$F = 1 - \Theta_1(\frac{\delta}{a})^2 - \Theta_2(\frac{\delta t}{a^2})$$

$$N = 1 - \Theta_3(\frac{s}{a})^3 - \Theta_4(\frac{\delta}{a})^2 - \Theta_5(\frac{\delta t}{a^2})$$

Where,

$$\Theta_1 = \frac{3}{10}$$
$$\Theta_2 = \frac{3}{2}$$
$$\Theta_3 = 1$$
$$\Theta_4 = \frac{9}{35}$$
$$\Theta_5 = \frac{9}{8}\{1 - (\frac{s}{a})^2\}$$

And parameters a, δ, s, t are defined as

a = instantaneous measured delamination crack length from the load point to the crack tip, corresponding to the load P causing crack growth.

δ = (vertical) opening displacement at the load point between two arms of the specimen

s = half width of the end block, or distance from the center of the loading pin (or hinge pin center) to its (inner) edge. This is shown in fig3.7.

t = the distance from the center of loading pin (or hinge pin) to the mid-plane of one specimen arm. This is shown in Fig. 3.7.

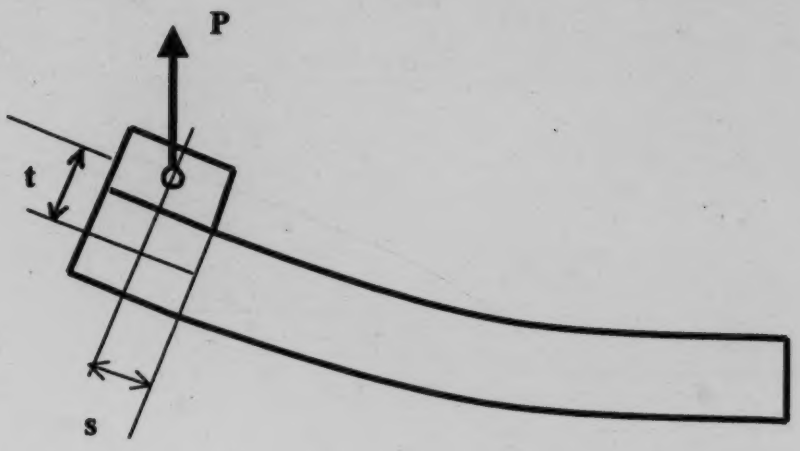

Fig 3.7 End Block Effects for the DCB Specimen

ANNEX 3.2
Large Displacement Corrections in Mode II ENF Specimen [54,82].

$$F = 1 - \Xi_1 (\frac{\delta}{L})^2$$

$$N = 1 + \Xi_2 (\frac{\delta}{L})^2$$

where,

$$\Xi_1 = \left[\frac{3}{5}\right]\left\{\frac{15\left[1-(\frac{a}{L})^3\right]^2 - 40\left(\frac{a}{L}\right)^2\left[1-(\frac{a}{L})^3\right] + 48\left(\frac{a}{L}\right)^4}{\left[2+3(\frac{a}{L})^3\right]^2}\right\}$$

$$\Xi_2 = \left[\frac{3}{35}\right]\left\{\frac{37+147\left(\frac{a}{L}\right)^3 + 210\left(\frac{a}{L}\right)^6 + 105\left(\frac{a}{L}\right)^9}{\left[2+3(\frac{a}{L})^3\right]^3}\right\}$$

And parameters a, δ, L are defined as

a = instantaneously measured delamination crack length

δ = (vertical) displacement at the load point

L= specimen half-length

Chapter 4

FINITE ELEMENT MODEL OF THE TEST SPECIMENS

4.1 INTRODUCTION

The finite element method is increasingly becoming an attractive and frequently indispensable part of engineering analysis and design. The finite element analysis solves a mathematical idealization of a physical problem, which is arrived at, after employing certain assumptions that together lead to differential equations governing the mathematical model [97,98,99]. Its own accuracy depends upon the selected mathematical model. It is often employed as a useful numerical tool to model structures having complex geometry, loading or significant non-linearity. Further the FE analysis has been, for several years applied directly to the fracture mechanics calculations with or without the crack tip singularities. The very first, and the most popular application of the finite element method, however, has been the linear elastic static analysis of solids and structures. Alternatively, higher order finite elements may be employed to achieve the desired accuracy for the complex problems.

Although most works for evaluating the interlaminar Mode I and Mode II fracture toughness of the standard test specimens have involved experimental studies, computational simulation using finite elements has been attempted by many authors [94,95,101-105]. In the present finite element study a two-dimensional linear elastic model of the composite specimens for the DCB and the ENF tests are analyzed using the ANASYS package version 5.6 [100]. The composite specimens consist of two-laminae unidirectional orthotropic homogeneous beams with starter defect in the middle interlaminar region.

Though may times elusive, the most fruitful situation calls for corroboration of the experimental evidence with the analytical results. In the DCB and ENF specimen models, the exact analytical approach to express G_{IIC} is too complex and cannot proceed without another set of simplifying assumptions (in addition to homogeneity) viz.; neglection of the crack tip singularity on global deformation field, empirical relation simplification to avoid complex calculation for the large deflection and non- linearity effects; empirical relation simplification to avoid complex calculation for the loading end

block effects, neglection of friction effects between crack faces etc. The finite element model developed could be used to validate or refute the corrected fracture toughness expressions derived analytically (after using simplifying assumptions and employing some empirical parameters) as in the equations 3.15 and 3.37. In addition experimental procedure always involves an element of human error in specimen preparation, geometry of the starter delamination, or recording of the crack length observations. These errors are absent in the finite element analysis. Hence, finite element analysis of the ENF and DCB specimen models can provide a very useful insight into the specimen behaviour and performance, and also lead to interesting explanations to some experimental findings.

In the finite element model each of the specimens for the DCB and ENF test has three layers. The top and the bottom layers are of orthotropic material (properties similar to glass–epoxy composite). The middle layer is of isotropic material and represents the thin resin rich interlaminar region. Schematic diagram of the DCB and the ENF specimen models are shown in Fig 4.4 and Fig. 4.7, respectively. The material properties of these three layers are defined subsequently. Both the specimen models are similar except for the lengths, the boundary conditions, and the loading, which are described subsequently. For the DCB and the ENF specimen models, eight-nodded plain strain element PLANE82 is used in the analysis with option of nodal stress calculation. Consistent with our earlier discussion on standard nomenclature in literature, the two-dimensional model is in x-z plane with the specimen length along the x-direction and the specimen thickness in the z-direction (however, it may be noted this 2-D geometry is in ANSYS x-y plane and we will stick to the standard convention in literature while defining the directional material properties, etc.). Each node has three degrees of freedom: U_x,U_y, and ROT_z in ANSYS notation.

The starter defect details, the crack tip geometry, and the material properties of the DCB and ENF specimens are the exact same. The starter insert defect is in the center of the middle interlaminar layer. Conforming to the ASTM standards, the thickness of the starter defect is 13 microns. The insert defect is not pre-cracked. In the models, the crack tip bluntness of the starter defect is assumed to be mathematically represented by an ellipse. In the model the ellipse at the crack tip is modeled by four-point-centre circular arc method. So the crack tip contour can be expressed as:

$$\left(\frac{x}{a}\right)^2+\left(\frac{z}{b}\right)^2=1,\begin{pmatrix}0\le x\le a\\ -b\le z\le b\end{pmatrix} \qquad 4.1$$

where $2a=13/2\mu m$, $2b=13\mu m$

The starter defect contour is shown in the Fig 4.1. The ratio of semi-major axis (perpendicular to the crack length = 13 micron) to semi-minor axis (along the crack length) is 2. The aspect ratio of 2 gives the maximum principal stress at the corner of the crack tip (away from the center of the crack tip) and represents the physical situation in the experiments [104,105]. In the experiments, the crack initiates from the corner of the

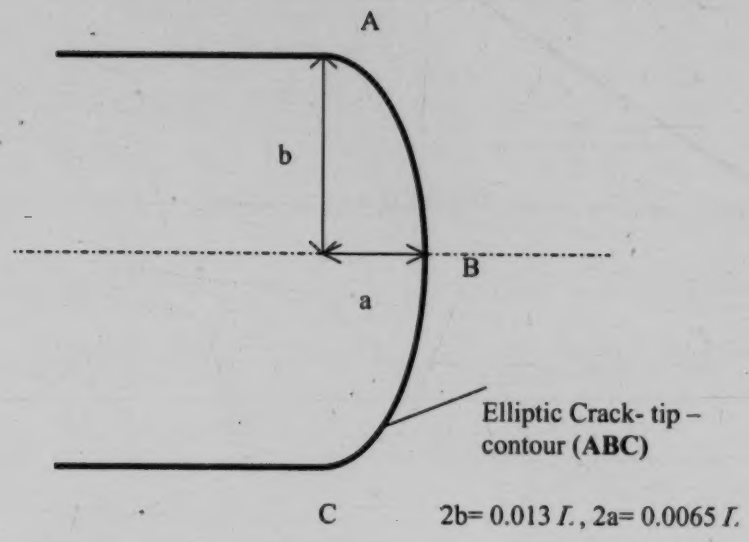

Fig 4.1 Starter defect crack contour

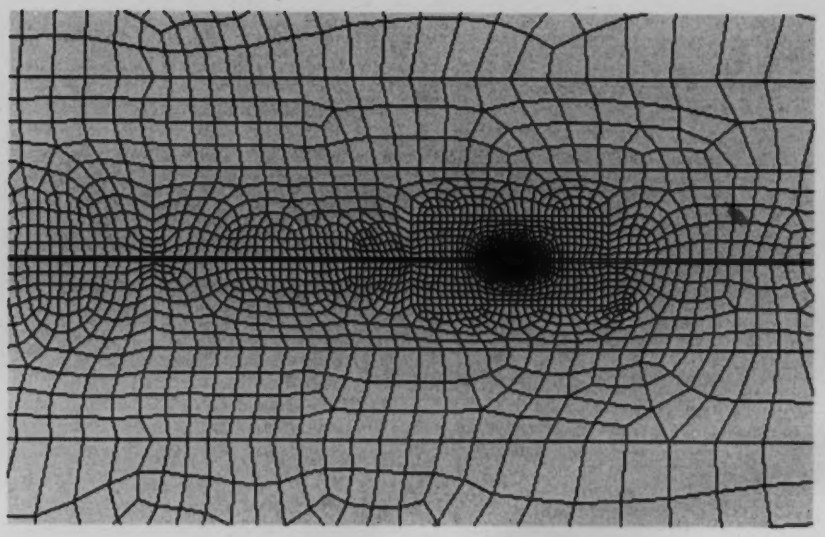

Fig 4.2 Finite element discretization of the DCB / ENF specimen model

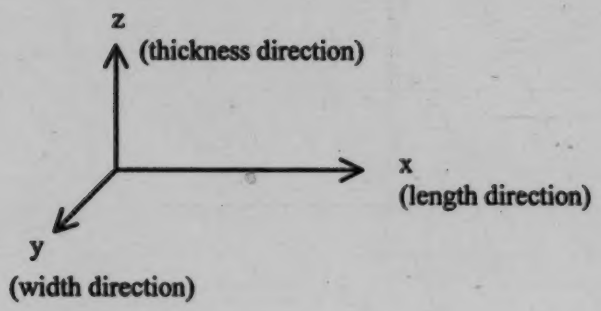

Fig. 4.3 Mesh Details of crack tip elements and Ref axes.

starter crack tends to grow close to the fibre/matrix interface along the boundary of the resin-rich region. Although most finite element work has been done with sharp starter delaminations, similar models of blunt crack tip in contrast to a sharp crack tip are available [104,105]. In reality a sharp crack tip in the DCB or ENF specimens does not exist in the testing coupons either with or without pre-cracking. So the assumption of blunt crack tip with crack growth from the corner of the crack tip is more reasonable. However, it may be noted that since the real crack tip contour may not be exactly elliptic, the FEM models used here do not represent the realistic stress distribution and deformation behaviour at the crack tip, even though the global deformation behaviour is adequately represented.

As noted earlier the two specimens are similar with similar mesh discretization. The mesh discretization of the specimen models and the details of the crack tip elements are shown in Fig 4.2 and Fig. 4.3. The manual [100] recommends at least one element for every 15-30 degrees arc along a circular crack tip contour and the results of stress analysis may vary depending upon the refinement of mesh near the crack tip. However, our mesh size along the elliptic crack tip contour conforms to the above criterion.

The current focus is to study the specimen geometry effects on the Mode I and Mode II fracture toughness. In the past, the specimen width has shown no significant effect on the fracture toughness values, except for the free edge effects, both for the Mode I and Mode II tests. However the specimen thickness effect on fracture toughness values has created controversy for the ENF test [49,61,83,107]. Hence, for the current study the specimen thickness effect is investigated. To achieve this objective, DCB and ENF test specimens of different thickness values of 5mm, 10mm, and 15mm are modeled and analyzed. The dimensions and boundary conditions of the models correspond to the full-scale test coupons. The specimen thickness is controlled by varying the thickness of each of the two orthotropic laminae of the composite specimens, while keeping the middle interlaminar region and the starter delamination region exactly the same.

In the literature there are many approaches to evaluate the fracture toughness numerically by the finite element model [95]. Three methods are popular. The first involves a curve fitting polynomial for plot of C with 'a', the crack length, computing the correction factor χ_I, χ_{II} using equation 3.13 or 3.34, respectively, for the DCB and the ENF specimen. Fracture toughness can be evaluated using equation 3.15 and 3.37. Second is the use of J-integral calculations [14,22,57]. The third technique is the virtual crack closure method in which crack tip is released [44,94].

For the present study a simpler method is used. The stress distribution and specifically, the stress at the maximum stress location on the crack tip contour and its neighbourhood from which the crack growth is most likely to originate is analyzed. The stress value considered along the crack tip contour is the maximum principal stress for the DCB specimen. For the ENF specimen, the stress values considered along the crack tip contour are for the interlaminar shear stress, the normal stress along x-axis, the von Misses stress, and the maximum principal stress. In addition, for the ENF specimen the values at

another location - the interface of the interlaminar region (having low modulus isotropic properties) and the lamina (having orthotropic properties) – need to be considered for these stresses. These values at the interface location need to be considered as there is abrupt shift in material properties at the interface and the stress values shoot up at the interface in the high modulus orthotropic lamina region. Crack initiation may occur directly from the interface if bond strength is sufficiently low as explained further in section 4.3.1 and section 5.2. Evidently, any of these stress values at either of the two locations may yield the most critical stress corresponding to crack growth in the ENF specimen.

For the specimens of varying thicknesses, load of appropriate value is applied in specimens in accordance with equations 3.15 and 3.37 for the DCB and ENF specimens, respectively. It can be argued that if most critical stress at some location on the crack tip contour remains the same for specimens of varying thicknesses, the fracture toughness of the specimens stays the same. This is expected based on the assumption of self-similarity, and neglection of non-linearity effects. Such a study is believed to be an important step in characterization of fracture toughness as a material property.

Surprisingly, given the amount of work performed on analysis and widespread use of ENF specimen, remarkably little work has been performed to establish whether the test yields results that are independent of specimen thickness. This appears to be an important step along the long road to the standardization of the ENF test. The author of this work has found no finite element study to investigate the thickness effect on the DCB and ENF specimens except possibly one for the ENF specimen [101].

4.2 THE DCB SPECIMEN MODEL

The model for the composite Double Cantilever Beam test specimen consists of three layers. The top and the bottom layers are orthotropic layers representing two unidirectional laminae, and the isotropic matrix layer sandwiched between the two laminae represents the resin-rich interlaminar region. The dimensions of the test specimen are 100 mm in length (L), and '2h' mm in the overall thickness of all the three layers. The width ('B'= 20mm) of the specimen is inputted as a real constant. The middle resin-rich interlaminar layer is 26μ m thick. In the center of this 26μ interlaminar region, there is starter defect of 13μ thickness. The length of this starter defect is 50 mm ('a'). The schematic of the DCB specimen model is shown is Fig 4.4.

The mesh details near the crack tip region can be obtained from Fig 4.2 and Fig. 4.3, and the crack tip bluntness from Fig. 4.1. The specimen thickness (=2h) varies as 5mm, 10mm, and 15mm for the various cases. For the case of specimen thickness of 10 mm, a

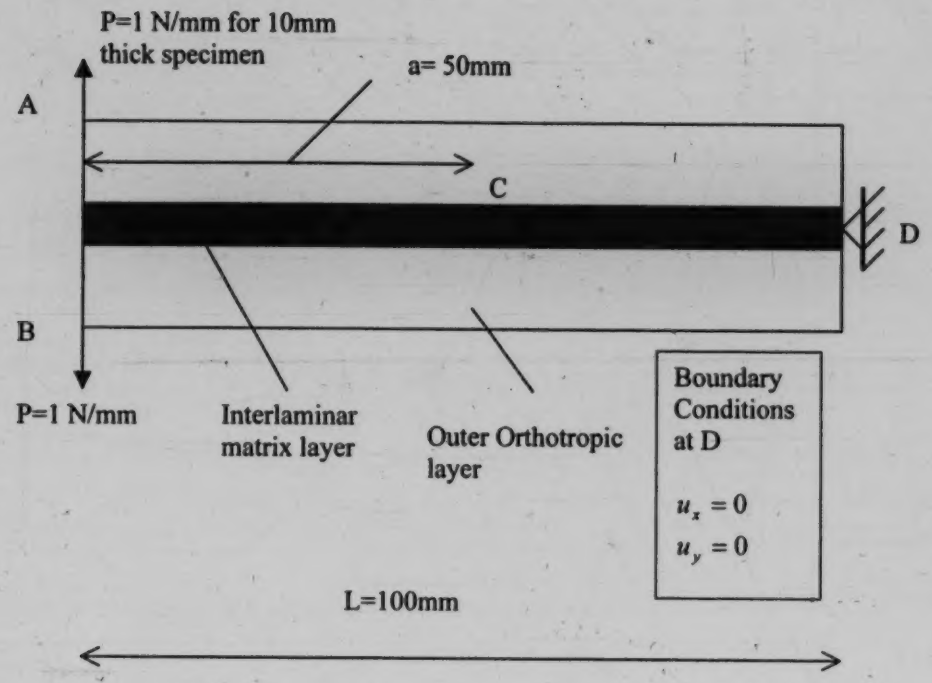

Fig 4.4 Model of the DCB Specimen

tensile load of 1 N/mm is applied on the nodes of loading points (located at the top and bottom free end of the beam containing the insert defect) as shown in Fig 4.4. For other thicknesses, appropriate loading is applied as explained later in this section. In the finite element model there is no end block. The node at the center of the other end is pinned with boundary condition of zero displacements in 'x' and 'y' directions (ANASYS notation).

The material properties of the specimen are given below:

For the composite outer layers:
$E_1 = 26{,}600 MPa$,
$E_2 = 4{,}700 MPa, \nu_{21} = 0.09, G_{12} = 2800 MPa$

For resin-rich interlaminar region:
E=3100 MPa, $\nu = 0.35$,

The Mode I fracture toughness is given by equation 3.15

$$G_{IC} = \frac{F}{1}\frac{12P^2(a+\chi_I h)^2}{B^2 E_1 h^3} \qquad 4.2$$

where P corresponds to the load causing fracture.

We will examine the need for the corrections factors involved in the above equation, due to crack tip extension and rotation accounted by parameter χ_I, and effect of geometrical non-linearity arising due to large displacements, accounted for by parameter 'F'

The correction factor χ_I depends upon the elastic properties of the material and can be found from equations 3.11 and 3.12 from beam on elastic foundation model. We have,

$$\Gamma = 1.18\frac{a_{66}}{\sqrt{a_{11}a_{22}}}$$

The coefficients a_{11}, a_{22}, a_{66} are the elastic compliances of the composite specimen, with notations similar to the equation 1.6 of section 1.4. in the chapter 1. The elastic compliances are the inverse of elastic (stiffness) constants. The values of a_{11}, a_{22}, a_{66} are respectively (37.594, 212.766, 357.143) x $10^{-3}(GPa)^{-1}$ for our model. Using the empirical relation '18K' =11 in equation 3.11, the correction factor χ_I for the DCB specimen works out to be:

$$\chi_I = 1.19 \qquad 4.3$$

To investigate thickness effects on G_{IC} values, we adopt a semi-analytical approach. To begin with, we assume that left-hand side of equation 4.2 represents a toughness value, that is a material property, independent of thickness. Now, let the load applied on 10mm DCB specimen be P = 1 N/mm. This load is an arbitrary load and need not correspond to the actual fracture load. So for varying thickness values, for 2h = 5, 10, and 15mm, using expression in equation 4.2 if expression on right-hand side has to be constant, we obtain the corresponding load values as 0.3734, 1.0, and 1.7444, respectively, (F is assumed unity at this stage). These values are appropriate loads which must be applied to the specimens of different thicknesses of 5mm, 10mm, and 15mm, to produce the same G_{IIc}. Now, to check the validity of our initial assumption, for the appropriate loads derived thus, the three specimens should have the same 'most critical' stress. The 'most critical' stress is represented by the maximum principal stress at the corner of the crack tip for the DCB specimen. If this stress is the same for the three specimens, so is the fracture stress, and the expression 4.2 is indeed independent of thickness effect.

Now, we examine the correction factor 'F'. Using the values of δ / a it is observed that the ratio of the opening displacement to the crack length is almost 0.5% for thickness 2h=15mm, and almost 2% for 2h=5mm. The values of F to be used can be obtained from the equation in ANNEX 3.1. The value of 't', the distance from the center of loading pin (or hinge pin) to the mid-plane of one specimen arm is taken as h/2. Using $\Theta_1 = \frac{3}{10}$, and $\Theta_2 = \frac{3}{2}$, F is given by

$$F = 1 - \frac{3}{10}\left(\frac{\delta}{a}\right)^2 - \frac{3}{2}\left(\frac{\delta t}{a^2}\right)$$

The 'F' values calculated from above equation for various thickness can be obtained as given in Table 4.1 below.

Table 4.1
Large Deformation Corrections

Specimen Thickness (2h)	δ	δ / a (%)	F
15	2 x 0.12364	0.4946	0.9994
10	2 x 0.20387	0.8154	0.9993
5	2 x 0.51812	2.0724	0.9991

It can be seen that the corrections factor (F) due to the effect of large deflection is very small and is unwarranted for the present study. Hence F may be omitted. The neglection of F in present case is also supported by the test protocol [54]. (Also, for the finite element model, N is taken as unity as there is no end-block effect).

4.2.1 RESULTS AND DISCUSSION

For the DCB specimen, as noted earlier, the fracture stress is believed to be guided by the maximum principal stress. The maximum principal stress contours near the crack tip region for the three thicknesses of the specimens are shown in Fig 4.5. Also variation of maximum principal stress for a path along crack tip is shown in Fig. 4.6. The maximum principal stress values for various specimen thickness are given in the Table 4.2

Table 4.2
Study on Dependence of Mode I Fracture Toughness on Specimen Thickness

Thickness(2 h) (mm)	Maximum Principal Stress (N/mm^2)
5.0	100.205
10.0	99.072
15.0	98.609

This leads to the conclusion that there is no significant effect of the specimen thickness on the maximum principal stress values and hence on the fracture stress values.

This finding is in accordance with earlier studies [61 83,106]. All these references are based on experimental results using corrected beam theory expressions in the analysis. Although there was an experimental scatter in values, there was no preferred trend. Davies et. al. [61] studied carbon/epoxy and carbon/PEEK specimens of thickness values: 1.6mm, 3.2mm and 5.2 mm. The starter films of 30-20 μ m thickness were introduced at mid-thickness during moulding. Reasonably constant G_{Ic} propagation values were found for carbon/epoxy specimens of varying thickness. However, for carbon/PEEK specimens, an increase of about 10% in the G_{Ic} propagation values was noted, which was close to the standard deviation of the measured values. Hence, they concluded Mode I delamination resistance to be reasonably independent of the specimen geometry. Hashemi et. al. [83] studied the thickness effect of carbon/PEEK specimens on Mode I initiation and stick/slip (s/s) propagation G_{Ic}(s/s-prop) values. The specimen thickness used were: 1.55mm, 3.16mm, 4.35mm, and 5.30mm. They noted no significant effect of the specimen thickness on the $G_{Ic,ini}$ and G_{Ic}(s/s-prop) values. However in thickest specimen, increase of G_{Ic}(s/s-prop) values was observed, but attributed to the crack-tip splitting ahead of the crack tip and fibre-bridging behind the crack in thick specimens. Hojo et. al. [106] have again studied carbon-AS4/PEEK and T800/Epoxy specimens having 30 μ m inserts with and without pre-cracks for the $G_{Ic,ini}$ and G_{Ic}(prop) values for the specimen thickness 3mm, 4mm, 5mm and 8 mm. Both, carbon-AS4/PEEK and T800/epoxy specimens showed no thickness effect on the $G_{Ic,ini}$ values; the thickness effect on the G_{Ic}(prop) values was perceptible but smaller than obtained by Davies [61] and attributed to prominent fibre-bridging in thicker specimens.

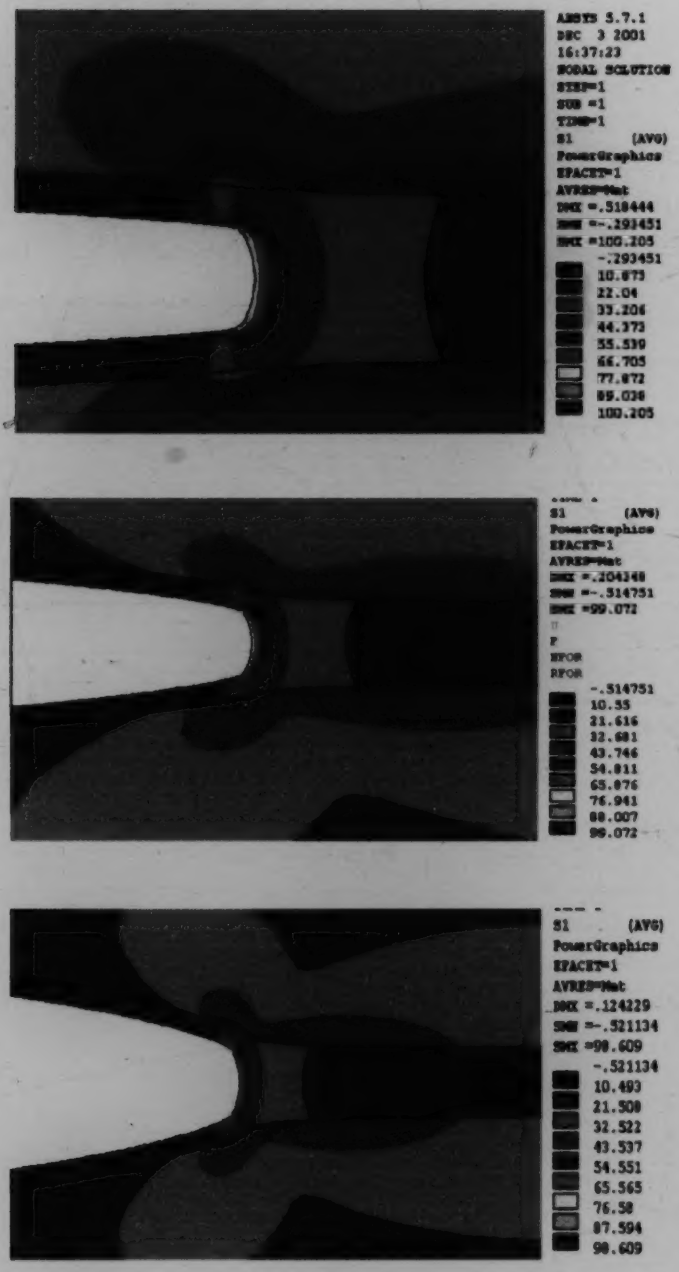

(a) Specimen thickness=5mm

(b) Specimen thickness=10mm

(c) Specimen thickness=15mm

Fig.4.5 Maximum principal stress contours near the crack tip of DCB specimens

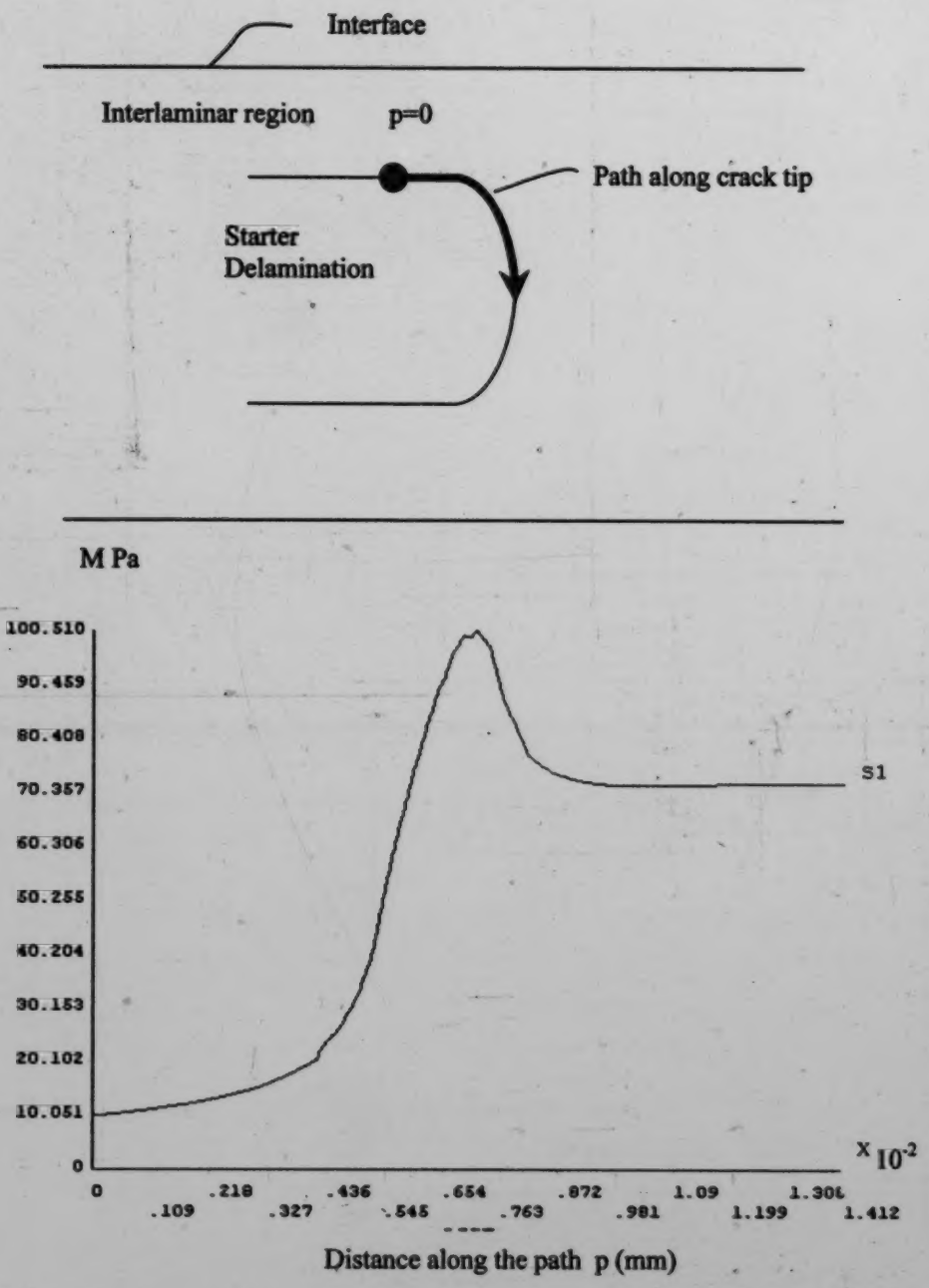

Fig 4.6 Variation of the max principal stress (S1) for the path along crack tip of 10mm DCB specimen

4.3 THE ENF SPECIMEN MODEL

The model for the composite End Notched Flexure test specimen consists of three layers similar to the DCB specimen. The top and the bottom layers are orthotropic layers representing two unidirectional laminae, and the isotropic matrix layer sandwiched between the two laminae represents the resin-rich interlaminar region. A schematic diagram of the ENF specimen model is shown in Fig. 4.7. The dimensions of the test specimen are span length ('2L') = 100mm, and specimen thickness ('2h') =5, 10 and 15 mm. The specimen width is 20mm. The thickness of the middle resin-rich interlaminar layer is 26μm with a starter (through-thickness) defect of 13μm thickness in its center. The length of starter delamination crack ('a') is 25mm. This gives the ratio of **a/L** equal to 0.5 as recommended by the ESIS. The crack contour in the center of the interlaminar layer is same as that for the DCB specimen model; i.e. the crack-tip bluntness is mathematically represented by an ellipse of an aspect ratio of 2 as shown in Fig. 4.1.

The mesh details can be obtained from Fig 4.2 and Fig 4.3. The elements near the crack tip have an aspect ratio of unity and are at least 12-20 times smaller than the smallest crack dimension. The elements along the crack further down towards the ends of the specimen have an aspect ratio of about 10-20. The model is subjected to 3-point bending under unit load at the center of the beam and the ends of the beam are simply supported as shown in Fig 4.7. The boundary condition gives zero displacement in the 'x', and the 'y' directions at node B and zero displacement in the 'y'-direction at node A (ANSYS notation).

The material properties of the outer orthotropic layer and that of the resin rich middle interlaminar layer are the same as those for the DCB specimen.

For the composite outer layers:
$E_1 = 26{,}600MPa$,
$E_2 = 4{,}700MPa, \nu_{21} = 0.09, G_{12} = 2800MPa$

For resin-rich interlaminar region:
E=3100 MPa, $\nu = 0.35$,

The earlier finite element studies [94,95,101,102,103,105] to analyze the behaviour and performance of the ENF specimen have involved calculations of the specimen compliance and the strain energy release rate to compare the results with the modified beam theory solutions. Various studies have affirmed better correlation for the compliance and fracture toughness values between the FE results and modified beam theory as compared to the simple beam theory. The FE results for G_{II} were higher by about 2-7 % than the corrected beam theory with shear deformations [94]. The FE analyses have assumed, both, the blunt crack tip [105] and sharp crack [94, 101-103] in their models.

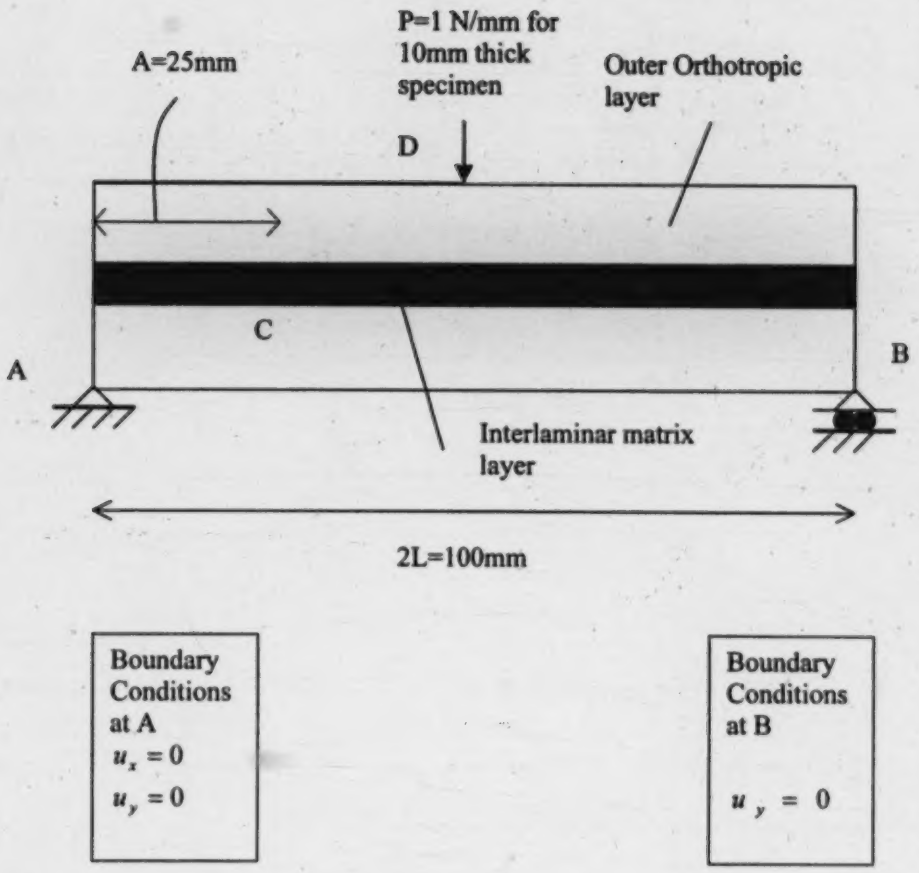

Fig 4.7 Model of the ENF Specimen

Previous investigators have encountered the problem of elements on either side of the insert defect crossing into each other without any restraint. Since this is physically not possible, suitable crack face constraints have to be employed into the model. To prevent the overlapping of elements various approaches have been used in the past: (i) use of bar element (or non-linear truss element) to connect the two crack faces and there by inducing a compressive stress [101,105], (ii) use of multiple-point constraints equations or a coupling technique at the nodes on the opposite crack faces [94,95,103] (iii) analysis of a contact problem accounting for frictional effects or use of contact (or interface elements) [101,102,103]. The contact element approach is more rigorous and directly accounts for the necessary friction, which is encountered when the two crack faces come into contact and slide past each other. Friction opposes the sliding and is responsible for the load that is transferred from the lower beam to the upper beam through tractions on the crack faces. Actually, the determination of contact pressure is extremely difficult task and even numerical contact analysis is computationally demanding. Contact analysis memory requirements may be many times and the computation time goes to more than 100 times as solution is obtained iteratively. However it has been found that error induced by neglecting the effect of friction is less than 2-4 % [72,101,102,103,112] for standard specimens with **a/L**=0.5 and friction coefficient values in range of 0.1-0.5, within the constraints of small deformation theory. However, the frictional effects could shoot up to 20% for specimens with **a/L** as small as 0.2 [103]. The effect of friction is to lower the maximum stress, by a small amount, i.e. neglection of friction results in slight overestimate of G_{IIC} [94].

In the present study analysis was performed by using all the three approaches for the purpose of providing constraints to the opposite crack faces. The results were found very close, within 1% variation. Based on the previous studies regarding significance of frictional effects in composite specimens [101,103] and the fact that the coefficient of friction at the interface is not well known, it was observed that inclusion of friction will not significantly add to the accuracy of the solution. So friction is ignored in the present analysis. It was decided that the crack region be meshed with bar elements as shown in the Fig 4.8. The crack faces are thus smooth. This approach can account for the compressive stress to be experienced by the crack faces as they tend to crush into each other, but are physically prevented to do so in the actual experimental set up. Such model appears sufficient for the present purpose. For the bar elements, $E=3100N/mm^2$ and $\nu = 0.35$, are used, which are same as those of the interlaminar resin rich region.

The use of bar elements across the crack contour though adequate from the above reasoning to prevent the two crack faces from overlapping, created some confusion. From the graphical representation shown by ANSYS seemingly the bar element was not sufficient to constrain the opposite crack faces and the faces appeared crossing over each other. However, the actual nodal deflection values of the nodes on the crack contour indicated that faces have not actually crossed each other, as expected. The discord between the numerical values representing the deflected crack contour and the graphical

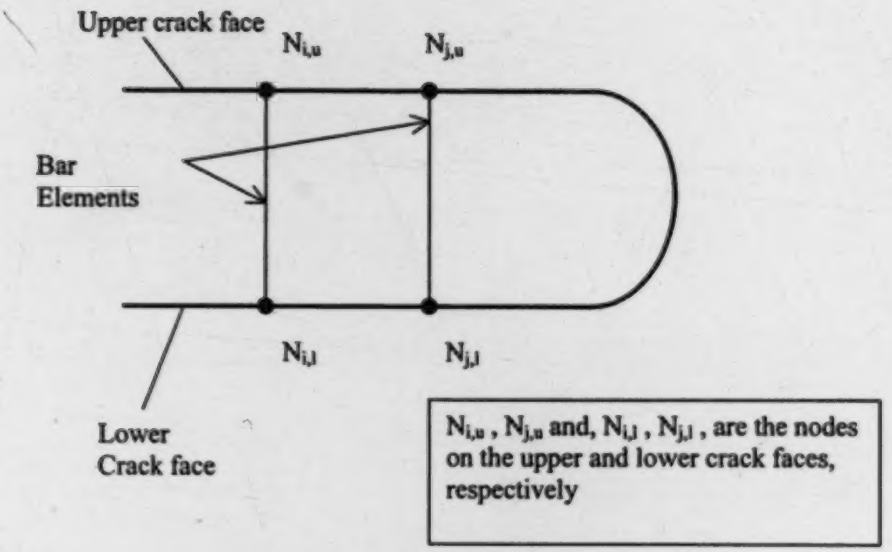

Fig 4.8 Use of Bar elements to constraint the opposite crack faces

picture shown by the ANSYS, was examined and explained in the Appendix 1. The unexpected graphical picture occurred due to the high magnification used by the ANSYS package of the deflection profile superimposed on the original undeflected configuration of an object.

Now, the expression for the Mode II fracture toughness including the correction factor in the beam theory can be obtained from equation 3.37

$$G_{IIC} = \frac{9P^2(a+\chi_{II}h)^2}{16B^2h^3E_1} \qquad 4.4$$

The correction factor χ_{II} for the Mode II is supposed to be approximately half that of the DCB test and some authors [85,95,96] have suggested the correction factor for Mode II to be, typically, 0.42 times that of the Mode I. Using this relation, for Mode II ENF specimen the shear deformation correction factor in equation 4.4 is given by:

$$\chi_{II} = 0.50 \qquad 4.5$$

To investigate the thickness effects on G_{IIC} values, we adopt the same semi-analytical approach as for the DCB specimen. To begin with, we assume that the left-hand side of equation 4.4 represents a toughness value, which is a thickness-independent material property. Let the load applied on 10mm ENF specimen be P = 1 N/mm. Again, this load is an arbitrary load and need not correspond to the actual fracture load. So for varying thickness values, for 2h = 5, 10, and 15mm, using expression on right-hand side of equation 4.4, we obtain the corresponding load values as : 0.3704, 1.00, and 1.7572, respectively. These values are appropriate loads which must be applied to the specimens of different thicknesses of 5mm, 10mm, and 15mm, so that right hand side of equation is constant, i.e. to generate the same G_{IIC} values.

It may be noted that correction factors for the large deflection effects can be employed to modify the equation 4.4 by suitably using the correction parameters 'F' and 'N' which can be obtained from the equations 3.39 and 3.40, respectively. However, in our case, for thinnest specimen with thickness 2h=5mm, we have δ / L= 0.03337 / 50*100= 0.067 %. As the δ / L values are smaller than 0.2, the correction factors 'F' and 'N' may be neglected for all the specimen thickness cases [54].

4.3.1 RESULTS AND DISCUSSION

The fracture stress for the Mode II loading can be guided by the maximum stress values in terms of the principal stress (S1), shear stress (τ_{xz}), the normal stress in longitudinal direction (σ_x) or the von Misses stress (Ψ). It can also be guided by the stress at the interface location as explained below. The stress contours near the crack tip region are given in Fig 4.9. The variation of associated stresses along the path close to the crack tip corner is shown in Fig 4.10. Further, it may be noted that the direction of the maximum principal stress is always tangential to the crack tip contour. This is shown in the Fig. 4.11. The relevant stress values at the corner of the insert crack tip from where the crack may supposedly initiate are tabulated in the Table 4.3.

Table 4.3
Study on Dependence of Crack Tip Corner Stresses on ENF Specimen Thickness

2. h	S1	τ_{xz}	σ_x	Ψ
5	15.668	7.606	12.643	13.573
10	15.463	7.508	12.472	13.395
15	15.322	7.442	12.357	13.273

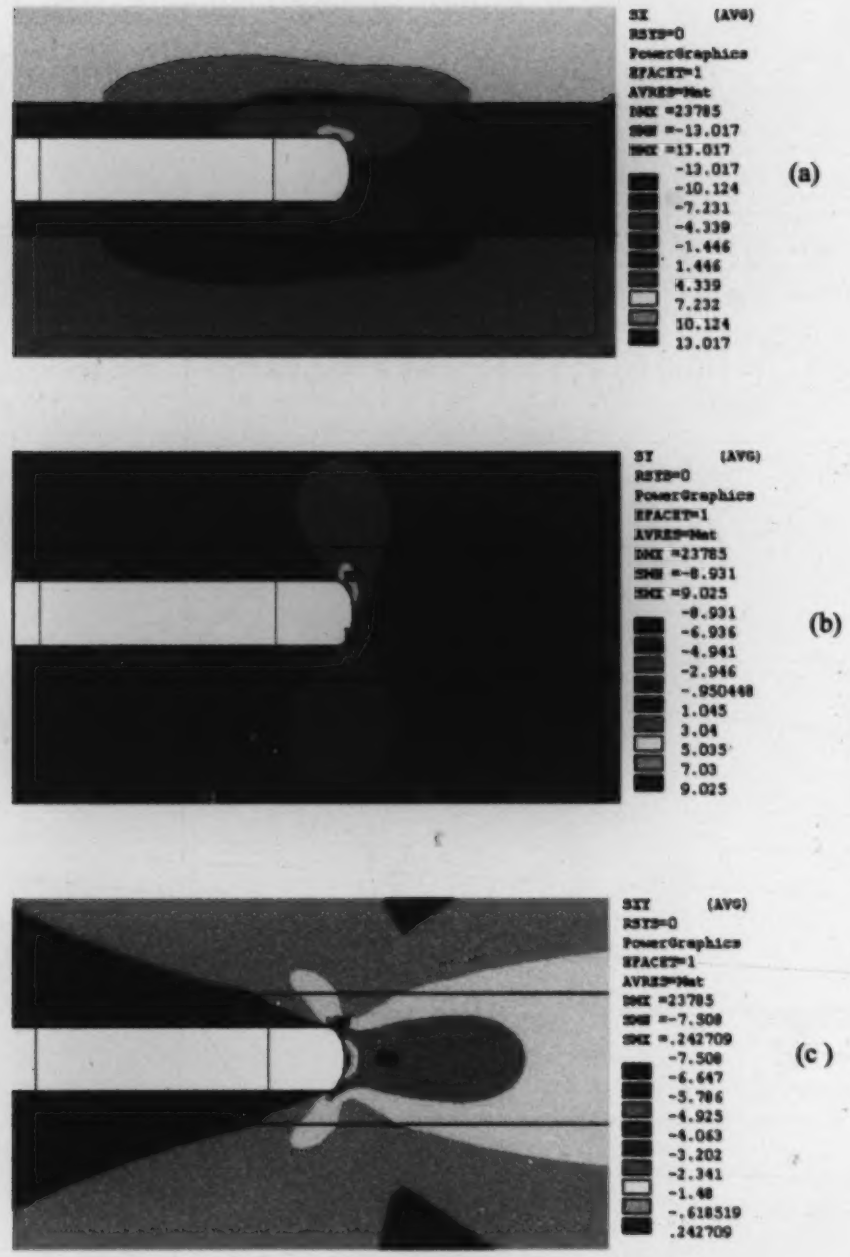

Fig. 4.9 Stress contours near crack tip for 10mm thick ENF Specimen:
(a) normal stress in x-dir (σ_x), (b) normal stress in z-dir (σ_z), (c) shear stress τ_{xz}, (d) max principal stress (S1), (e) von Misses stress (Ψ).

(d)

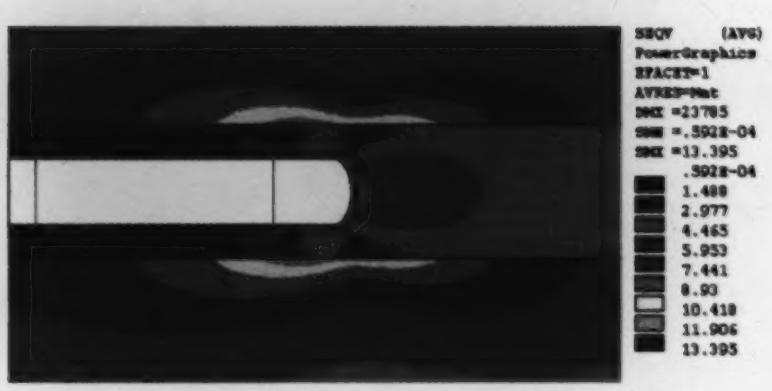

(e)

(Fig. 4.9 Cont.): Stress contours near crack tip for 10mm thick ENF Specimen: (a) normal stress in x-dir (σ_x), (b) normal stress in z-dir (σ_z), (c) shear stress τ_{xz}, (d) max principal stress (S1), (e) von Misses stress (Ψ).

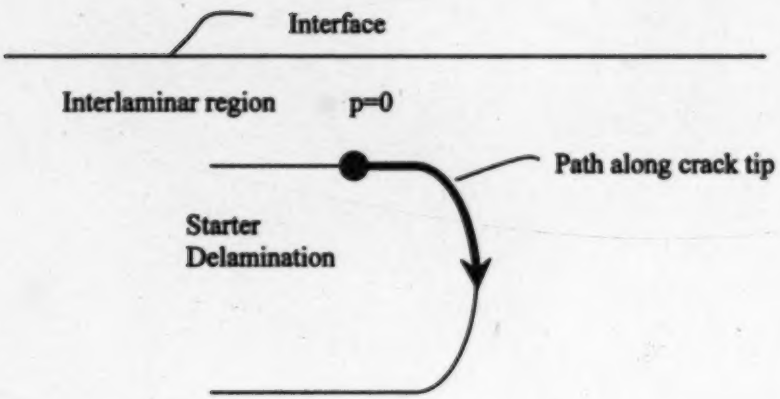

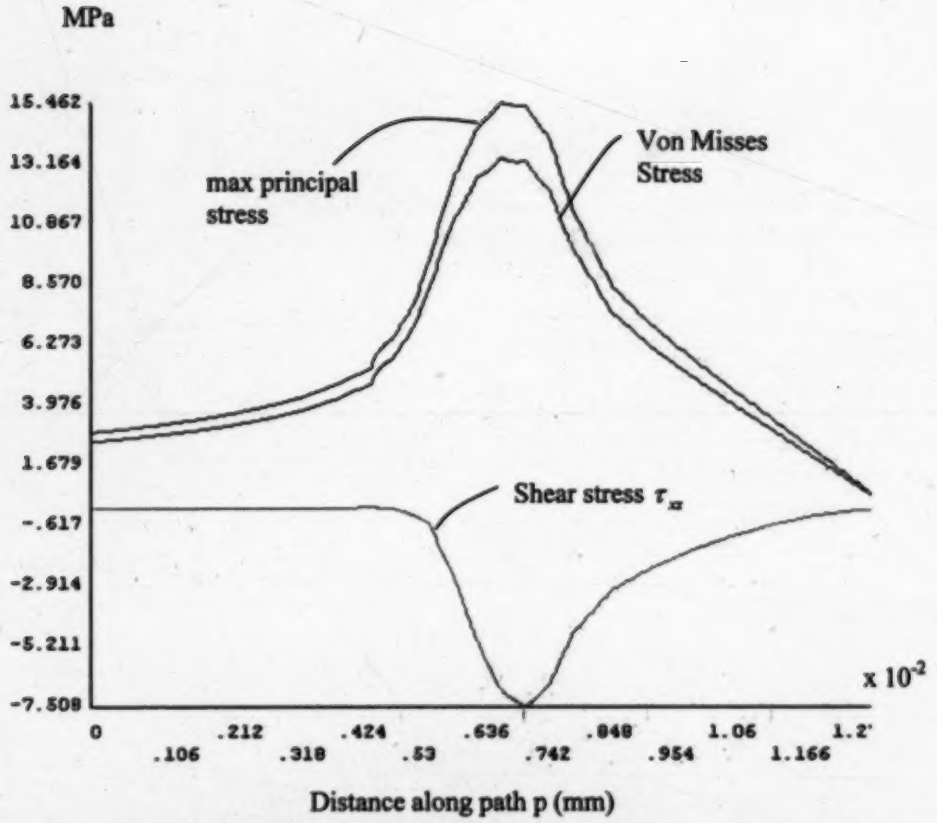

Fig 4.10 Variation of the max principal stress (S1), shear stress τ_{xz}, and von Misses stress for the path along crack tip of 10mm ENF specimen

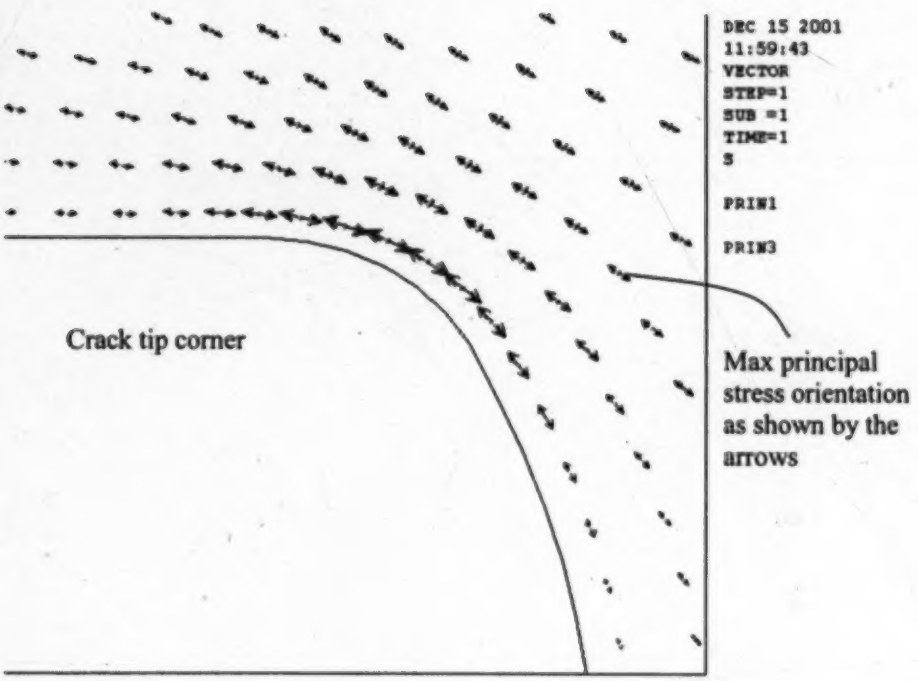

Fig 4.11 Vector plot showing the orientation of max principal stress near the crack tip

In addition, the stress values at the interface location in the orthotropic lamina region near the crack tip corner for normal stress in z-direction called the interlaminar direct stress (σ_z), and the von Misses stress (Ψ) are to be considered. The shear stress and the principal stress have a low value at the interface. Hence the principal stress (S1), and the shear stress (τ_{xz}) at the interface are not considered as critical. The variation of relevant stresses along the path over the interface, near the crack tip, is shown in the Fig 4.12. The values for relevant stress are tabulated in the Table 4.4

Table 4.4
Study on Dependence of Interface Stresses on ENF Specimen Thickness

2. h	Interlaminar Direct Stress σ_z	von Misses Stress Ψ
5	2.44	12.14
10	2.41	11.95
15	2.39	11.77

The above values in the Table 4.3 and Table 4.4 show that as the thickness increases, the critical stress stays unchanged. It may be mentioned that the variation in the von Misses stress values at the interface with thickness is more as compared to the variation for the other stress values with thickness, the absolute percentage variation is too small to indicate a definite trend. Hence each of the specimens has essentially the same fracture stress. For the mode II fracture toughness values again, the present finite element results conclude no significant influence of specimen thickness.

Earlier works [49,61,83,107,108,109] have reported varying results regarding the influence of specimen thickness. All the results are based on experimental studies. Some studies have observed the trend of thickness dependence, viz. the increase of fracture toughness with specimen thickness. This is clearly in contradiction to our present conclusion. We will examine the results of other studies closely as below.

The study by Davies et. al. [61] involved tests on carbon/PEEK and carbon/epoxy specimens with 20-25 μ release-agent-coated aluminium, and 30 μ PTFE insert films, respectively. The specimen thicknesses used were: 1.6mm, 3.2 mm and 5.2mm. Apparently, a/L was 0.5., and apparently specimens were pre-cracked in mode I. Results for carbon/epoxy showed no specimen thickness effect on Mode II propagation values using simple beam theory. However, for the carbon/PEEK specimens increase was noted. Values obtained for G_{IIc} were 1492, 1927, and 2406 J/m^2 for the three thicknesses. The investigators attributed this increase to the Mode I pre-cracking of the specimens resulting in multiple cracks in the thicker specimens. They also noted that corrections to simple beam theory can increase G_{IIc} by 30% for the ENF specimen.

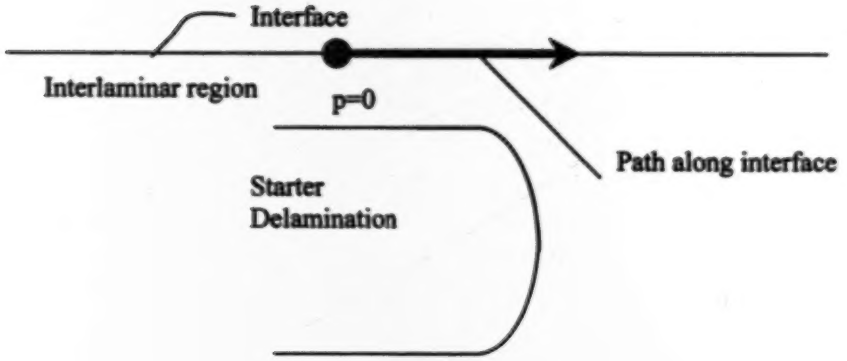

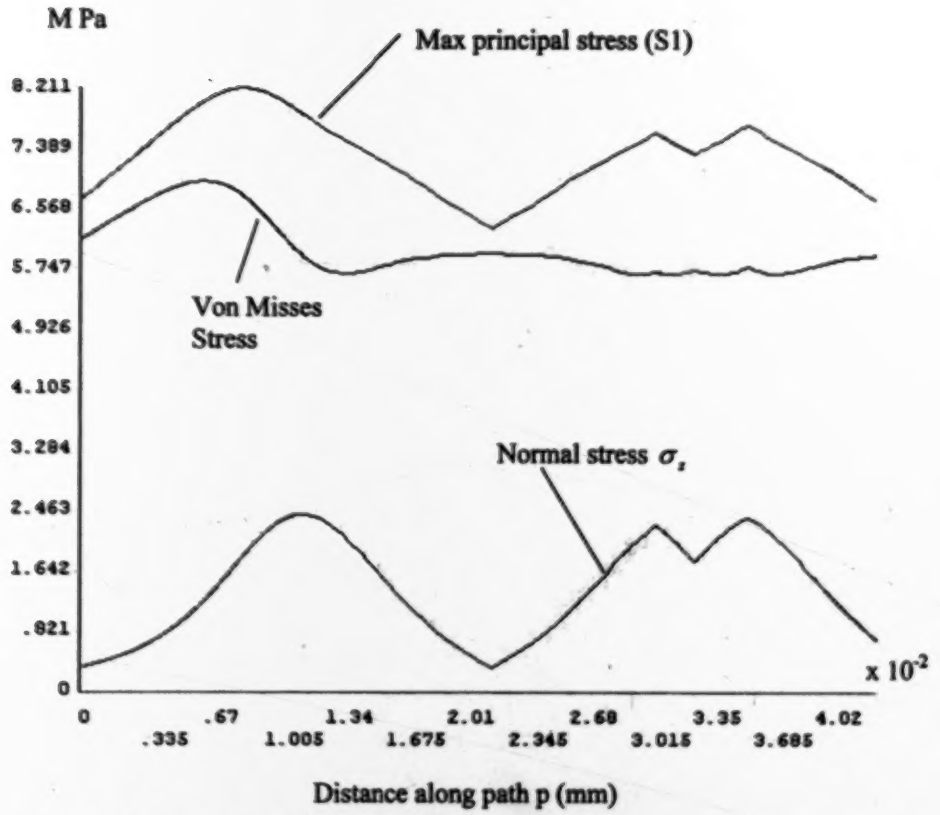

Fig 4.12 Variation of the max principal stress (S1), normal stress σ_z, and von Misses stress for the path along interface of 10mm ENF specimen

Another study by Davies et. el. [109] on carbon/PEEK composites in thickness range of 2, 3 and 5mm with PTFE insert film showed increased values for thicker specimens. This was believed to be due to the quality of Mode I precrack causing multiple crack and/or fibre bridging. Significantly, the NL point using simple beam theory expression was used to determine the G_{IIc}.

Recently, Cantwell [108] conducted a study on the ENF specimens of wide range of composite materials. The specimens were shear precracked ahead of 25 μm aluminium insert film, and a thin Teflon film was placed in the precrack prior to the test. Shear deformation effects were included in G_{IIc} values obtained from the maximum load point. The thicknesses used were 1.6mm, 3.2mm, and 5.3mm. The results indicated distinguishable increase of G_{IIc} with the thickness at loading rate of 1mm/min. The difference between the values of G_{IIc} for the highest and lowest thickness was about 30%. The increase was attributed to processing effects, leading to greater scope for fibre movement, and hence greater fibre-bridging in thicker specimens.

Another study by Compston [49] involved tests on glass/epoxy specimens with 15 μ thick aluminium insert film with release agent. The modified beam theory expression was used. The a/L ratio was 0.5 and specimens were not precracked. The thickness used were from 4.5 to 7mm. The $G_{IIc,i}$ based on the NL point (corresponding to deviation from linearity, and, difficult to identify) showed an increase with the thickness, and it was believed to be related to the effect of friction. However, $G_{II,\ max}$ results showed no influence of specimen thickness.

In contrast to the above results, a study by Hashemi et. al. [83] involved carbon/PEEK composites for ELS test using 20 μ release-coated folded aliminium foil as insert without precreaking the specimen, for thickness 3.16mm, 4.35mm and 5.30mm. A small roller was inserted between the beam halves. Modified beam theory expression was used in analysis. They concluded no dependence of $G_{IIc,i}$ and G_{IIc}(s/s-prop) values on specimen thickness.

Lately, Davies et. al. [107] conducted ENF specimen studies on carbon/PEEK composites for thickness 1.6mm, 3.2 mm, and 5.2 mm. The a/L ratio was 0.5 and the specimens were not pre-cracked. The shear deformation effects were considered in the beam theory. Values for the $G_{IIc,i}$ (NL point), and the $G_{IIc,max}$ (corresponding to the maximum load which immediately preceded unstable crack propagation) showed thickness independence for tests, with 25 μm PTFE separator film between starter crack surfaces. Thickness dependence was observed for tests without the separator film. The increase in toughness values with thickness in absence of separator film was attributed to the overestimation due to effect of friction by as much as 20%. Based on their argument, for a given crack length the error in toughness due to friction increases linearly with specimen thickness.

In the finite element study by Gillespie et. al. [101], the effect of specimen thickness and friction was examined by a 2-D linear elastic model. They conducted contact problem analysis with and without friction effects. Excellent correlation was found for the compliance between the finite element results and modified beam theory expressions. However, the toughness values were not well correlated. The reason for disagreement was not exactly clear, but crack tip shear deformation due to elastic supports and the friction were considered as possible sources causing the discrepancy. The beam theory gave the conservative values for all cases. For specimens of the same 'a', and 'L' having the same properties E_1, and G_{13}, the correlation between the fracture toughness results from the finite element analysis and the beam theory expressions, both, with and without the shear deformation effects, worsened as the specimen thickness increased. Frictional error increased linearly with **h/a** ratio and it was postulated that friction effects could be minimized through a judicious choice of specimen geometry.

4.4 DISCUSSION

The effect of specimen thickness on the Mode I and Mode II fracture toughness values is investigated in the present study using finite element models of the DCB and ENF specimens. It is assumed that an anisotropic linear elastic fracture mechanics approach can be used satisfactorily to predict the stress distribution around the crack tip. The deformations are assumed small, and suitable corrections are employed to account for large deformation effects. Having said this, till date, some features are daunting with regard to Mode II interlaminar fracture toughness characterization using the ENF specimen. Unless these features are resolved a test standard is unlikely to emerge. These complexities are illustrated below:

(1) PRECRACKING AND STARTER DELAMINATION THICKNESS

Starter crack has a very significant influence on results. Precracking may be desirable to simulate a natural crack and overcome the influence of resin pocket ahead of insert which may increase the toughness values (the size of pocket depends upon the insert thickness, with no obvious resin pocket with 13 μm insert). However, the disadvantage is that, Mode I precracking may cause fibre bridging [70,104]. Only the values of G before fibre bridging begins are relevant as a material property. For the Mode I DCB specimen single generic toughness value may be obtained as insert thickness is decreased, thereby achieving a composite material property, where the insert successfully simulates an initial delamination crack without having to resort to precracking. However shear precracks may be used for DCB specimens [70,83].

The problem of precrcaking is more complicated in the Mode II test. For the ENF specimen, a Mode II precrack which is known not to cause fibre bridging may be used. But a shear precrack causes damage micro-cracks ahead of the delamination front. There is much controversy amongst the results obtained by the different precracking methods. One group has reported the NL values for insert higher than for Mode II precrcaks, which were higher than for Mode I precrcaks; and same trend was observed for the max load G_{IIc} values [63]. In contrast, another group has obtained higher NL point values for shear precrack, with Mode I and insert values being the same [70]. Other studies have reported higher G_{IIc} values from insert than shear precrack [62,108]. Generally it is believed that inserts produce higher values than precrcaks [60]. Furthermore, as the insert thickness is decreased, the G_{IIc} values decrease continuously, and never reach a single value that may be considered a generic material property [70]. Consequently, G_{IIc} measured from an insert has been reported sometimes greater and sometimes less than G_{IIc} measured from a shear precrack [60]. The dispute is apparently somewhat resolved by a study obtaining almost identical values from Mode I precracks, and $7.5\mu/12.5\mu$ inserts [64]. More validation is awaited. Interestingly, a unique R-curve is obtained as the crack grows from Mode I precracks of different lengths [83].

(2) DATA REDUCTION METHOD

Various methods used to calculate interlaminar fracture toughness values numerically are mentioned in the section 4.1. The compliance calibration although recommended for high accuracy data reduction [110], is used seldom for G_{IIc} calculation [62]. The method is generally unavailable, as a set of values at varying crack length need to be measured. Also, data analysis requires careful examination and a small variation in specimen compliance with crack length makes experimental compliance calibration inaccurate. Hence beam theory solutions as in equation 3.8 and equation 3.32, employing single measurement of critical load are most often employed:

$$G_{Ic} = \frac{3}{2}\frac{P.\delta}{B(a+|\Delta|)} \qquad 4.6$$

$$G^{SH}{}_{IIc} = \frac{9}{16}\frac{P^2a^2}{B^2E_1h^3}\left(1+0.2\frac{E_1h^2}{G_{13}a^2}\right) \qquad 4.7$$

For Mode I the method has been standardized and validity and interpretation of various load points on the load versus deflection plot has been ascertained in determining the fracture toughness values [53].

For the Mode II calculation methods, there is significant discord. There still exists some disagreement from the fracture mechanics point of view on the best method to obtain the critical point on the load-deflection curve [61,64,107]. The problem is enhanced in toughened materials with significant non-linear behaviour, where NL point loses much meaning, but may give only a lower bound. Only max load point is clearly defined.

Additionally, if the compliance change is more before the max load, the 5% offset value looks arbitrary. To resolve these issues, in addition to the NL point and 5% compliance offset point, NL point and 5% compliance offset point on load versus the crack shear displacement (CSD) plot has been recommended [64]. Unlike the values for NL point on load versus CSD plot, the values for 5% compliance offset point on load versus CSD plot do not show scatter and were found suitable for standardization. However, it is also reasonable to standardize multiple points as characteristics of the material.

Another issue associated with ENF specimen is its inherent instability. As dG_{II} / da is positive excepting when a/L ≥ 0.7, an unstable growth occurs. The ENF test yields unstable delamination growth unless the initial crack is very long or is stabilized. Control methods may be applied to prevent unstable fracture propagation and obtain distinct initiation values [64].

(3) NON-LINEARITY

For tougher composites a significant period of geometrical non-linearity is observed on the load-displacement plot requiring a more precise criterion for the onset of propagation than the maximum load value. The large deflection non-linearity effects may be significant if mid-surface slope of deformed specimen is large. The actual beam deflections need to be modified in light of curvature expression being evaluated as:

$$\frac{1}{R} = \frac{d^2w/dx^2}{[1+(dw/dx)^2]^{3/2}} \qquad 4.8$$

where 'w' is the deflection along the z-direction, and R is radius of curvature.

The non-linearity effects may be prevented through suitable specimen sizing [31,72]. In general, a larger crack length has relatively large errors due to non-linearity, but small errors due to shear deformation. Finite element studies have shown that the deflection should be less than '2h' to avoid non-linearity effects [103].

(4) ALTERNATE ASYMMETRIC BEAM THEORY MODEL

An improvement in the G_{IIc} expression over the equation 4.7 has been attempted considering asymmetrical flexure about span and including shear deformations [96]. The modified beam theory used in equation 4.7 assumes zero slope at the center of the span on account of symmetry [72]. This is erroneous representation of the actual situation. Owing to delamination, the flexure has to be asymmetric and slope at the center of the span is not zero. The line of load introduction is not the line of symmetry. Hence, the point of max deflection deviates to the cracked half segment from the central point. This new point has the zero slope. This gives the expression for the G_{II} as below [96]:

$$G_{II}^{ASH} = \frac{9P^2a^2}{16B^2h^3E_1}[1+\frac{1}{6}(E_1/G_{13})(h/a)^2] \qquad 4.9$$

(5) SINGULARITY EFFECT

The ENF specimen compliance is dominated by the total beam bending and shear deformations, and the contribution from the crack tip deformations, which govern the fracture process is small. Neglect of singularity has negligible influence on the G_{II} values in the analytical expression. Hence, the compliance obtained from such model is not sufficiently sensitive to the delamination growth process at singular crack tip. Therefore it is inappropriate to assess the accuracy of the model for ENF strain energy release rate by use of specimen compliance.

The shear deformation beam theory is insufficient. More rigourous elasticity methods considering the singularity contribution need to be considered to obtain accurate analytical expression for G_{IIc}. It has been shown that local warping of the cross-section occurs in region near the crack tip due to intense shear deformation at the region of singular field [88,101,111,113]. Consequently, the analytical expressions as in equation 4.7 always under-predict the finite element results [94,101,102]. In one model [101] employing different specimen geometries, the departure is very significant. For practical ranges of properties of advanced graphite reinforced polymers, the beam theory with shear deformation gives conservative estimate by 12-25%.

Elasticity solutions based on the singular field are available [113]. For practical purposes, it reduces the expression for G_{IIc} as below, with errors less than 1% with the FE results.

$$G^{SG-SH}{}_{IIc} = G^{BT}{}_{II}\left\{1+0.13[\frac{E_1}{G_{13}}]^{1/2}\frac{h}{a}\right\}^2 \qquad 4.10$$

Such results will be helpful in choosing the geometry of the ENF specimen. Special care should be taken when delamination length is large compared to thickness, and through-thickness shear modulus is small ($G_{13} << E_1$).

To account for the singularity effect equation 4.9 has also been modified to account for the shear deformation at the singular elastic crack tip 'root' to give [96]:

$$G_{II}^{ASG-SR} = \frac{9P^2a^2}{16B^2h^3E_1}[1+\frac{4}{3}\{2(\frac{\chi_{II}h}{a})+(\frac{\chi_{II}h}{a})^2\}] \qquad 4.11$$

This expression has been found to agree with the finite element solution closely for the practical range of E_1/G_{13} values.

One of the requirements of the Mode II test specimen is to promote shear fracture at the crack tip without introducing excessive friction between the crack faces. Friction between crack surfaces opposes the sliding and is an energy absorbing mechanism. However, the effect of friction can be estimated from the extent of hysteresis observed during loading and unloading of the specimen, and was found to result in an overestimate of G_{IIc} by less than 2% [112]. For a/L = 0.5, assuming the coefficient of friction $\mu = 0.3$, the finite element results have indicated that effect of friction on G_{IIc} is negligible, less than 2-4% [101,102,103]. However the effect is pronounced for shorter crack lengths. In contrast, experimental work has reported much larger effect of the friction up to 20% for thick specimens [107].

The frictional contact between the crack faces is located symmetrically about the outer support pin along delaminated length in the region less than *'4h'* and carries a load P/4 on each face [72,102]. The distribution length depends upon the ratio E_1 / G_{13}. Rollers between the cracked faces at support pin location are advisable [103,112].

(7) PLANE STRAIN VS PLANE STRESS

While one group of authors has assumed the plane strain condition [94, 101-105, 112], various authors in other group [114] have assumed the plane stress condition. The plane stress condition is valid for specimens where the cracked and uncracked regions are long and narrow, and the plane strain condition is valid for specimens where the cracked and uncracked regions are short and wide. The difference between the two may be characterized by a non-dimensional ratio D_e, defined as 1 minus the ratio of plane stress to plane strain rigidities, which is reduced to [111].

$$D_e = D_{12}^{\ 2} / (D_{11} D_{22}) \qquad 4.12$$

The coefficients D are the elastic bending constants given by equation 1.7(c). For the practical purposes the difference is very small, less than 1-2% [94]. In reality for ENF test geometries, it is likely that neither the plane stress nor the plane strain conditions apply.

(8) THREE-DIMENSIONAL EFFECTS

(8-i) *Delamination Front Curvature*:

In the DCB specimens the anticlastic curvature (saddle-shaped deformation) effect causes the crack length to be larger in the center than at the edges. The computed value of G may be 1.6% higher than the true value for unidirectional specimens, and could be 7.3%

higher for the [±45] specimens [115]. However, the crack front shape in an ENF specimen is reverse to that in a DCB specimen [111]. For the ENF specimen, a mode III component may also be induced at the outer edges of the crack front due to anticlastic curvature of the individual sublaminates [111].

(8-ii) *Free Edge/ Finite Width Effects*

The effect of finite width is relatively unimportant, especially for unidirectional specimens. However, local increase in mode II energy release rate will occur at the free edges. Since such boundary layer region is normally effective in one laminate thickness (section 2.2.1), an increase in effective ply thickness causes a decrease in fracture stress due to larger interlaminar stress distribution [116].

(8-iii) *Bending-Twisting Coupling*

These effects occur in laminates of multidirectional lay-ups, and need to be considered in the analysis [111].

Chapter 5

CONCLUSIONS

5.1 GENERAL

The delamination resistance of polymer composites, characterized by the interlaminar fracture toughness, is an important material property. Possible specimen thickness effects on the Mode I and the Mode II fracture toughness values is investigated in the present study, and has concluded thickness independence for both the modes. A broader objective of the study has been to assess the current status quo of characterization of Mode I and Mode II interlaminar fracture toughness. With regard to the DCB specimen for Mode I IFT testing, the ASTM standardization is available. Nonetheless, the DCB specimen was included in the present study on account of its various similarities in procedure, analysis, data interpretation, and associated complexities, with the ENF specimen. Also the results from the finite element stress analysis of the DCB specimen can be used to gain more confidence in the FE model and its various common features. In this perspective, it can serve as useful groundwork for the more challenging ENF specimen. It may be noted that there is no singularity in our model and a mesh size convergence study is not required. The size of the elements near the crack tip is selected on the basis of experience and reference [100], and the finite element mesh refinement appears adequate for our study.

With regard to the ENF specimen, the specimen thickness independence for the Mode II IFT as evidenced in this study, is clearly a significant step in the development of an acceptable test standard. Other geometry effects have been investigated; broad width-independence excepting edge effects [83,109]; independence for overhang length beyond supports [103]; span length independence [107,109] and some unexplained span length effects [62]; independence of initiation and s/s-prop values with respect to crack length 'a' [83, 84, 87], with desirable 'a' > 25mm [101]; **a/L** ratio effect on the friction and other corrections, with recommendation of **a/L** ≥ 0.5 [101,103]. Most of these geometry effects have been explored satisfactorily to affirm no significant influence under stated limitations. As a valuable attribute, the ENF specimen is relatively insensitive to the offset of the starter delamination about the mid-plane, although beam theory solution suggests sensitivity of the G_{II} solution for the ELS specimen [88,101,102]. Interestingly, the complexities discussed in section 4.4 have some hope of being resolved. However, the Mode II IFT testing has other chilling hurdles as discussed in section 5.2.

5.2 COMPOSITE INTERLAMINAR G_{IIC}: SHEER MYTH OR TRUE SHEAR MEASUREMENT ?

Apart from the unresolved issues discussed in section 4.4, the interpretation of the property being measured in the test appears elusive, and the Mode II interlaminar toughness testing remains contentious. The study of the micromechanisms involved in the failure reveals that the apparent G_{IIc}, as typically measured, is inconsistent with the original definition of a shear fracture. It has been shown that failure under Mode II loading in the specimen actually consists of local tension microcracks in the interlaminar resin-rich region between the plies followed by their coalescence [50,60,105]. A Mode I fracture surface has a clean cleavage plane, while Mode II fracture surface exhibits a very rough zigzag pattern [49,83]. This is usually accompanied by damage in resin inside the adjacent plies with characteristic 'hackles'. For tough composites the Mode II fracture surfaces have been found similar to those of Mode I with extensive evidence of matrix yielding at the delamination front [60]. The delamination front has a significant Mode I component (at failure location accounting at least half of the total G), with the max principal stress tangential to the corner of the starter defect as shown in Fig 4.11. The matrix fails in tension, as matrix tensile strength is often lower than its shear strength. Such 'secondary' tension microcracks exist ahead of the main crack front close to the fibre-matrix interface where high stress concentration occurs. The growth of tension microcracks forms the final interlaminar shear fracture surface. Finally, this Mode I initiated fracture is expected to follow a Mode II growth along the fibre-matrix interface. So the complex failure process is far removed from an idealized sliding of two crack planes relative to one another. Interestingly, the mechanisms do not give toughness values anywhere close to the Mode I delamination fracture toughness. It is believed that the ENF specimen measures something important for the composite strength, even though what is being measured is still a mystery.

A three-dimensional model of the ENF specimen with blunt crack tip showed high tensile stress concentration over the fibre-matrix interface surface causing strong preference for the interlaminar failure crack to start from the fibre-matrix interface rather than from the starting defect, when interfacial strength was estimated 28% below the matrix strength [105]. Similar preference for the crack to grow from the fibre-matrix interface occurs in the DCB specimen for interfacial strength 50% below the matrix strength [104]. Details of interfacial failure are available elsewhere [117]. The crack tip stress contours in Fig 4.9 and Fig. 4.12 show that in some situations, fracture may not initiate at all from starter defect and the failure values may correspond to some Mode I matrix failure at the interface on account of low bond strength for ENF specimen.

Clearly, in such cases there is no self-similarity and the application of the present fracture mechanics expressions is questionable. Hence, what is required is the continuum and the microscopic modeling, in parallel. Micro modeling alone is not very fruitful as models for crack splitting, pullout, or delamination are rarely precise. Understanding of the micromechanisms of failure and their dominance is important to resolve the anomaly.

5.3 CONCLUDING REMARKS

The effect of specimen thickness on the Mode I and the Mode II fracture toughness is investigated for specimen thicknesses 5, 10, and 15mm, using finite element models of the DCB and ENF specimens. The results for the DCB model show that the thickness effect is not significant, as expected. This is also in accordance with earlier experimental studies [61,83,106], which were conducted prior to the standardization of the test [53]. These references are based on corrected beam theory expressions, and although there was an experimental scatter in the values, no preferred trend was observed.

For the Mode II interlaminar testing, again, the present finite element results of the ENF specimen model conclude no definite trend in fracture toughness values with specimen thickness. The test is under review for Mode II characterization, and controversy exits regarding thickness effect [49,61,83,101,107,108]. These are reported in section 4.3.1. A closer examination reveals that the relevant references that have used shear deformation beam theory, are few [49,107,108]. Studies [49,108] conclude thickness independence if friction effect is accounted for. In contrast, a study [108] has reported an increase of G_{IIc} with thickness by 30% owing to processing effects. Though experimental limitations are understandable, such huge increase needs further explanation. Nonetheless, G_{IIc} appears thickness independent in light of present results. But standardization of the ENF test does not look forthcoming, owing to other issues discussed in section 4.4 and section 5.2.

The results for the Mode I and the Mode II specimen models are valid within the constraints of small linear elastic deformation theory. The features discussed in the section 4.4 do not undermine the validity of our results. The present model uses the empirical correction factors χ_I and χ_{II}, as in equation 4.2 and equation 4.4, respectively. It appears that the empirical correction factors are more satisfactory. For Mode I such correction factors give better results compared to any analytical beam theory solution available. Probably, the same is true for the Mode II [95]. It may be mentioned that any of the corrections in section 4.4 not adequately accounted for, may be manifested as specimen thickness and other specimen geometry effects and influence the fracture toughness results.

For the Mode II characterization, the progress in precracking technique is promising with preference for Mode I precrcaks. The friction effects at the crack faces can be avoided by using a roller between the delamination faces near the support pin. The only real hurdle remains the data reduction. Equation 4.7 may not be realistic as it neglects singularity effects, and equation 4.10 though simple, looks promising. However, more validation is needed. This is if at all the property being measured by the ENF specimen is the shear interlaminar fracture toughness. It may be mentioned that fibre-matrix interface failure is a different micromechanism as discussed in section 1.6.3 and can be discarded from the controversy. However, due to the presence of hackles the assumption of self-similarity may be jeopardized, and the governing expressions for the G_{II} need to be reexamined.

5.4 FUTURE WORK

A number of future directions are proposed in order to provide a further understanding of the interlaminar fracture behaviour of polymer composites. It is necessary to accurately evaluate the values of the correction factors in the beam theory expressions for the ENF specimen to have a more definitive conclusion regarding the specimen thickness effects, and clearing the way to its standardization. The issues regarding the validity of self-similarity of crack growth in the light of fracture initiation by the tensile matrix cracks need a rigorious examination. Features such as precracking techniques and data reduction may provide the long awaited break-through in the test procedure. It will be an interesting exercise to investigate the desired and suitable specimen dimensions and crack length to minimize the effects of various corrections. The requirements may be conflicting and would need a careful judgment.

It has been reported that for the Mode I test the matrix toughening enhances the fracture toughness values [49]. For the Mode II test, the effect of matrix toughening may be investigated. Also, impact induced delamination will be a useful study with immediate practical aerospace and other industrial applications.

A three dimensional model for the ENF specimen including the plasticity effects would be most appropriate to study the crack growth resistance in terms of the micromechanisms occurring close to the crack tip. Issues such as fibre-matrix bond strength may be incorporated in the FE model.

REFERENCES

1. Sheldon R.P., "*Composite Polymeric Materials*", Applied Science Publishers Ltd., 1982.

2. Lee Stuart M., Ed., "*International Encyclopedia of Composites*", vol 1-6, VCH Inc. Publishers, New York, 1990.

3. Hollaway L., "*Glass Reinforced Plastics in Construction: Engineering Aspects*", Surrey University Press, Glasgow, 1978.

4. Whipple L.D., "*Progress Report-Development of Advanced Composite Structures*", Advanced Fibrous Reinforced Composites, Society of Aerospace Material and Process Engineers, San Diego, vol 10, 1966, pp:C13-C20.

5. Daniel I. M. and Ishai O., "*Engineering Mechanics of Composite Materials*", Oxford University Press, 1994.

6. Zweben C., Hahn H.T., & Tsu-Wei Chou, "*Mechanical Behaviour and Properties of Composite Materials*", vol 1, Delaware Composites Design Encyclopedia, Reviewing Eds., L.A. Carlsson & J.W. Gillespie Jr., Technomic Pub, U.S.A., 1989.

7. Peters S.T., Ed, "*Handbook of Composites*", Chapman & Hill, U.K. 1998.

8. Agrawal A., "*Finite Element Analysis of Arbitrarily Curved Thin Composite Shells*", M. Tech. Thesis, Department of Aerospace Engineering, I.I.T., Kharagpur, India, 2000.

9. Jones R.M., "*Mechanics of Composite Materials*", McGraw-Hill Book Company, 1975.

10. Carman G.P., Lesko J.L., & Reifsnider K.L., "*Micromechanical Analysis of Fibre Fracture*", Composite Materials: Fatigue and Fracture, 4th vol, ASTM, STP1156, Eds. Stinchcomb W.W and Ashbaugh N.E., Philadelphia, 1993, pp: 430-452.

11. Chen Yu, "*Finite Element Micromechanical Modeling of Glass Fibre/Epoxy Cross-ply laminates*", M.S. Thesis, Department of Mechanical Engineering, University of Alberta, Canada, 2000.

12. Halpin J.C. and Tsai, S.W., "*Effects of Environmental Factors on Composite Materials*", AFML-TR 67-423, 1969.

13. Aliabadi M.H., and Rooke D.P., "*Numerical Fracture Mechanics*", Kluwer Academic Publishers, 1991, pp: 1-2.

14. Knott J.F., "*Fundamentals of Fracture Mechanics*", Butterworths Publication, London, 1973.

15. Anderson T.L., "*Fracture Mechanics: Fundamentals and Applications*", II Edition, CRC Press, London, 1995.

16. Williams J.G., "*Fracture Mechanics of Polymers*", Ellis Horwood Limited, England, 1984.

17. Larsson L.H., "*Basic Principles of Fracture Mechanics and an Overview of ASFM6*", The Assessment of Cracked Components by Fracture Mechanics, Eds. Larsson L.H., EGF Publication 4, London, 1989, pp: 1-26.

18. Bradley W.L., "*Relationship of Matrix Toughness to Interlaminar Fracture Toughness*", Composite Materials Series, 6, Application of Fracture Mechanics to Composite Materials", Ed Klaus Friedrich, Elsevier, 1989, pp 159-187.

19. Beaumont P.W.R., "*The Failure of Fibre Composites: An Overview*", J of Strain Analysis, vol 24 no 4, 1989, pp: 189-194.

20. Sih G. C., "*Fracture Mechanics of Composite Materials*", Fracture of Composite Materials, Eds., G.C. Sih & V.P. Tamuzs, Proceedings of first USA-USSR Symposium, Riga, USSR, 1979, pp: 111-128.

21. Boniface L, Ogin S.L., & Smith P.A., "*Fracture Mechanics Approaches to Transverse Ply cracking in Composite Laminates*", Composite Materials: Fatigue and Fracture (third vol) ASTM STP 1110, T.K. O'Brien Ed, 1991, pp: 9-29.

22. Williams J.G., "*Fracture Mechanics of Anisotropic Materials*", Composite Materials Series, 6, Application of Fracture Mechanics to Composite Materials", Ed. Klaus Friedrich, Elsevier, 1989, pp: 3-38.

23. Hart-Smith L.J., "*Some observations on the Analysis of In-plane Matrix Failures in Fibrous Composite Laminates*", Composite Materials: Fatigue and Fracture, 4th vol, ASTM, STP1156, Eds., Stinchcomb W.W and Ashbaugh N.E., Philadelphia, 1993, pp: 363-380.

24. Kanninen M.F., Rybiciki E.F. & Brinson H.F., "*A Critical Look at the Current Applications of Fracture Mechanics to Failure of Fibre-Reinforced Composites*", Composites, Jan 1977, pp: 17-22.

25. Kim Jang-Kyo & Mai Yiu-Wing, "*Micromechanics of Fibre-Matrix Interface and Fracture of Advanced Composites with Engineered Interfaces*", Fracture Mechanics: 25th vol, ASTM STP 1220, Ed Erdogan F., 1995.

26. O'Brien T.K., "*Characterization of Delamination Onset and Growth in a Composite Laminate*", NASA Langley Technical Memorandum 81940, Jan 1981& Damage in Composite Materials, ASTM STP 775, Ed K.L. Reifsnider, 1982, pp: 140-167.

27. Schulte K. & Stinchcomb W.W., "*Damage Mechanisms-Including Edge Effects in Carbon Fibre-Reinforced Composite Materials.*" Composite Materials Series, 6, Application of Fracture Mechanics to Composite Materials", Ed Klaus Friedrich, Elsevier, 1989, pp: 273-325.

28. Agarwal B.D., "*Fracture Toughness of Fibre-Reinforced Composites*", Handbook of Ceramics and Composites, vol 1, Synthesis and Properties Ed Cheremisinoff Nicholas P., 1990, pp: 269-305.

29. Batdorf S.B., "*Tensile Strength of Unidirectionally Reinforced Composites- I*", J of Reinforced Plastics and Composites, vol 1, 1981, pp: 153-177.

30. Kanninen M.F., Rybiciki E.F. & Griffith W.L., "*Preliminary Development of a Fundamental Analysis Model for Crack Growth in a Fibre Reinforced Composite Material*", ASTM STP 617, 1977.

31. Whitney. J.M., "*Experimental Characterization of Delamination Fracture*", Interlaminar Response of Composite Materials, Composite Materials Series 5, Ed N.J. Pagano, Elsevier Science Publishers B.V., 1989, pp: 161-250.

32. O'Brien T.K., "*Delamination of Composite Materials*", Fatigue of Composite Materials, Composite Materials Series 4, Ed K.L. Reifsnider, Elsevier Science Publishers, B.V., 1990, pp 181-198.

33. Davies P., "*Delamination*", Seminar on Advanced Composites, Cranfield, 1986.

34. Datoo M.H., "*Interlaminar Stresses*", Mechanics of Fibrous Composites, Elsevier Applied Science, London, 1991.

35. Garg A.C., "*Delamination- A damage Mode in Composite Structures*", Eng Fracture Mechanics, vol 29, no 5, 1988, pp: 557-584.

36. Wang A.S.D., "*Fracture Analysis of Interlaminar Cracking*", Interlaminar Response of Composite Materials, Composite Materials Series 5, Ed N.J. Pagano, Elsevier Science Publishers, B.V., 1989, pp: 69-110.

37. Herakovich C.T., "*On the Relationship Between Engineering Properties and Delamination of Composite Materials*", J of composite Materials, 15, 1981, pp: 336-343.

38. R.B. Pipes,& Pagano N.J., "*Interlaminar Stresses in Composite Laminates under Uniform Axial Extension*", J of Composite Materials, 4, 1970, pp:538-458.

39. Pagano N.J., "*Stress Fields in Composite Laminates*", Intl J of Solids and Structures, 14, 1978, pp: 385-400.

40. Kim R.Y. & Soni S.R., "*Experimental and Analytical Studies on the Onset of Delamination in Laminated Composites*", J of Composite Materials. 18, 1984, pp: 70-80.

41. Pagano N.J. & Pipes R.B., "*Some Observations on the Interlaminar Strength of Composite Laminates*", Intl. J of Mechanical Sciences, 15, 1973, pp: 679-688.

42. Raju I.S. & Crews J.H., "*Interlaminar Stress Singularities at Straight Free Edge in Composite Laminates*", Journal of Computers and Structures, vol 14, No 1-2, 1981, pp: 21-28.

43. Silva A. & Freitas de M., "*Computational Prediction of Strain Energy Release Rates of Delamination in Composite Materials*", Fracture of Polymers, Composites, and Adhesives, Eds. J.G. Williams and A. Pavan. ESIS Publication 27, Elsevier, 2000, pp:149-160.

44. Rybicki E. F. & Kanninen M. F., "*A Finite Element Calculation of Stress Intensity Factors by a Modified Crack Closure Integral*", Eng. Fracture Mechanics, vol 9, 1977, pp: 931-938.

45. Robinson P., Besant T. & Hitchings D., "*Delamination Growth Prediction Using A finite Element Approach*", Fracture of Polymers, Composites, and Adhesives, Eds. J.G. Williams and A. Pavan, ESIS Publication 27, Elsevier, 2000, pp:135-147.

46. Lu Xianqiang & Liu Dahsin, "*Assessment of Interlayer Shear Slip Theory for Delamination Modeling*", Composite Materials: Fatigue and Fracture, 4th vol, ASTM, STP1156, Eds. Stinchcomb W.W and Ashbaugh N.E., Philadelphia, 1993, pp: 218-235.

47. Chen Xiao-hong, Mai Yiu-Wing, Tong pin & Zhang Liang-Chi, "*Numerical Simulation of the Essential Fracture Work Method*", Fracture of Polymers, Composites, and Adhesives, Eds. J.G. Williams and A. Pavan, ESIS Publication 27, Elsevier, 2000, pp:175-186.

48. Bjeletich J.G., Crossman F.W., & Warren W.J., "*The Influence of Stacking Sequence on Failure Modes in Quasi-Isotropic Graphite-Epoxy Laminates*", Failure Modes in Composites, IV, Eds. J.R. Cornie F.W. Crossman, American Institute of Mining, Metallurgical and Petroleum Engineers, New York, 1979, pp:118.

49. Compston P., "*Matrix-to-Composite Toughness Transfer in the Mode I and Mode II Interlaminar Fracture of Glass-Fibre/Vinyl Ester Composites*", Ph.D. Thesis, The Australian National University, Australia, 1999.

50. O'Brien T.K., "*Interlaminar Fracture Toughness: The Long and Winding Road to Standardization*", Composites Part B, 29B, 1998, pp:57-62.

51. Whitney J.M., Browning C.E. & Hoogsteden W., "*A Double Cantilever Beam Test for Characterizing Mode I Delamination of Composite Materials*", J of Reinforced Plastics Composites, vol 1, 1982 pp:297-313.

52. Wilkins D.J. et. al., ASTM STP 775, 1982, pp:168-183.

53. *Standard Test Method for Mode-I Interlaminar Fracture Toughness of Unidirectional Fibre Reinforced Polymer Matrix Composites*, ASTM Standard, D 5528-94a, ASTM Annual Book of Standards, vol 15.03, ASTM, 1999, pp: 283-291.

54. *Protocols for Interlaminar Fracture Testing of Composites*, European Structural Integrity Society, 1993, Delft, Netherlands.

55. *Testing Methods for Interlaminar Fracture toughness of Carbon Fibre Reinforced Plastics*, JIS K 7086, 1993, Japan Industrial Standards Group, Tokyo, Japan.

56. Davies P., Cantwell W., & Kausch H.-H., "*Measurement of Initiation value of G_{Ic} in IM6/PEEK Composites*", Composites Science and Technology, 35, 1989, pp: 301-313.

57. Broek D., "*Elementary Engineering Fracture Mechanics*", 4th revised edition, Martinus Nijhoff Publishers, Dordrecht, Netherlands, 1986.

58. Anon, "*The standard K_{Ic} Test*", ASTM Standards 31, 1969, pp:1099-1114.

59. *Standard Test Method for Plane-Strain Fracture Toughness and Strain Energy Release Rate of Plastic Materials*", ASTM D5045 – 91a, 1991.

60. O'Brien T.K., "*Composite Interlaminar Shear Fracture Toughness, G_{IIc} : Shear Measurement or Sheer Myth?*", Composite Materials : Fatigue and Fracture, 7th vol, ASTM STP 1330, Ed R.B. Bucinell, ASTM, 1998 , pp:3-18.

61. Davies P. et al., *"Round-Robin Interlaminar Fracture Testing of Carbon-Fibre-Reinforced Epoxy and PEEK Composites"*, Composites Science and Technology, 43, 1990, pp: 129-136.

62. Davies P., *" Summary of Results from Second VAMAS Mode II Round Robin Test Exercise using 4ENF specimens*", IFREMER Internal Report ref TMSI/RED/MS 99.82, 1999.

63. Davies P., et al., "*Comparison of Test Configuration for Determination of Mode II Interlamilar Fracture Toughness Results from International Collaborative Test Programme*", Plastics, Rubber and Composites, vol 28, No 9, 1999, pp: 432-437.

64. Tanaka K, Kageyama K, & Hojo M., "*Prestandardization study on Mode II Interlaminar Fracture Toughness Test for CFRP in Japan*", Composites, 26, 1995, pp: 257-267.

65. Martin R. Davidson B.S., Plastics, Rubber, & Composites, 28(8), 1999, pp: 401.

66. Giare G.S. & Campbell D., "*A Method to Determine the Fracture Toughness of Unidirectional Fibre Reinforced Composites in Mode II (Forward Shear), Using Thin tubular Specimen*", Eng Fracture Mechanics, 27, 1987, pp: 683.

67. Barrett J.D. Foschi R.O., "*Mode II Stress-Intensity Factors for Cracked Wood Beams*", Eng Fracture Mechanics, 9, 1977, pp: 371.

68. Bradley W.L., "*Presentation at ASTM Task Group Meeting*", Committee D-30, Charleston, SC, April 30, 1986.

69. AECMA Aerospace Series, Carbon Fibre Reinforced Plastics, "*Determination of Interlaminar Fracture Toughness Energy for Mode I (prEN6033) and Mode II (prEN6034)*", Dec 1995.

70. Murri G.B. & Martin R.H., "*Effect of Initial Delamination on Mode I and Mode II Interlaminar Fracture Toughness and Fatigue Fracture Thresholds*", Composite Materials: Fatigue and Fracture, 4th vol, ASTM, STP1156, Eds., Stinchcomb W.W and Ashbaugh N.E., Philadelphia, 1993, pp: 239-256.

71. Russell A. J. & Street K.N., "*Factors Affecting the Interlaminar Fracture Energy of Graphite / Epoxy Laminates*", Proc. Fourth International Conference on Composite Materials, ICCM-IV, Eds. T. Hayashi, K Kawata and S. Umekawa, Tokyo, 1982, pp: 279-286.

72. Carlsson L.A., Gillespie Jr J.W., & Pipes R.B., "*On the Analysis and Design of the End Notched Flexure (ENF) Specimen for Mode II testing*", Journal of Composite Materials , vol 20, 1986, pp :594-605.

73. ASTM D-2234, ASTM Standards and Literature Reference for Composite Materials, 2nd Edition, ASTM, Philadelphia, 1990.

74. Vanderkley P.S., "*Mode I-Mode II Delamination Fracture Toughness of a Unidirectional Graphite /Epoxy Composite*", M. Sc. Thesis, Texas A & M University, Dec. 1981.

75. Lee S.M.,"*An Edge Crack Torsion Method for Mode III Delamination Fracture Testing*", ASTM J of Composite Tech. and Res., JCTRER, 1993, 15(3), pp 193-201.

76. Trantina, G. & Nimmer R., "*Structural Analysis of Thermoplastic Components*", Ed Peggy Malnati, Chap-3: FEA Tech and Nonlinear Issues & Chap-4: Stiffness, McGraw-Hill Inc, 1994.

77. Kanninen M.F., "*A Dynamic Analysis of Unstable Crack Propagation and Arrest in the DCB Test Specimen*", Intl J of Fracture, 9, 1974, pp: 415-430.

78. Crandall, Dahl, S.H, & Lardner T.J., "*An Introduction to the Mechanics of Solids*", 2nd Edition, McGraw-Hill, New York, 1978.

79. Hashemi S., Kinloch A.J., & Williams J.G., "*Corrections Needed in Double Cantilever Beam Test for Assessing the Interlaminar Failure of Fibre Composites*", J of material Science letters, 8, 1989, pp: 125-129.

80. Williams J.G., "*End Corrections for Orthotropic DCB Specimens*", Composites Science and Technology, 35, 1989, pp: 367-376.

81. Williams J.G., "*The Fracture Mechanics of Delamination Tests*", J of Strain Analysis, IMechE, vol 24, No 4, 1989, pp: 207-214.

82. Hashemi S., Kinloch A.J., & Williams J.G., "*The Analysis of Interlaminar Fracture in Uniaxial Fibre-Polymer Composites*", Proceedings of the Royal Society of London, Series A, vol 427, Issue 1872, Jan 1990, pp:173-199.

83. Hashemi S, Kinloch A.J., & Williams J.G., "*The Effect of Geometry, Rate and Temperature on Mode I, Mode II, and Mixed –Mode I/II Interlaminar Fracture of Carbon-fibre/ Poly(ether-ether Ketone) Composites.*" Journal of Composite Materials, vol 24, 1990, pp:918-955.

84. Hashemi S, Kinloch A.J., & Williams J.G., "*Mechanics and Mechanisms of Delamination in a Poly(ether sulphone)- Fibre Composites*", Composites Science and Technology, 37, 1990, pp: 429-462.

85. Kinloch A.J., Wang Y. Williams J.G., & Yayla P., "*The Mixed Mode Delamination of Fibre Composite Materials*", Composites Science and Technology, 47, 1993, pp 225-237.

86. Berry J.P., "*Determination of Fracture Surface Energies by the Cleavage Technique*", J of Applied Physics, 34, 1, 1963, pp:62.

87. Giare G.S.,"*Fracture Toughness of Unidirectional Fibre reinforced Composites in Mode II*", Eng Fracture Mechanics, vol 20, No 1, 1984, pp: 11-21.

88. Carlsson L.A. & Gillespie Jr. J.W., "*Mode-II Interlaminar Fracture of Composites*", Composite Materials Series, 6, Application of Fracture Mechanics to Composite Materials", Ed Klaus Friedrich, Elsevier, 1989, pp: 113-157.

89. Timoshenko S.P., "*Strength of Materials*", Part I, Krieger Publishing, 1964.

90. Ugural A.C. , Fenster S.K., "*Advanced Strength and Applied Elasticity*", American Elsevier Publishing Company, 1975.

91. Kazimi S.M.A., "*Solid Mechanics*", 5th Edition, Tata McGraw-Hill Publishing Company, New Delhi, 1981.

92. Au Tung, "*Elementary Structural Mechanics*", Prentice-Hall of India (Pvt.) Ltd., New Delhi, 1965.

93. Timoshenko S.P.,& Goodier J.N., "*Theory of Elasticity*", 3rd Edition, McGraw-Hill Book Company, Singapore, 1970.

94. Salpekar S.A., Raju I.S., and O'Brien T.K., "*Strain Energy Release Rate Analysis of the ENF Specimen using the Finite Element Method*", J of Composite Technology & Research, vol 10 no 4, 1988, pp:133-139.

95. Wang Y., & Williams J.G., "*Corrections for Mode II Fracture Toughness Specimens of Composite Materials*", Composites Science and Technology, 43, 1992, pp: 251-256.

96. Zhou Jiang & He Tianbai, "*On the Analysis of the End-Notched Flexure Specimen for Measuring the Mode II Fracture Toughness of Composite Materials*", Composites Science and Technology, 50, 1994, pp:209-213.

97. Bathe K.J., "*Finite Element Procedures*", Prentice-Hall of India, New Delhi, 1997.

98. Cook R. D. , Malkus D. S. & Plesha M. E., "*Concepts and Applications of Finite-Element Analysis*" Third edition, 1994.

99. Zienkiewicz O. C. & Taylor R. L., "*The Finite Element Method*" vol 2, 4th Edition, 1991.

100. *ANSYS*, "Online ANSYS User Manual", Version 5.6

101. Gillespie J.W. Jr., Carlsson L.A., & Pipes R.B., "*Finite Element Analysis of ENF Specimen for Measuring Mode II Fracture Toughness*", Composites Science and Technology, vol 27, 1986, pp:177-197.

102. He M. T. and Evans A.G. *"Finite element Analysis of Beam Specimens Used to Measure the Delamination Resistance of Composites*", J of Composites Technology and Research, vol 14, no 4, 1992, pp: 235-240.

103. Mall S., and Kochar N.K., "*Finite Element Analysis of ENF Specimens*", J of Composites Tech. & Res., vol 8, No 2, 1986, pp: 54-57.

104. Todo M., and Jar P.-Y. B., " *Study of Mode–I Interlaminar Crack Growth in Specimens of Fibre-Reinforced Composites.*", Journal of Composite Science and Technology, 58, 1998, pp:105-118.

105. Todo M. and Jar P.-Y. B., *"Initiation of a mode-II interlaminar crack from an insert film in the end-notched flexure composite specimen.*", Journal of Composite Science and Technology, 60, 2000, pp:263-272.

106. Hojo Masaki & Aoki Takahira, "*Thickness Effect of Double Cantilever Beam Specimen on Interlaminar Fracture Toughness of AS4/PEEK and T800/ Epoxy Laminates*", Composite Materials: Fatigue and Fracture, 4th vol, ASTM, STP1156, Stinchcomb W.W and Ashbaugh N.E. Eds., Philadelphia, 1993, pp: 281-298.

107. Davies P., "*Influence of ENF Specimen Geometry and Friction on the Mode II Delamination Resistance of Carbon / PEEK*", J of Thermoplastic Composite Materials, vol 10, July 1997, pp: 353-361.

108. Cantwell W.J., "*The Influence of Loading Rate on the Mode II Interlaminar Fracture Toughness of Composite Materials*", J of Composite Materials, vol 31, No 14, 1997.

109. Davies P., Cantwell W., Richard H., Moulin C., & Kausch H.H., "*Interlaminar Fracture Testing of Carbon Fibre / PEEK Composites: Validity and Applications*", pp 746-755.

110. O'Brien T.K., Murri G.B., & Salpekar S.A., "*Interlaminar Shear Fracture Toughness and Fatigue Thresholds for Composite Materials*", Composite Materials: Fatigue and Fracture, Second vol, ASTM STP 1012, Eds. P.A. Lagace, 1989, pp 222-250.

111. Davidson B.D., Kruger R, & Kong M., "*Three-D Analysis and Resulting Design Recommendations for Unidirectional and Multi-directional End-Notched Flexure Tests*", J of Composite Materilas, vol 29, No 16, 1995. pp: 2108-2133.

112. Russell A.J. & Street K.N., "*Moisture and Temperature Effects on the Mixed Mode Delamination Fracture of Unidirectional Graphite/ Epoxy*", Delamination and Debonding of Materials, ASTM STP 876, Ed. W.S. Johnson, 1985, pp: 349-370.

113. Chatterjee S.N., "*Analysis of Test Specimens for Interlaminar Mode II Frcature Toughness, Part I. Elastic Laminates*", J of Composite Materials, vol 25, May 1991, pp: 470-493.

114. Trethewey B.R., Carlsson Jr., L.A., Gillespie Jr., J.W., & Pipes R.B., "*Mode II Interlaminar Fracture During Static and Fatigue Loading*", CCM-86-26, Centre for Composite Materials, Univ. of Delaware, Newark.

115. Davidson B.D., "*An Analytical Investigation of Delamination Front Curvature in Double Cantilever Beam Specimens*", J of Composite Materials, vol 24, Nov 1990, pp:1124-1137.

116. Lagace P., Brewer J., & Kassapoglou C., " *The Effect of Thickness on Interlaminar Stresses and Delamination in Straight-Edged Laminates*", 1987, J of Composites Technology & Research, vol 9, pp :81-87.

117. Daniel I.M., Anastassopoulos G., & Lee J.W., "*Failure Mechanisms and Interfacial Shear Strength in Brittle-Matrix Composites*", AD-vol 29, AMD-vol 146, Advances in Experimental Mechanics and Biometrics, ASME 1992, pp: 57-69.

Appendix I

A NOTE ON GRAPHICAL REPRESENTATION IN ANSYS

Like most packages with special graphical abilities, ANASYS package has the characteristic to appropriately magnify the displacements to make it visible to the naked eye. We need to examine this feature in order to correctly understand the actual deformed shape of the crack contour for the ENF specimen model. This is required because the crack faces are only 13 micros apart, where as the length of the crack is 50mm. The deformations of the node points of the crack face are of the order of .001mm and .01 mm in x- and y-directions, respectively (ANSYS notation).

For the above purpose, let us consider a simple undeformed configuration as shown in fig A1.1(A). The deflection profile is as follows. The deflection of all the node points is uniform along the y-axis, where as the deflection along x-direction is given by the deflection profile superimposed on the original configuration in the figure. The deformed configuration after the magnification of the displacements along x and y directions is given in fig A1.1--(B): (i), (ii), (iii). We see that in the last figure the top and the bottom faced appear to cross each other. So the magnification effect of the deformations sometimes distorts the actual deformed configuration.

To get rid of this distorted picture, the stress contour are plotted on the undeformed model. This can be obtained by using a spurious link element with a small pre-strain of 1.0×10^{-6}. The spurious link connects the two keypoints which are not actually connected to the model of the ENF Specimen. The element carries no force, but undergoes large deformation (infinite, as it is not constrained). So magnification of all the deformations is brought down and stress contours can be obtained superimposed on the undeformed shape. This procedure is used to obtain the figures 4.9 (a)-(e) for the stress contours of the ENF specimen.

The actual deformed configuration of the crack contour in the ENF specimen can be arrived at from the numerical values of the nodal deformations on the crack contour. This is shown in the Table A1.1. The plot of the crack faces and the crack tip in the actual deformed configuration is shown in fig A1.2.

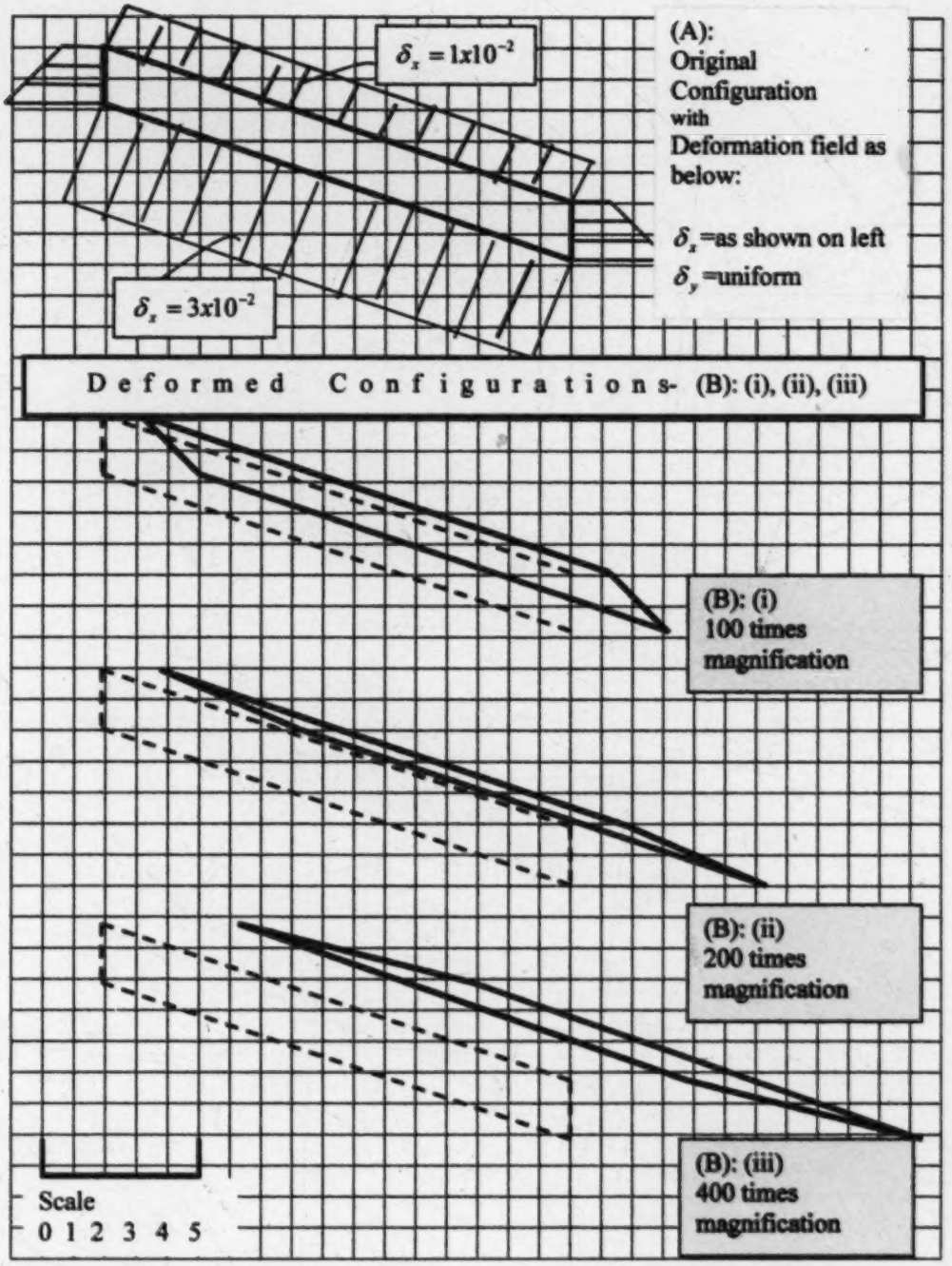

Fig A1.1 Orginal and deformed configurations showing that in (B): (iii) the top and the bottom faces cross over each other.

Table A1.1
Actual Deformed Crack Contour from Numerical Nodal Deflection Values

S.No.	Node Number	Initial Configuration x-cor	y-cor	Deflection δ_x	δ_y	Deformed Configuration x-cor	y-cor
nodes on top crack face							
2top	2	49.99	0.0065	0.0014937	-0.010066	49.991494	-0.00357
3top	72691	49.95	0.0065	0.0014803	-0.010054	49.95148	-0.00355
4top	76981	49.93741	0.0065	0.0014775	-0.010051	49.938888	-0.00355
5top	76979	49.92139	0.0065	0.0014741	-0.010047	49.922863	-0.00355
6top	76975	49.85104	0.0065	0.0014618	-0.01003	49.852506	-0.00353
7top	72627	49.8	0.0065	0.0014543	-0.010018	49.801454	-0.00352
8top	76989	49.61372	0.0065	0.0014316	-0.0099737	49.615156	-0.00347
9top	79846	49.40939	0.0065	0.0014114	-0.0099252	49.410797	-0.00343
10top	79856	49.08134	0.0065	0.001384	-0.0098462	49.082726	-0.00335
11top	77001	48.77311	0.0065	0.001361	-0.0097705	48.77447	-0.00327
12top	79698	48.50165	0.0065	0.0013434	-0.0097026	48.502996	-0.0032
13top	79680	47.88017	0.0065	0.0013057	-0.0095424	47.881477	-0.00304
14top	79670	47.52517	0.0065	0.0012858	-0.009448	47.526458	-0.00295
15top	70453	46	0.0065	0.0012084	-0.0090179	46.001208	-0.00252
16top	77060	45.00641	0.0065	0.0011628	-0.0087162	45.007573	-0.00222
nodes on bottom crack face							
2bot	226	49.99	-0.0065	1.58E-03	-0.010065	5.00E+01	-0.01657
3bot	72979	49.95	-0.0065	0.0015885	-0.010055	5.00E+01	-0.01656
4bot	76982	49.93741	-0.0065	0.0015914	-0.01005	4.99E+01	-0.01655
5bot	76980	49.92139	-0.0065	0.0015946	-0.010046	4.99E+01	-0.01655
6bot	76976	49.85104	-0.0065	0.0016069	-0.010029	4.99E+01	-0.01653
7bot	72659	49.8	-0.0065	0.0016145	-0.010016	4.98E+01	-0.01652
8bot	76990	49.61372	-0.0065	0.0016371	-0.0099724	4.96E+01	-0.01647
9bot	79897	49.40939	-0.0065	0.0016572	-0.0099239	4.94E+01	-0.01642
10bot	79907	49.08134	-0.0065	0.0016846	-0.0098449	4.91E+01	-0.01634
11bot	71002	48.77311	-0.0065	0.0017071	-0.0097692	4.88E+01	-0.01627
12bot	79777	48.50165	-0.0065	0.0017252	-0.0097013	4.85E+01	-0.0162
13bot	79759	47.88017	-0.0065	0.0017805	-0.0095411	4.79E+01	-0.01604
14bot	79749	47.52517	-0.0065	0.0017829	-0.0094467	4.75E+01	-0.01595
15bot	71389	46	-0.0065	0.0018604	-0.0090166	4.60E+01	-0.01552
16bot	77059	45.00641	-0.0065	0.0019016	-0.0087149	4.50E+01	-0.01521

S.No.	Node Number	Initial Configuration x-cor	y-cor	Deflection δ_x	δ_y	Deformed Configuration x-cor	y-cor
nodes on the crack tip							
C1	68484	50.00201	0.0053	0.0015136	-0.010076	50.003522	-0.00482
C2	68496	50.00317	0.0014	0.0015293	-0.010079	50.0047	-0.00872
C3	68506	50.00307	-0.002	0.001542	-0.010078	50.004615	-0.01211
C4	68512	50.00255	-0.004	0.0015497	-0.010077	50.004096	-0.01408
C5	68406	49.999	0.0065	0.0015019	-0.01007	50.000502	-0.00357
C6	68436	49.999	-0.0065	0.001567	-0.01007	50.000567	-0.01657
C7	68520	50.00081	0.0063	0.0015065	-0.010073	50.002317	-0.00372
C8	68524	50.00151	0.0059	0.0015099	-0.010075	50.003021	-0.00416
C9	68490	50.00276	0.0034	0.0015217	-0.010078	50.004281	-0.00672
C10	68482	50.00179	-0.0056	0.0015571	-0.010075	50.003347	-0.01569
C11	68476	50.00081	-0.0063	0.0015624	-0.010073	50.002372	-0.01641

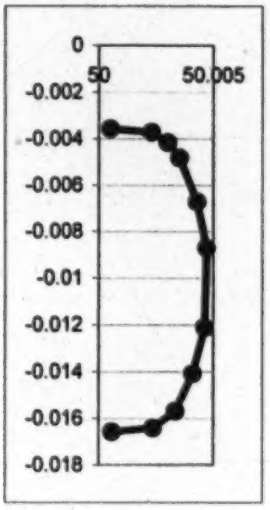

(a)

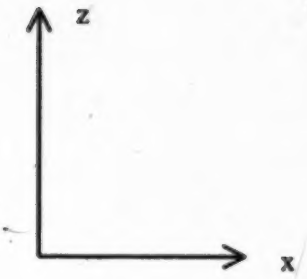

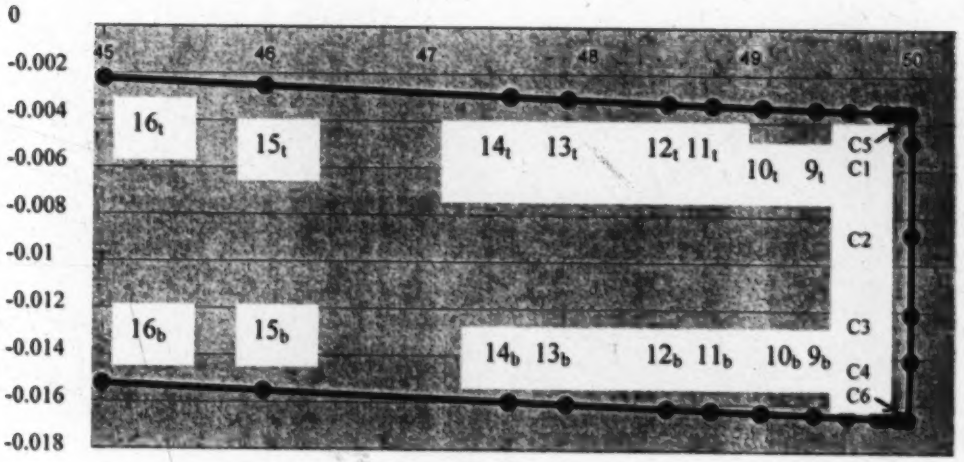

(b)

Fig A1.2 Actual deformed crack contour configuration (a) Deformed crack tip on 1:1 scale (b) Crack faces on an elongated scale